INDIRECT SOIL SALINITY DETECTION IN IRRIGATED AREAS USING EARTH OBSERVATION METHODS

SYBRAND JACOBUS MULLER

Thesis presented in fulfilment of the requirements for the degree of Master of Science in the Faculty of Science at Stellenbosch University.

Supervisor: Prof A Van Niekerk

March 2017

DECLARATION

By submitting this thesis electronically, I declare that the entirety of the work contained therein is my own, original work, that I am the sole author thereof (save to the extent explicitly otherwise stated), that reproduction and publication thereof by Stellenbosch University will not infringe any third party rights and that I have not previously in its entirety or in part submitted it for obtaining any qualification.

With regard to Chapters 3 and 4 the nature and scope of my contribution were as follows:

Chapter	Nature of contribution	Extent of contribution (%)
Chapter 3	This chapter was published as a journal article (Muller & van Niekerk 2016a) and was co-authored by my supervisor who helped in the conceptualization and writing of the manuscript. I carried out the literature review, data collection and analysis components and produced the first draft of the manuscript.	SJ Muller 85% Prof A van Niekerk 15%
Chapter 4	This chapter was published as a journal article (Muller & Van Niekerk 2016b) and was co-authored by my supervisor who helped in the conceptualization and writing of the manuscript. I carried out the literature review, data collection and analysis components and produced the first draft of the manuscript.	SJ Muller 85% Prof A van Niekerk 15%

Date: March 2017

Signature:

SUMMARY

Excessive accumulation of salt in the plant root zone has a deteriorating effect on vegetation growth, resulting in reduced crop yield and rendering fertile soil barren, and ultimately leads to decreasing food production. This problem motivates the critical need for active salinity monitoring, with an aim to implement rehabilitation and preventive measures. Conventional salinity monitoring methods, such as regular field visits and laboratory analyses of soil samples, are ineffective for frequent salt accumulation monitoring over large areas. Earth observation techniques can complement conventional methods and potentially improve the cost- and time-efficiency of the regular salt accumulation monitoring.

A review of literature identified a number of direct and indirect approaches for detecting accumulated salts using remote sensing. Given that salt accumulation in South Africa is most prevalent in irrigation schemes, the indirect approach, which mainly focusses on salt induced vegetation response, was identified as the preferred approach. Little is known about the optimal combinations of very high resolution satellite imagery and image classification techniques in South African irrigation schemes, where accumulated salt generally occurs in small localized patches. Consequently, two experiments were carried out to: identify suitable spectral and spatial resolutions of imagery; test the value of various image-derived features and classification techniques; and evaluate the spatial scale at which salt accumulation is best identified. The first experiment, applied on an agricultural field scale, analysed WorldView-2 imagery with statistical (regression) and machine learning (decision trees) techniques, and found clear relationships between salt accumulation and image transformations (vegetation indices and image texture). Spatial resolutions of six metres or higher were found to be most suitable. A higher spectral resolution marginally improved classification accuracies, but the increases were insignificant. The second experiment, applied on an irrigation scheme level, assessed SPOT-5 imagery with statistical (regression) and machine learning (various algorithms) techniques in two irrigation schemes. The failure to highlight any consistent image transformation or classification techniques for both irrigation schemes emphasised the negative effect of varying salinity tolerances of crop types and growing phases in identifying salt accumulation. Knowledge gained from the two experiments aided the development of a field level object-based monitoring system that showed sufficient transferability.

The quantitative experiments answered key research questions and will serve as a point of departure for future research regarding indirect methods for detecting salt accumulation in agricultural fields. This work will be instrumental in the establishment of a South African

salinity monitoring system – with the aim of rehabilitation – and will help to maximize agricultural production and ultimately contribute to sustainable food production.

KEYWORDS

Soil salinity, salt accumulation, irrigated agriculture, remote sensing, earth observation, regression analysis, decision tree analysis, supervised classification, machine learning, geographic object-based image analysis

OPSOMMING

’n Oormaat sout in ’n plant se wortelarea het ’n nadelige effek op die plant se groei, veroorsaak ’n afname in oesopbrengs en maak vrugbare grond onvrugbaar, wat uiteindelik tot ’n afname in voedselproduksie lei. Hierdie probleem motiveer die kritiese behoefte aan ’n stelsel wat grondversouting aktief moniteer, met die doel om versoute areas te rehabiliteer en te voorkom. Tradisionele metodes om grondversouting te moniteer sluit gereelde veldwerk en laboratoriumontleding van grondmonsters in, maar is nie vir die gereelde monitering van groot grondversoute-areas effektief nie. Afstandswaarnemingmetodes kan konvensionele metodes aanvul en moontlik tot ’n afname in die tyd en koste verbonde aan die gereelde montering van soutophoping lei.

’n Literatuuroorsig het direkte en indirekte metodes vir die identifisering van grondversouting met behulp van afstandswaarneming uitgelig. Aangesien grondversouting in Suid-Afrika grootliks in besproeiingskemas voorkom, word die indirekte metode, wat die afname in plantegroei as gevolg van grondversouting monitor, verkies. Min inligting is beskikbaar oor die optimale kombinasies van baie hoë resolusie satellietbeelde en beeldklassifikasie-metodes in Suid-Afrikaanse besproeiingskemas, waar grondversouting in klein, gelokaliseerde areas voorkom. Gevolglik is twee eksperimente uitgevoer om geskikte spektrale en ruimtelike resolusies te identifiseer; kenmerke afgelei van beelde en beeldklassifikasie-tegnieke te toets; en die mees geskikte ruimtelike skaal vir die identifisering van grondversouting te evalueer. Die eerste eksperiment, toegepas op ’n landeryskaal, het WoldView-2 beeldmateriaal met statistiese (regressie) en masjienleer- (beslissingsboom) metodes geanaliseer en het gevind dat daar duidelike verhoudings tussen grondversouting en beeldtransformasies (plantegroeiindeks en beeldtekstuur) bestaan. Ruimtelike resolusies as ses meter of kleiner was as aanvaarbaar beskou. ’n Hoër spektrale resolusie het die resultate effens verbeter, maar was nie betekenisvol nie. Die tweede eksperiment, wat op ’n skema-vlak toegepas was, het SPOT-5-beeldmateriaal met statistiese (regressie) en masjienleermetodes (verskeidenheid algoritmes) op twee verskillende besproeiingskemas geëvalueer. Geen konsekwente beeldtransformasies of -klassifikasies vir die twee studieareas kon uitgelig word nie, wat op die negatiewe effek van die wisselende versoutingstoleransies en verskillende groeistadiums van die gewasse dui. Die kennis wat deur die twee eksperimente opgedoen is, het gelei tot die ontwikkeling van ’n objekgebaseerde-moniteringsisteem op landeryskaal wat voldoende oordraagbaarheid getoon het.

Die kwantitatiewe eksperimente het kernnavorsingsvrae beantwoord en sal as ’n vertrekpunt dien vir enige toekomstige navorsing oor die gebruik van indirekte afstandswaarneming metodes vir die identifisering van grondversouting. Die navorsing sal ook bydra tot die vestiging van ’n Suid-

Afrikaanse grondversoutingmoniteringsisteem – met die oog op rehabilitasie – wat tot die maksimalisering van landbouproduksie en uiteindelik tot volhoubare voedselproduksie kan lei.

TREFWOORDE

Soutgehalte van grond, soutophoping, besproeide landbou, afstandswaarneming, aardobservasie, regressie-analise, beslissingsboomanalise, gerigte klassifikasie, masjienleer, geografiese objekgebaseerde beeldanalise

ACKNOWLEDGEMENTS

I sincerely thank:

- the staff of the Department of Geography and Environmental Studies for helpful comments and constructive criticism during scheduled feedback sessions;
- the staff of the Department of Soil Science for aiding with laboratory work; and
- Prof Adriaan van Niekerk for excellent guidance and meaningful advice and suggestions.

I am also thankful to the Water Research Commission (WRC) for initiating and funding the project titled “Methodology to monitor the status of waterlogging and salt-affected soils on selected irrigation schemes in South Africa” (contract number K5/1880//4), of which this work forms part. More information about this project is available in the 2015 WRC Report (No. TT 648/15; ISBN 978-1-4312-0739-8), available at www.wrc.org.za. I also acknowledge and thank the project leader, Dr Piet Nell of the Agricultural Research Council, for providing the soil data used in this study and for his invaluable guidance and insight, particularly during the field surveys.

CONTENTS

TABLES

FIGURES

ACRONYMS AND ABBREVIATIONS

ANOVA	Analysis of variance
ARC	Agricultural Research Council
ASTER	Advance space-borne thermal emission and reflection radiometer
AUC	Area under the curve
AVIRIS	Airborne visible infrared imaging spectrometer
BR	Brightness ratio
BRE	Best relative error
CART	Classification and regression tree
CASI	Compact airborne spectrographic imager
CBERS	China-Brazil earth resources satellite
COSRI	Combined spectral response index
DEM	Digital elevation model
DN	Digital numbers
DT	Decision tree
EC	Electroconductivity
EM	Electromagnetic
ETM	Enhanced thematic mapper
EVI	Enhanced vegetation index
FAO	Food and Agriculture Organization
FCC	False colour composite
GCP	Ground control points
GEOBIA	Geographical object-based image analysis
GIS	Geographical information system
GLCM	Grey level co-occurrence matrix
GLDV	Grey level difference vector
GPS	Global positioning system
GVMI	General vegetation moisture index
IHS	Intensity, hue, and saturation
IRS	Indian remote sensing
IFOV	Instantaneous field of view
KC	Kappa coefficient
KNN	k-Nearest neighbour

KZN	KwaZulu-Natal
LiDAR	Light detection and ranging
LISS	Linear imaging self-scanning system
LMM	Local mean matching
LMVM	Local mean and variance matching
LO	Longitude of origin
LSU	Linear spectral unmixing
MeaD	Mean difference
MinD	Minimum distance
ML	Maximum likelihood
MODIS	Moderate resolution imaging spectroradiometer
MRS	Multi-resolution segmentation
NDVI	Normalized difference vegetation index
NIR	Near-infrared
NN	Nearest neighbour
OA	Overall accuracy
OBIA	Object-based image analysis
OI	Optical imagery
PA	Producer’s accuracy
PCA	Principal component analysis
PLS	Partial least squares
PRI	Physiological reflectance index
RADAR	Radio detection and ranging
RF	Random forests
RGB	Red, green, blue
RSA	Republic of South Africa
ROC	Receiver operating characteristics
RVI	Ratio vegetation index
SAM	Spectral angle mapper
SANSA	South African National Space Agency
SAVI	Soil-adjusted vegetation index
SEBAL	Surface balance algorithm for land
SFF	Spectral feature fitting
SLR	Stepwise linear regression

SMA	Spectral mixture analysis
SMR	Stepwise multiple regression
SPOT	Satellite pour l'observation de la terre
SVM	Support vector machine
SWIR	Shortwave infrared
SWSI	Salinity and water stress indices
TIR	Thermal infrared
TM	Thematic mapper
US	User's accuracy
USDA	United States Department of Agriculture
VHR	Very high resolution
VIL	Variable importance list
VIs	Vegetation indices
VIS	Visible spectrum
WFAD	Within-field anomaly detection
WI	Water index
WRC	Water Research Commission
WV2	WorldView-2

CHAPTER 1: INTRODUCTION

Soil salinity, for the purpose of this study, is defined as the accumulation of soluble salts in the topsoil. Salinity can be classified as primary (i.e. when soil salinity occurs naturally), or secondary (when induced by human interference). Secondary salinity mainly occurs due to a lack of proper planning or maintenance of irrigation infrastructures and is a major concern, especially in irrigated areas. Extreme salt accumulation leads to the death of vegetation and consequently to a reduction in crop yield and general degradation of fertile soil (Ghassemi, Jakeman & Nix 1995). Previous estimates of global salinity effects indicate that around 77 million hectare of the earth's surface is affected by secondary salinity and that more than half of this area is made up of irrigated soil (Metternicht & Zinck 2003). The negative economic impact of salt-affected soils on the agricultural sectors' production capacity is immense, with the added pressure of maintaining sustainable food production in a world with a growing population. With quality crop and soil management, good irrigation and drainage systems design and political and social support, irrigation can be a thriving, sustainable practice (Hillel & Vlek 2005; Van Rensburg et al. 2012). Quality management practice includes tracking and identifying salinity changes to anticipate further degradation and to undertake suitable reclamation and rehabilitation practices (Metternicht & Zinck 2003).

1.1 SOIL SALINITY

The term salinity is used to describe both the processes and impacts of salt on soil and water, while also being a measure of the amount of salt in soil or water (Hillel 2000; McGhie & Ryan 2005). The electrolytic mineral solutes most commonly associated with salinity are the cations Na^{+}, K^{+}, Ca^{2+} and Mg^{2+} and the anions Cl^{-}, SO_4^{2-}, NO, HCO and CO_3^{2-} (Hillel 2000). The sources and processes of salt accumulation are vast and dynamic. Soil salinity can occur naturally (primary) or as a result of human interference (secondary) (Ghassemi, Jakeman & Nix 1995). Salts occur naturally in soils formed in arid regions simply because they have not been leached by rain (Hillel 2000). However, the salt content in such soils depends greatly on the nature of the soil. The salt content for sandy soils is generally lower than that of soils with a high content of clay minerals (Ghassemi, Jakeman & Nix 1995). Brackish groundwater can also infuse salts into top soil, typically where the subsoil contained accumulated salts from previous geologic eras. Rising water tables can transport these salts from the subsoil to the crop root zone. Rainwater is also considered a natural cause and can indirectly contribute to soil salinity, especially near industrialized regions where rainwater mixes with emitted gasses, or near coastal regions where sea spray can mix with rainwater.

The more insidious form of soil salinity occurs when previously productive soils are subjected to salinity due to human interference. This secondary salinity is mainly due to the extra water provided by human activities, such as irrigation and land clearing (Ghassemi, Jakeman & Nix 1995).

Some of the processes that give rise to human-induced salinity include:

- When water containing mineral salts is used for irrigation, the salts are transported to the crop root zone. Through the processes of transpiration and evaporation, the water is returned to the atmosphere and the salts are left behind in the soil. Highly arid regions require more irrigation and have less rainfall to leach out the accumulated salts (Hillel 2000; Umali 1993).
- Irrigation in poorly drained areas leads to increased water infiltration and the rising of the natural water table (Ghassemi, Jakeman & Nix 1995). This effect is exacerbated by the over-application of irrigation water, which especially happens when water is priced below its true economic value (Umali 1993). Similar to the natural process, the rising water table (artificial rise) leads to the transportation of salts to the crop root zone.
- Irrigation systems often have an intricate canal system for the transportation of irrigation water. The canals are mostly unlined and have a high seepage rate. The infiltrating water accumulates and over time can raise the water table to within a few metres of the land surface (Ghassemi, Jakeman & Nix 1995).
- A change in the hydrological balance that occurs when land is cleared for farming and pastoral activities can be another major cause of rising water tables. When land is cleared, the deep-rooted natural vegetation is removed, leading to less evapotranspiration. Consequently, more water infiltrates the soil, supplementing the natural water table (Ghassemi, Jakeman & Nix 1995).

An overview of secondary salinity, specifically in irrigated areas, is shown in Figure 1.1. Umali (1993) ascribes most of the human-induced salinity to poor water-use efficiency on farms owing to a lack of awareness; poor engineering and maintenance on the canal systems (leading to increased seepage); insufficient or non-existing artificial drainage infrastructure; and poor design and maintenance of artificial drainage infrastructure. In irrigation schemes, most salt accumulation occurs as a result of the secondary process.

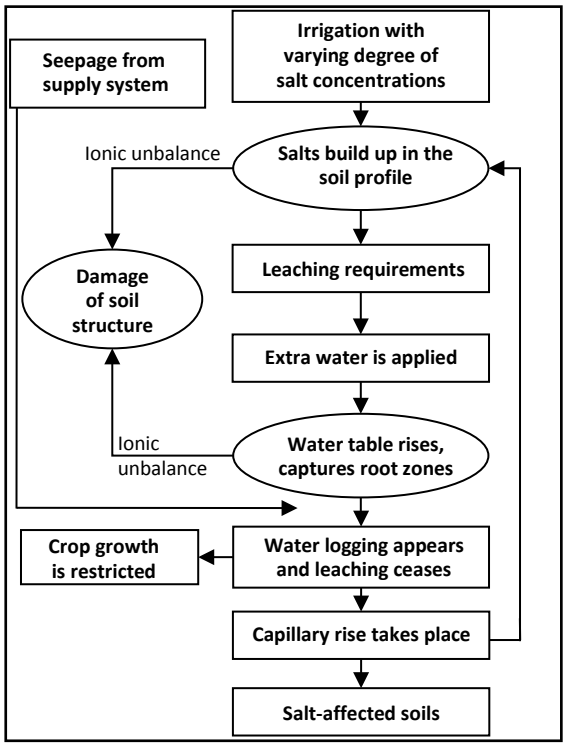

Source: Abbas et al. (2013)

Figure 1.1 Induced secondary salinization in irrigated areas

1.1.1 Waterlogging

Waterlogging, a process very closely related to soil salinity (Figure 1.1), is the saturation of the soil as a result of the water table being located at or near the surface (Barrett-Lennard 2003; McDonagh & Bunning 2009). The secondary salinity processes that lead to a rising water table similarly contributes to the occurrence of waterlogging. Waterlogging can also be caused by high sodicity levels in soils, which limit the infiltration of surface water as a result of compaction and crusting (Ghassemi, Jakeman & Nix 1995; Qureshi & Barrett-Lennard 1998). Soil sodicity occurs when clay particles in the soil becomes dominantly charged with sodium (Na) ions, rather than calcium (Ca) ions (Hillel 2000; Qureshi & Barrett-Lennard 1998).

1.1.2 Effects and indicators of soil salinity and waterlogging

Halophytic plants are adapted to grow in saline conditions (Hillel 2000; Qureshi & Barrett-Lennard 1998). Some of these plants only occur in saline conditions and can therefore be used to identify areas affected by salt accumulation. These salinity indicator plants, however, vary between different regions (McGhie & Ryan 2005). Glycophytes, plants that are not adapted to survive in saline conditions, show indications of physiological stress in the presence of salinity. Most crop plants are glycophytic (Hillel 2000).

If the accumulation of salts in the root zone is higher than the plant's tolerance level, the plant will have a reduced ability to take up water. The plant then goes into an "osmotic adjustment"

process, using additional metabolic energy (i.e. from photosynthesis) in an attempt to take up more water (Hillel 2000). This inevitably leads to the dehydration and wilting of plant leaves and stems, known as the osmotic effect (McGhie & Ryan 2005).

When a plant absorbs water and nutrients during transpiration, small amounts of salt will accompany the water. In persistent saline conditions, over time, these salts will accumulate and may have a toxic effect on the plant. Some of the ions related to salinity that cause the toxic effect are an abundance of chloride (Cl^-) and sodium (Na^+) (Hillel 2000). The toxicity can lead to internal structural damage and more commonly leads to leaf injury symptoms (leaf tips of plants turn yellow) (Hillel 2000; McGhie & Ryan 2005).

In the case of waterlogging, there is an oxygen deficiency in the soil due to the low solubility and diffusivity of oxygen in the water, which causes a state of hypoxia (Armstrong et al. 1991; Barrett-Lennard 2003). Since plant roots require oxygen for optimal production, the lack thereof results in a rapid decrease of growth, the loss of its ability to screen out salts at the root zone and the loss of its ability to absorb organic nutrients. Physiological indicators include discolouring of vegetation, defoliation, wilting and plant death (Barrett-Lennard 2003; McGhie & Ryan 2005; Qureshi & Barrett-Lennard 1998). McGhie & Ryan (2005) observed that waterlogging symptoms are very similar to those caused by an excess of salt.

It should be clear from the above discussion that physiological vegetation stress is a potential indicator of salinity and waterlogging. There are also other, more direct, indicators of salinity and waterlogging. For instance, a white efflorescent salt crust on the soil surface is a direct sign of salt accumulation (McGhie & Ryan 2005). These efflorescent salt crusts form when saline water evaporates and salts crystalize on soil grains (Goodall, North & Glennie 2000). This results in a powdery or puffy texture that has a high reflectance (i.e. appear bright) (Metternicht & Zinck 2003) (Figure 1.2a). Other surface features of salinity include: black staining when iron in the soil reacts with sulphate salts (SO_4^{2-}), bare patches without salt encrustations and soil erosion due to the loss of protective vegetation cover. Waterlogging is directly detectable on the surface in the visible saturation of the topsoil and surface ponding (Figure 1.2b) (Dwivedi, Sreenivas & Ramana 1999). When the water of a surface pond evaporates, salt encrustation also tends to form.

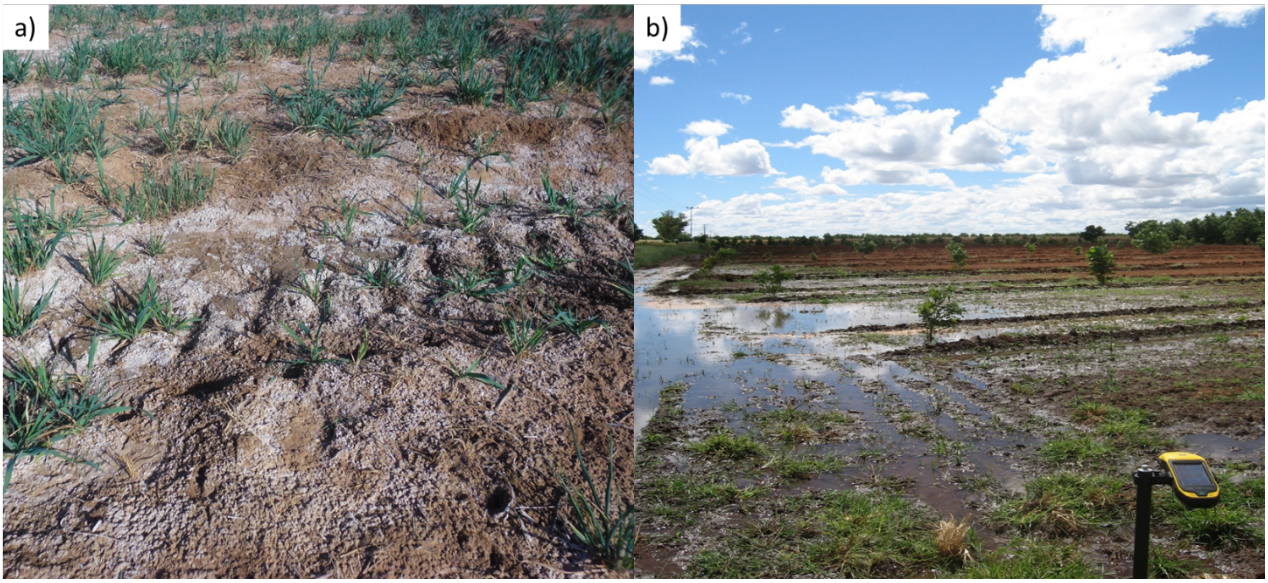

Figure 1.2 Examples of a) white efflorescent salt crust and b) surface ponding (waterlogging) in the Vaalharts irrigation scheme.

1.1.3 Salinity impacts

In an advanced stage, the cumulative effects of soil salinity and waterlogging on its surroundings can lead to adverse agricultural and environmental impacts. If salinity reaches high levels, it kills off all vegetation, resulting in reduced crop yield and quality, and renders the once fertile soil barren, stripped of any biodiversity (Ghassemi, Jakeman & Nix 1995). Salinity is not as dramatic or damaging as earthquakes or landslides, yet it is still one of the most severe environmental factors impairing the production of agricultural crops (Ghassemi, Jakeman & Nix 1995; Metternicht & Zinck 2003; Pitman & Läuchli 2002; Umali 1993; Zinck 2000).

Estimations of the extent of salt-affected areas vary greatly. Metternicht & Zinck (2003) estimated that primary salinity covers a total of 1 billion hectares of the earth surface – about 7% of the earth's continental extent Secondary salinity accounts for an additional 77 million hectares, with 58% occurring in irrigated areas. According to Hillel (2000), irrigated cropland makes up 17% of cropland globally, while contributing 30% of the total agricultural production – highlighting the importance of irrigation and the impact that secondary salinity can have on food security. Ghassemi, Jakeman & Nix (1995) estimate that 20% of these irrigated croplands are salt-affected. Globally, the economic impact of the loss in production capacity due to salinity is estimated at $US 11.4 billion and $US 1.2 billion per year in irrigated and dryland areas respectively (Ghassemi, Jakeman & Nix 1995). A more recent global estimate is urgently needed, especially given that dryland crops are increasingly being converted to irrigated agriculture to increase agricultural production, which could lead to a dramatic increase in induced soil salinity (Metternicht & Zinck 2003). Other problems linked to soil salinity includes

losses in property values, eutrophication of rivers, damage to infrastructure, increased soil erosion and engineering difficulties (Metternicht & Zinck 2003).

1.1.4 South African situation

In South Africa, the total area under irrigation is estimated at 1.3 million ha. Irrigation is critical for food security, specifically given that large parts of the country receives insufficient rainfall for dryland crop production (Backeberg 2003; Backeberg et al. 1996). In the comprehensive literature review by Ghassemi, Jakeman & Nix (1995), it is estimated that up to 9% of South African irrigated lands are susceptible to salt accumulation. Backeberg et al. (1996) reported that between 1% and 12% of the South African irrigation schemes suffer from severe waterlogging and salt accumulation, while between 5% and 20% are moderately affected. This percentage is much lower compared to other regions such as Argentina (34%), Egypt (33%), Iran (30%), Pakistan (26%) and USA (23%) (Ghassemi, Jakeman & Nix 1995). This favourable status is attributed to careful selection of irrigated areas, good drainage and the smaller sized irrigated areas in South Africa. Although the extent of salt-affected areas in South African irrigation schemes is less severe, Ghassemi, Jakeman & Nix (1995) warns that the salinization of reservoirs used for water supply can have a direct effect on salt accumulation in irrigation schemes. Also, there is no active programme in place to monitor the extent and changes in salt-affected and waterlogged areas (De Villiers et al. 2003). Such complacency can potentially lead to conditions that may cumulatively cause rapid salt accumulation and loss of scarce productive land.

1.1.5 Importance of irrigated agriculture

Irrigation is necessary for the sustainable maintenance of food production in South Africa. For example, the fruit and wine industries of the Western Cape are entirely dependent on irrigation, while cropping in the Eastern and Northern Cape also rely heavily on irrigation (Van Rensburg et al. 2011). The posing threat of salinity in irrigation schemes is real, but manageable. Letey (1994), Rhoades (1997) and Van Schilfgaarde (1990) as cited in Van Rensburg et al. (2012) are all in agreement that sustainable irrigation is possible with well-designed irrigation and drainage systems, good crop and soil management practices and support from political and social structures. These factors can, according to Hillel & Vlek (2005), help to strengthen irrigated agriculture and increase food production.

Pressure on agricultural land increases with an increase in population (currently at 1.6% per annum). Irrigation schemes account for almost 30% of the total crop production (De Villiers et al. 2003). Saline soils pose a threat to sustainable agriculture and can significantly reduce crop

yields – particularly in irrigation schemes. There is consequently a need for a systematic management of salt accumulation to mitigate further losses of fertile agricultural land. Salt accumulation management practice require monitoring to anticipate degradation and to make informed decisions about reclamation and rehabilitation (Metternicht & Zinck 2003). Monitoring includes identifying locations of salt accumulation and tracking its temporal and spatial dynamics.

1.1.6 Salt accumulation monitoring

An area's salinity status is usually determined by carrying out field surveys and performing laboratory analyses of collected soil samples. There are a number of ways to measure the salt content in soils. The saturated paste technique is widely used for measuring the salt content in a soil sample, and has shown sufficient accuracy. The process involves extracting the salt concertation of a soil sample with the use of water to ultimately determine its electroconductivity (EC). Electroconductivity is defined as the degree to which water conducts electricity, which is proportional to the amount of salts in the solution (Hanson, Grattan & Fulton 2006). The measured EC value is widely used as an indicator of soil salinity. In South Africa, soil samples with EC values of 4.0 dS/m (deci-siemens per metre) or higher are regarded as being salt-affected, while all samples with EC values below 4.0 dS/m are regarded as being unaffected (Bresler, McNeal & Carter 1982; Richards 1954; SASA 2007).

Conventional methods for monitoring salt accumulation are laborious and costly and not viable when frequent monitoring is required over extensive (e.g. national) areas. A cost-effective solution for monitoring salt accumulation over large areas is consequently needed.

1.1.7 Earth observation for monitoring soil salinity

Earth observation by remote sensing can capture data on both a temporal and spatial scale and has the potential for identifying salt-affected areas. If successfully applied, remote sensing can serve as a monitoring solution that would not be as costly and labour intensive as regular field surveys and laboratory analyses.

Various techniques and applications of remote sensing for the identification of salt-affected areas have been published. Salt accumulation can be detected either directly or indirectly using remotely sensed images (Bastiaanssen 1998; Mougenot, Pouget & Epema 1993). The direct detection of the accumulation of salts involves identifying salt encrustations on the bare ground, while the indirect method focuses mainly on vegetation responses to salt accumulation.

Several authors have successfully applied the direct approach for identifying salt accumulation (Abood, Maclean & Falkowski 2011; Dwivedi & Sreenivas 1998; Elnaggar & Noller 2010; Iqbal 2011; Khan et al. 2005; Metternicht & Zinck 2003; Rao et al. 1995; Setia et al. 2013; Sidike, Zhao & Wen 2014). Most of these studies reported that salt crusts generally have high reflectance in the visible and near to mid-infrared regions of the electromagnetic spectrum, depending on the chemical composition of the salts (Metternicht & Zinck 2009). Specific spectral ranges for direct salinity detection (identified by laboratory analyses) are in the visible region (550-770 nm), near-infrared region (900-1030 nm, 1270-1520 nm) and middle infrared region (1940-2150 nm, 2150-2310 nm, 2330-2400 nm) (Csillag, Pasztor & Biehl 1993). Metternicht & Zinck (2009) observed that applying laboratory techniques to optical remote sensing data to detect salt accumulation is complicated by the variations in reflectance that cannot be attributed to a single soil property and salt type. Spectral variation in salt crusts can be attributed to the difference in the quantity of salts, the mineralogy of the salts (e.g. carbonates, sulphates or chlorides), soil moisture, colour of the salt crust (white to dark) and surface roughness of the salt crust (smooth to rough), which all vary among chemical structures. The direct approach also fails to take into account salt accumulation that occurs in the sub-surface, since it is limited to monitoring surface conditions.

The indirect approach, which focuses mainly on vegetation monitoring, has also been successfully applied to remotely identify salt-affected areas. One approach is to identify halophytic vegetation types that commonly occur in salt-affected areas (Dehaan & Taylor 2002; Dehaan & Taylor 2003; Dutkiewicz, Lewis & Ostendorf 2009a; García Rodríguez, Pérez González & Guerra Zaballos 2007). However, this method is less suitable for application in irrigated areas where natural vegetation is removed during field preparations. A more common approach in irrigated areas is to monitor vegetation (crop) vigour. For this purpose, vegetation indices (VIs) are primarily used to distinguish between healthy vegetation and stressed vegetation. Two of the most used VIs are the NDVI (Abbas et al. 2013; Aldakheel 2011; Bouaziz, Matschullat & Gloaguen 2011; Elnaggar & Noller 2010; Hamzeh et al. 2012a; Platonov, Noble & Kuziev 2013; Sidike, Zhao & Wen 2014; Zhang et al. 2011) and the SAVI (Abood, Maclean & Falkowski 2011; Allbed, Kumar & Aldakheel 2014; Bouaziz, Matschullat & Gloaguen 2011; Elnaggar & Noller 2010; Hamzeh et al. 2012b; Koshal 2010; Zhang et al. 2011). However, using vegetation response for identifying salinity conditions should be used with caution because many factors besides soil salinity (e.g. farming practices) can contribute to loss of vegetation vigour (Metternicht & Zinck 2009). Different crops in different growing phases

also have different tolerances to soil salinity, which further complicates the implementation of the indirect approach.

1.2 PROBLEM FORMULATION

Conventional methods of monitoring the accumulation of salts include soil surveys and laboratory analyses. These methods are not practical for systematic monitoring over large areas. Earth observation has been shown to be effective for monitoring salt-affected areas by detecting vegetation stress caused by exposure to high levels of salts in the soil. Previous applications of the indirect approach have been carried out successfully in areas where soil salinity occurs at a grand scale (i.e. high levels of salinity and large affected areas). As a result, the satellite imagery most commonly employed for detecting soil salinity has low to medium spatial resolution. Examples include 30 m Landsat (Abdelfattah, Shahid & Othman 2009; Aldakheel 2011; Dehni & Lounis 2012; Gao & Liu 2008; Mohamed, Morgun & Goma Bothina 2011); 23 m IRS (Abbas et al. 2013; Dwivedi et al. 2001; Dwivedi & Sreenivas 1998; Eldiery, Garcia & Reich 2005; Khan et al. 2001; Koshal 2010) and 250 m MODIS (Lobell et al. 2010). Given the relatively small field sizes (e.g. 2 ha) in South African irrigation schemes and the narrowness of affected areas (generally only a few metres in width) (Nell et al. 2015), medium to low resolution imagery will be of little value for monitoring salt accumulation in South African irrigation schemes.

The increasing availability of high resolution satellite imagery enables the assessment of the extent to which remote sensing can detect saline soils beyond the medium and low resolution image domains. Very high resolution (VHR) satellite imagery consequently provides a greater amount of spatial information, which enables the use of sophisticated data mining and image analysis techniques. Finding the optimal combination of high resolution imagery and image analysis techniques for indirectly identifying salt accumulation in South African irrigation schemes would greatly benefit a systematic salinity monitoring approach. A literature review of published remote sensing and salt accumulation research revealed that no research has yet been done on the use of VHR imagery for indirectly identifying small patches of affected areas (such as those occurring in South Africa) in irrigation schemes. Early detection of affected areas (i.e. while they are still small) will facilitate the implementation of mitigating measures and may prevent losses of fertile agricultural land.

From a research perspective, very little is known about the optimal combinations of VHR spectral bands for detecting salt-affected areas. It is also not clear which image analysis

techniques are best for indirectly identifying salt accumulation. The following research questions were consequently set:

1. What spatial and spectral resolutions would be suitable for the indirect detection of salt-affected areas in a typical South African irrigation scheme?
2. Would the identified spatial and spectral resolutions be viable and robust for implementation over large areas?
3. To what extent would the dynamic nature of crops and their varying salinity tolerance influence the indirect monitoring of salt accumulation?
4. What observation scale (field level or scheme level) would be the most efficient for indirectly detecting salt accumulation over large areas?
5. Which image transformations and classification techniques are most robust (transferable) for indirectly identifying salt accumulation across multiple irrigation schemes?

1.3 RESEARCH AIM AND OBJECTIVES

The primary aim of this research is to implement and assess indirect earth observation approaches for detecting salt accumulation in soils, with a particular focus on irrigation schemes. The secondary aim is to develop and evaluate an earth observation methodology in the context of finding operational solutions for monitoring salt accumulation in South African irrigation schemes.

To achieve the research aim, the objectives are to:

1. review the literature on detecting salt accumulation using earth observation;
2. collect and prepare in situ reference data and acquire suitable remotely sensed imagery;
3. assess the value of high (spectral and spatial) image resolution for indirectly identifying salt accumulation in a single cultivated field;
4. identify the image features and classification techniques most successful in discriminating between salt-affected and unaffected areas at irrigation scheme level;
5. develop and demonstrate a semi-automated, transferable earth observation methodology for monitoring salt accumulation in South African irrigation schemes; and
6. critically evaluate the developed methodology in the context of finding operational solutions for monitoring salt-affected areas in South African irrigation schemes.

1.4 RESEARCH METHODOLOGY AND THESIS STRUCTURE

The research approach was deductive and experimental in nature. The quantitative analyses included statistical techniques (regression analysis), machine learning (decision trees, k-nearest neighbour, random forest, and support vector machines) and expert systems (rule-based classification models). Two experiments were carried out using empirical datasets obtained from in situ field surveys and remotely sensed imagery.

The first experiment focused on a single field analysis and aimed to contribute towards research questions one, two, four and five. The main aim of the experiment was to determine the optimal spatial and spectral resolutions required for identifying salt accumulation in a typical irrigated field. The experiment used empirically measured in situ EC data and WoldView-2 (WV2) imagery. The data was quantitatively analysed using regression modelling and a decision tree algorithm.

The second experiment was carried out at irrigation scheme level and aimed to contribute towards research questions three, four and five. Two irrigation schemes were selected for examining the influence of variations in crop type and salt tolerance on detecting affected areas. This experiment also aimed to identify specific image transformation or classification techniques that are consistently effective at monitoring soil salinity at irrigation scheme level. Empirically measured in situ EC data and SPOT-5 satellite imagery were used as main data sources. The data was quantitatively analysed using regression modelling, decision tree analysis and image classification techniques. The findings of the two experiments were applied in an inductive spatial modelling approach in order to develop a robust (i.e. transferable) salinity monitoring technique.

Figure 1.3 outlines the research design and illustrates how it relates to the thesis structure. The real world problem and research questions, together with the research aims and objectives, were outlined in this chapter. Chapter 2 provides an overview of earth observation and remote sensing, followed by a review of how remote sensing techniques have been used to detect salt accumulation.

Chapters 3 and 4 present the two experiments that evaluated the indirect earth observation approach's capability to detect salt accumulation at a field and a scheme level respectively. Chapter 5 builds on the knowledge gained from the two experiments, and proposes a robust and transferable monitoring technique. Chapters 3 and 4 are structured as independent research articles and consequently include theoretical discussions as well as overviews of the study areas,

datasets and quantitative methods used. Repetition of certain concepts and methods was consequently unavoidable.

Chapter 6 provides a summary and a critical evaluation of the research. It reflects on the research questions, aims and objectives, and discusses the key findings in the context of establishing an operational solution for monitoring salt accumulation in irrigated areas. Recommendations for further research are also made.

The next chapter provides a brief overview on the concepts of earth observation and remote sensing. Applications of remote sensing for detecting salt accumulation, identified in published literature, are then discussed.

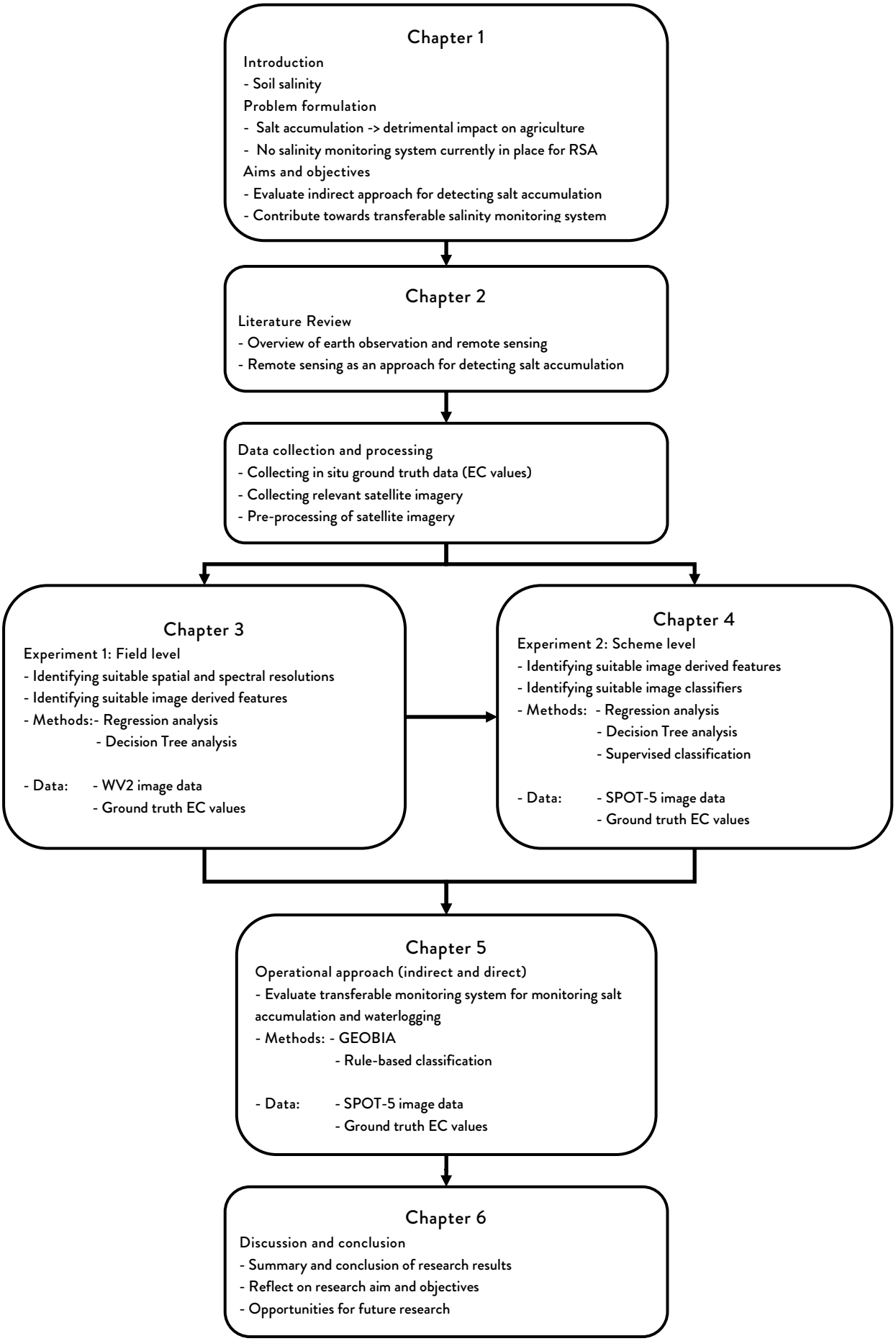

Figure 1.3 Research design and thesis structure

CHAPTER 2: EARTH OBSERVATION FOR SALINITY DETECTION

An understanding of salinity, its causes, effects and dynamic processes, together with remote sensing and its capabilities, was vital for achieving the aims and objectives of this study. The first section of this chapter consequently summarizes relevant earth observation concepts, while the rest of the chapter is dedicated to a review of remote sensing applications for detecting soil salinity.

2.1 EARTH OBSERVATION

Earth observation is a wide-ranging term used to describe remote sensing and geographical information systems (GIS) technologies and applications. Remote sensing is widely defined as attaining and recording information about a specific object without being in direct contact with it (Campbell 2007; Fischer, Hemphill & Kover 1976; Gibson 2000). For this study, it is more specifically defined as acquiring information about the earth's surface with satellite sensors by recording electromagnetic radiation through one or more regions of the electromagnetic spectrum reflected from the earth's surface (Campbell 2007). A GIS refers to a computerized system for capturing, storing, querying, analysing and displaying geospatial data (Chang 2010).

2.1.1 Electromagnetic spectrum

Electromagnetic (EM) energy, most commonly experienced as visible light, consists of two oscillating components, namely electric and magnetic fields (Tempfli et al. 2009). Electromagnetic energy is measured by its wavelength or frequency unit (Figure 2.1). This energy is generated by all matter with an absolute temperature above zero (Tempfli et al. 2009). The sun, however, is the prime source of this energy and produces a full spectrum of electromagnetic radiation, known as the electromagnetic spectrum. Of this full range, the visible spectrum only encompasses one ten-thousandth of one percentage of the total range (Gibson 2000). As the electromagnetic energy passes through the atmosphere to interact with objects on the earth's surface, its behaviour changes. The levels of reflection and absorption of each object on the earth's surface vary and each object uniquely interacts with the EM energy. By recording the changes in how surface objects behave under different EM energy spectra, scientists can attain knowledge of the different characteristics of objects (e.g. vegetation cover, water bodies, soils or urban structures) by using remotely sensed data (Campbell 2007). The most relevant regions of the electromagnetic spectrum for remote sensing applications are described by Chuvieco & Huete (2010) as the visible (VIS), near-infrared (NIR), shortwave infrared (SWIR) and thermal infrared (TIR) regions.

The VIS, with wavelengths ranging from 0.4 to 0.7 micrometres (µm), is named after the energy that human eyes are capable of sensing. It includes the blue, green and red areas of the spectrum (Figure 2.1). This part of the spectrum is also used to visualize the EM energy humans cannot directly see.

The NIR includes wavelengths of 0.7 to 1.2 µm, is invisible to humans and is well-known for its ability to record green vegetation. Healthy vegetation has a high reflectance in this region and reflectance decreases with increased plant stress (Tempfli et al. 2009).

The SWIR is delimited by 1.2 and 3 µm wavelengths and is known for its vegetation and soil moisture identification.

With wavelengths longer than the 3 µm, the TIR is associated with emissive electromagnetic radiation from the earth's surface. The earth's surface has a peak wavelength of 10 µm (Tempfli et al. 2009).

The shortest *microwave* wavelengths have properties similar to the thermal region and the longest wavelengths merge into radio wavelengths used for commercial broadcasts (Campbell 2007). The microwave wavelengths are commonly known for its capability to penetrate cloud cover.

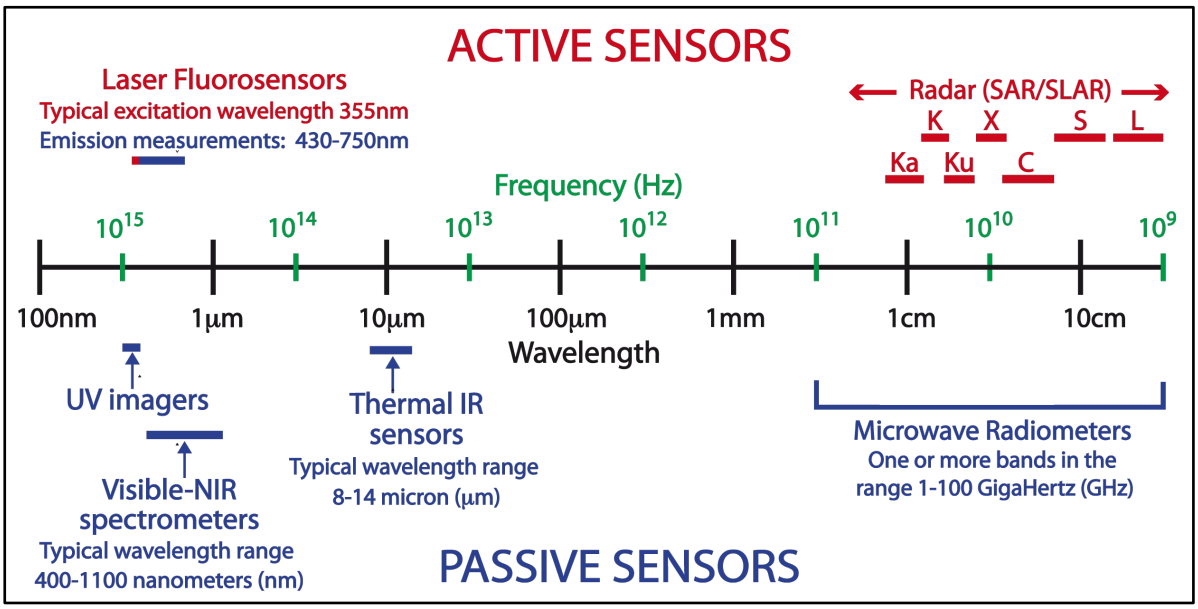

Source: SEOS (2016)

Figure 2.1 Electromagnetic spectrum and its relation to passive and active remote sensors.

2.1.2 Active (microwave) vs passive (optical) sensors

Remote sensors, the physical devices that detect EM energy, can be grouped into two main types, namely passive and active remote sensors. A passive remote sensor measures solar energy reflected from or radiation emitted by the earth's surface. To detect solar energy reflected from the earth's surface, instruments (known as optical sensors) must be capable of recording in the visible and preferably also in near-infrared spectrum. Some of the key variables in the process of capturing data with these sensors are atmospheric clarity, spectral properties of objects, angle and intensity of the sun, and choices of films and filters (Campbell 2007). To detect radiance emitted from the earth's surface, instruments (known as thermal sensors) must be capable of recording in the thermal infrared region. These sensors are also considered passive because they do not create electromagnetic energy themselves, but only record what is reflected or emitted from the earth.

An active remote sensor emits its own EM energy and then detects the energy returned from the target object or surface (Tempfli et al. 2009). Active remote sensors are independent of solar and terrestrial radiation and can thus operate during day or night. These sensors are represented by the NIR region, in the form of light detection and ranging (LiDAR) instruments, and the microwave region, in the form of radio detection and ranging (RADAR) instruments. The latter has wavelengths long enough to penetrate could cover.

2.1.3 Characteristics of optical imagery

Satellite sensors capture the reflected or emitted electromagnetic energy and convert it into a grid array of cells (pixels). Each pixel contains a raw digital number (DN), representing the amount of reflectance/emittance of a specific region in the electromagnetic spectrum (VIS, NIR or SWIR). This specific region is commonly known as a sensor band. The collective array of pixels forms a raster image, used for analysis. Each raster image is uniquely defined by certain characteristics relative to its satellite system, which ultimately determines its value for specific remote sensing problems. These characteristics are spatial, spectral, temporal and radiometric resolution.

Spatial resolution refers to the detail visible in an image, e.g. what is the smallest object detectable on the ground surface. For satellites, it is primarily determined by its instantaneous field of view (IFOV) (Figure 2.2) and measured by metres on the ground (Chuvieco & Huete 2010; Gibson 2000). The spatial resolution of satellite images can range from a few centimetres to kilometres, depending on the satellite system.

Spectral resolution determines how many sensor bands are provided. A larger spectral resolution means a greater coverage of the electromagnetic spectrum, which enables a better recording of surface objects' spectral characteristics. Multispectral raster images have spectral resolutions that range from three bands to more than 30, while hyperspectral images can contain in excess of 100 narrow spectral bands.

Temporal resolution is a measurement of how often a satellite system revisits a specific area. This resolution is determined by the satellite system's orbital characteristics and its swath overlap (Chuvieco & Huete 2010). Satellite systems with a high temporal resolution would be more valuable for monitoring change. Some satellite systems capture data of a specific region twice daily, while others capture data only a few times monthly.

Radiometric resolution refers to the sensitivity of a satellite's sensor and its ability to discriminate between variation in the recorded spectrum (Chuvieco & Huete 2010). A higher radiometric resolution generally refers to a higher number of grey levels within one band and is measured by the images' bit number (Gibson 2000).The resolutions described above are finely interconnected and an increase in one usually leads to a decrease in another (Chuvieco & Huete 2010). For instance, satellite sensors that capture images at a high spatial resolution generally have low temporal and spectral resolutions, and vice versa. This is due to a combination of factors, including the IFOV, the satellites scan speed, the optics of the satellite (e.g. aperture and lens) the sensor itself and download link speeds. Choosing which satellite data source is most appropriate for analysis thus greatly depends on the scope of the problem. Weather prediction, for example, needs constant hourly information (very high temporal resolution), but does not require a high spatial resolution. Geological exploration, on the other hand, needs a higher spatial resolution, where a low temporal resolution would be sufficient.

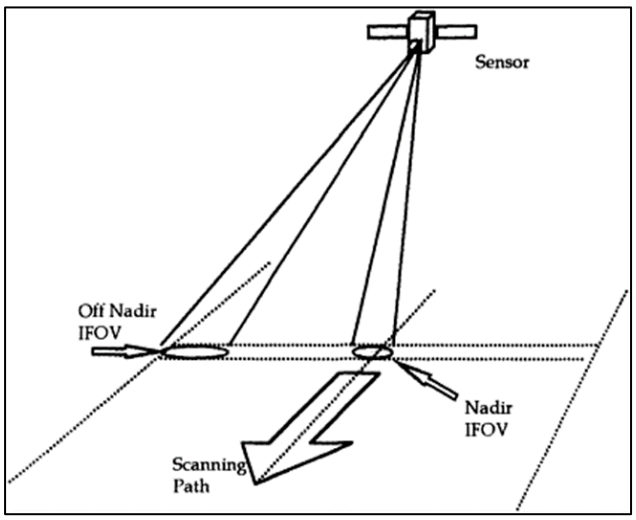

Source: Tso & Mather (2009)

Figure 2.2 Instantaneous field of view of a satellite sensor capturing data at nadir and of-nadir

2.1.4 Available optical imagery

Optical imagery is the most cost-effective way of gathering remotely sensed data, and offers the widest range of sources. Optical imagery can be acquired mainly from two platforms, namely aerial (including unmanned aerial vehicles) or space-borne (i.e. satellite-based).

Aerial imagery can be obtained by a camera system that points vertically or oblique down at the landscape from the aerial craft (Gibson 2000). Aerial imagery generally has a high spatial resolution that is dependent on the height of the aircraft or the obliqueness of the photo. The temporal resolution of aerial imagery is dependent on the image vendor and is generally very low. Most hyperspectral sensors, e.g. HyMap (126 spectral bands), Airborne Visible Infrared Imaging Spectrometer (AVIRIS) (224 spectral bands) and Compact Airborne Spectrographic Imager (CASI) (288 spectral bands), are also aircraft specific sensors.

There are approximately 1 381 operating satellites in orbit, of which roughly 344 satellites (including 152 optical imaging satellites) are used for earth observation (UCS 2016). From this list, there are a select few platforms that distribute optical imagery freely, commercially or for research purposes. Popular sources of optical imagery are listed in Table 2.1, together with relevant information regarding their spectral, spatial and temporal resolutions.

2.1.5 Image processing and interpretation

Specialized knowledge of and experience with image interpretation is required to extract useful information from remotely sensed data. Campbell (2007) suggests that there are three different levels of knowledge required for capable image interpretation. First, knowledge of the subject of interest is needed. The subject is the motivation for image interpretation and a sufficient knowledge is required to understand what the imagery is portraying. Second, the location of the study can be equally important given that each area has unique characteristics that influence patterns (tones and textures) on an image. Third, the type of remote sensing system is important, since each remote sensing system has a unique blend of resolution characteristics (spatial, spectral, temporal and radiometric resolutions). Therefore, knowing how these characteristics influence the ability to derive useful information about the subject of interest is essential.

Table 2.1 Popular sources of optical imagery (OI) and their characteristics

	Satellite(launch year)	Sensors	Spectral bands	Spatial resolution	Revisit Time	Availability
Low resolution OI	**MODIS** Terra (1999) Aqua (2002)	Moderate Resolution Imaging Spectroradiometer (MODIS)	36	Red, NIR (250 m) Blue, Green, IR (500 m) Thermal (1 km)	2 times, daily	Freely available
	AVHRR NOAA (1978 - 2009) multiple	Advanced Very High Resolution Radiometer (AVHRR)	6	VIS, NIR, Thermal, (1 km)	2 times, daily	Freely available
Medium resolution OI	**Landsat** Landsat-4 (1982)	Multispectral Scanner (MSS); Thematic Mapper	4	VIS, NIR, Thermal (68 m by 83 m)	18 days	Freely available
	Landsat-5 (1985)	Thematic Mapper (TM) MSS TM	7 4 7	VIR, NIR, Mid IR (30 m), Thermal (120 m) VIS, NIR, Thermal (68 m by 83 m) VIR, NIR, Mid IR (30 m), Thermal (120 m)	16 days 18 days 16 days	Freely available Freely available Freely available
	Landsat-7 (1999)	Enhanced Thematic Mapper Plus (ETM+)	8	Panchromatic (15m), VIR, NIR, Mid-IR, SWIR (30m) Thermal (60m)	14 days	Freely available
	Landsat- 8 (2013)	Operational Land Imager (OLI) Thermal Infrared Sensor (TIRS)	9 2	Panchromatic (15m), VIR, NIR, Mid-IR, SWIR (30m) Thermal (100m)	15 days 16 days	Freely available Freely available
	ASTER Terra (1999)	Advance Space-borne Thermal Emission and Reflection Radiometer (ASTER)	14	VIS, NIR (15 m), SWIR (30 m), Thermal (90 m)	16 days	Commercially, Research
	Hyperion EO-1 (2000)	Hyperion	220	VIS, NIR, SWIR (30 m)	16 days	Freely available
	CBERS China-Brazil Earth Resources satellite CBERS (1999) multiple	High Resolution CCD Camera (HRCCD)	5	Panchromatic, VIR, NIR (20m)	26 days	Freely available
		Infrared Multispectral Scanner	4	Panchromatic, SWIR (80 m), Thermal (160 m)	26 days	Freely available
	IRS IRS-1A (1988)	Linear Imaging Self Scanning Sensor (LISS)- I	4	VIR, NIR, (72.5 m)	22 days	Commercially, Research
		LISS-II	4	VIR, NIR (36.25 m)	22 days	Commercially, Research
	IRS-1B (1991)	LISS-I	4	VIR, NIR, (72.5 m)	22 days	Commercially, Research
		LISS-II	4	VIR, NIR (36.25 m)	22 days	Commercially, Research
	IRS-1C (1995)	LISS-III	4	Panchromatic (5.8 m), VIR, NIR (23 m)	24 days	Commercially, Research
High resolution OI	**IRS** Resourcesat - 1 (2003)	LISS-IV	4	Panchromatic, VIR, NIR (5.8 m)	5 days	Commercially, Research
	Resourcesat - 2 (2011)	LISS-IV	4	Panchromatic, VIR, NIR (5.8 m)	5 days	Commercially, Research
	Sentinel Sentinel -2 (A & B)(2015 & 2016)	Multispectral Instrument (MSI)	13	VIS, NIR (10 m), SWIR (20 m), other (60 m)	5 days	Freely available
	SPOT SPOT-1 (1986)	Visible High Resolution sensor (HRV)	4	Panchromatic (10m), VIS, NIR (20m)	26 days	Commercially, Research
	SPOT-2 (1990)	Visible High Resolution sensor (HRV)	4	Panchromatic (10m), VIS, NIR (20m)	27 days	Commercially, Research
	SPOT-3 (1993)	Visible High Resolution sensor (HRV)	4	Panchromatic (10m), VIS, NIR (20m)	28 days	Commercially, Research
	SPOT-4 (1998)	Visible and Infrared High-Resolution sensor (HRVIR)	5	Mono-spectral (10m), VIS, NIR, SWIR (20 m)	26 days	Commercially, Research
	SPOT-5 (2002)	High Resolution Geometric sensor (HRG)	5	Panchromatic (2.5 m), VIS, NIR (10m), SWIR (20m)	26 days	Commercially, Research
	SPOT 6 & 7 (2012 & 2014)	New AstroSat Optical Modular Instrument (NAOMI)		Panchromatic (1.5 m), VIS, NIR (6 m)	5 days	Commercially, Research
Very high resolution OI	**IKONOS** IKONOS (1999)	Optical Sensor Assembly (OSA)	5	Panchromatic (0.82 m), VIS, NIR (3.2 m)	Approx. 3 days	Commercially
	QuickBird QuickBird (2001)	Ball's Global Imaging System (BGIS 2000) sensor	5	Panchromatic (0.65 m), VIS,NIR (2.6 m)	3.5 days	Commercially
	RapidEye RapidEye (2008)	RapidEye Earth Imagin System (REIS)	5	VIS, NIR (5 m)	5.5 days	Commercially
	GeoEye-1 GeoEye-1 (2008)	GeoEye Imaging System (GIS)	5	Panchromatic (0.41 m), VIS, NIR (1.65 m)	8 to 10 days	Commercially
	WorldView WorldView-1 (2007)	WorldView-60 camera	1	Panchromatic (0.5 m)	2 to 6 days	Commercially
	WorldView-2 (2009)	WorldView -110 camera	9	Panchromatic (0.5 m), VIS, NIR (2 m)	1 to 3 days	Commercially
	WorldView-3 (2014)	WV-3 imager, CAVIS	17	Panchromatic (0.3 m), VIS, NIR (1.2 m), SWIR (3.7 m)	1 to 5 days	Commercially

2.1.5.1 Image pre-processing

Due to radiometric (measuring electromagnetic energy) and geometric (shape, size and relative position of objects) distortions, satellite imagery has to undergo a rigorous pre-processing phase prior to interpretation and analysis. The rectification and restoration of the acquired imagery are necessary for both spatial and spectral comparisons.

Geometric distortions can be caused by various factors such as oblique viewing distortions (objects in the foreground appear larger than objects farther away), relief displacement and displacement effects caused by the rotation of the earth and satellite sensors' scan speed (Chuvieco & Huete 2010; Tempfli et al. 2009). These geometric distortions occur either systematically (predictably) or randomly, and are dealt with accordingly. Predictable errors (e.g. the movement of the earth) are better understood and can be corrected by applying mathematically derived formulas. Remaining random distortions are corrected by comparing the distorted image to known, well-distributed ground control points (GCP's). Least squares regression, used to determine coefficients for two coordinate transformation equations, interrelates the geometrically correct coordinates and the distorted image coordinates (Lillesand, Kiefer & Chipman 2004). Resampling then occurs during which the image is essentially warped to accurately fit the ground coordinates. The preferred approach for image resampling for scientific analysis is the nearest neighbour approach, mainly because it is computationally simplistic and the original input pixel values are not compromised. Other resampling methods include bilinear interpolation and cubic convolution, which are more appropriate for continuous variables and display purposes. The quality of the geometric correction is largely attributed to the selected GCP's and is a process that generally requires human input (Chuvieco & Huete 2010; PCI Geomatics 2014).

Similar to geometric distortions, radiometric effects are highly variable and sensor-specific. Main causes of radiometric distortions are the deterioration of the sensor's general performance, discrepancies due to the earth-sun distance and distortions due to the atmospheric effects on EM reflectance (e.g. haze). The sensor effects are compensated for by sensor-specific calibration coefficient values, which are applied in a mathematical model for rectification. When images from different seasons are compared to one another, the seasonal earth-sun elevation differences need to be accounted for. This rectification process normalizes the pixel brightness values, assuming the sun was at the zenith on each date of image sensing (Lillesand, Kiefer & Chipman 2004). When EM energy is reflected or emitted from the earth and move through the atmosphere, it experiences degradation due to atmospheric scattering (which is wavelength dependant) (Tempfli et al. 2009). This effect reduces the contrast in the image. A principle used to correct

this degradation is based on measuring the radiance recorded over areas of essentially zero reflectance (e.g. water) and applying the offset correction to the distorted image (Lillesand, Kiefer & Chipman 2004). Atmospheric correction is particularly important when converting the DN's of the raw image file to units such as absolute radiance or percentage surface reflectance. This conversion is essential when image data needs to be compared to ground measurements, or when imagery of different sensors acquired at different times needs to be compared to one another.

Image fusion is a component of image pre-processing and refers to the process of combining images of two separate resolutions, for example the high spatial resolution of a panchromatic band with the coarser spatial but wider spectral resolution of the corresponding multispectral image (Campbell 2007). This technique assumes that the two images to be fused are compatible, since they were acquired at the same date and time. It is also vital that the two images to be fused share the exact same geometry and have similar spatial properties, emphasising the importance of the geometric correction step. Various image fusion algorithms exist to accommodate different kinds of image fusion needs. Less processing-intensive fusion algorithms, for example the intensity hue and saturation (IHS) spectral domain technique, can usually not be used for quantitative image analysis and is best suited for visualization purposes only. The fusion techniques that can be used for quantitative analysis purposes include the Pansharp, local mean matching (LMM) and local mean and variance matching (LMVM) algorithms (Nikolakopoulos 2008; Zhang 2002).

2.1.5.2 Image transformations

Image transformation is the process of generating a new image from one or more spectral bands with the use of arithmetic operators. The purpose of image transformation is to generate a new image with properties more suitable for a specific purpose compared to the original spectral bands from which it was derived. Various image transformations have been proposed through scientific research and each transformation serves a unique purpose.

Some of the well-known image transformations include band ratios and vegetation indices (VIs); principal component analysis (PCA); IHS transform; and image textures. Band ratios are quotients that enhance or reveal underlying information where there is an inverse relationship between bands (Campbell 2007). VIs are based on the principle of band rationing and use addition, subtraction, division and/or multiplication to yield a single value that represents the degree of vegetation vigour in a single pixel (Campbell 2007). A wide range of VIs exits, with the most popular being the normalized difference vegetation index (NDVI) (Table 2.2). Some

VIs are empirically derived from taking into account factors that are not addressed by the NDVI. The soil-adjusted vegetation index (SAVI) (Table 2.2), for example, includes a soil-adjustment factor that accounts for background reflectance/noise in less dense vegetation. The enhanced vegetation index (EVI) (Table 2.2) furthermore includes aerosol coefficient values to minimize the effect of atmospheric disturbances on the vegetation response.

Table 2.2 Commonly used VIs

Vegetation Index	Equation
Normalized difference vegetation index (NDVI)	$\mathbf{NDVI} = (NIR - Red)/(NIR + Red)$
Soil-adjusted vegetation index (SAVI)	$\boldsymbol{SAVI} = (1 + L)((NIR - Red)/(NIR + Red + L))$
Enhanced vegetation index (EVI)	$\boldsymbol{EVI} = G((NIR - Red)/(NIR + C_1 Red - C_2 Blue + L))$

* where L is the soil-adjustment factor, G is a gain factor and C1 and C2 are aerosol resistance coefficients

Principal component analysis (PCA) is a data reduction technique that reduces the feature dimensionality of the input dataset. This statistical technique essentially identifies optimum linear combinations of the original amount of input channels (bands), which accounts for most of the variation of pixel values within an image. The statistical procedure (Gould 1967) calculates the optimum set of coefficients that will concentrate the maximum amount of information in a few principal components (often stored as image bands) (Campbell 2007).

The IHS is a spectral domain transformation that alters multispectral data from the red, green and blue (RGB) domain to the IHS domain. Intensity relates to the total brightness of a colour, hue to the dominant/average wavelength or light contributing to a colour, and saturation to the pureness of a colour, relative to grey (Campbell 2007; Lillesand, Kiefer & Chipman 2004). The IHS transformation is useful when the intensity (brightness) of a colour needs to be separated from the colour itself. This transformation is also widely used in image fusion.

Image texture is loosely defined as the local brightness variation from pixel to pixel in a small neighbourhood (Russ 1999). The earth's surface and the angle of illumination are two vital contributors to image texture. The observation of image texture is determined by two factors, namely the scale of variation and the scale of observation (Mather & Magaly 2011). Perhaps the most well-known texture analysis involves extracting various texture measurements from a grey level co-occurrence matrix (GLCM) (Haralick, Shanmugam & Dinstein 1973). This approach uses second order statistics of the grayscale image histograms. Texture is valuable for image interpretation, because humans have the ability to perceive the subtle pattern differences contained in image texture measures.

2.1.5.3 Image classification

Image classification is a key part of image interpretation and is the process of assigning image pixels or objects to specified informational classes. Computer algorithms, called classifiers, are often used to perform image classification. Image classification varies in levels of complexity. For instance, a classification of land use may have more than ten classes, while a binary classification only differentiates between two classes.

There are two main approaches to image classification, namely unsupervised classification and supervised classification. Unsupervised classification is a technique that defines certain clusters or structures in multidimensional data space, which are then matched to informational categories (classification classes) (Campbell 2007). Well-known unsupervised classification (clustering algorithms) are generally based on distance measuring algorithms, e.g. the Euclidean or Mahalanobis distance (Mather & Magaly 2011). The ISODATA algorithm is one of the most popular clustering algorithms, known for its flexibility and robustness (Chuvieco & Huete 2010).

Supervised classification is the process of using pixels with known identity (training areas) to classify pixels with an unknown identity (Campbell 2007). This classification approach therefore requires prior knowledge of the study area. An advantage of supervised classification, compared to unsupervised classification, is that the analyst has more control over the informational categories. Results from different supervised classifications are also more comparable.

The minimum distance (MinD) classifier is one of most simple supervised classifiers and is based on the Euclidean distance algorithm. Its simplicity and low processing requirements can be beneficial for classifications with limited class overlap, as it does not account for class variance (Campbell 2007; Chuvieco & Huete 2010). The maximum likelihood (ML) classifier addresses the class variability limitation of MinD and is one of the most used classifiers of remotely sensed data. The algorithm deals with class overlap by using training data to compute the mean and variability of brightness for each class, thereby maximizing the probability of a correct classification (Campbell 2007; Foody, Warner & Nellis 2009). One of the main limitations of the ML and MinD classifiers is that they require a normal distribution of input datasets. The classifiers are also highly sensitive to the quality of training data, as outliers can substantially influence the distance and probability calculations (Campbell 2007; Chuvieco & Huete 2010).

The k-nearest neighbour (KNN) classifier is another algorithm based on distance measurements. The advantage of this simple yet efficient non-parametric classifier over ML and MinD is that it makes no prior assumptions about the data distribution. KNN examines each pixel value in the context of its neighbouring pixel values (in feature space). These neighbouring values were

either labelled during the classification process itself or prior knowledge (i.e. training data) was used to label them (Campbell 2007). The candidate pixel is then assigned to the class that is most represented by its k-defined neighbours. Inverse distance weighting calculations assign a higher significance to closer neighbours than distant neighbours (Campbell 2007).

A decision tree (DT) classifier generates a set of binary rules that are sequentially applied to specified features to differentiate between chosen target classes (Chuvieco & Huete 2010). DTs are non-parametric, robust, flexible and easy to interpret. DTs can, however, suffer from overfitting, which occurs when a model achieves a high accuracy on a training set, but fails to produce an accurate classification on different data. This points to the actual underlying relationships and exposes patterns arising purely by chance (Schaffer 1993). The support vector machine (SVM), a classifier more recently introduced to the field of remote sensing, is also non-parametric and less sensitive to training samples' size (Foody, Warner & Nellis 2009; Myburgh & Van Niekerk 2014). SVM finds the optimal hyperplane between classes by using training data. Mountrakis, Im & Ogole (2011) state that SVM is superior to most of the alternative algorithms because of its quick learning, self-adaptability and limited reliance on training size.

The random forests (RF) classifier, an ensemble of DT classifiers, makes use of bootstrapping and an unit voting system for each tree classifier (Breiman 2001; Gislason, Benediktsson & Sveinsson 2006). When comparing the SVM classifier to the RF classifier, Pal (2005) found that the RF produced comparable results and that its capability to handle categorical, unbalanced and even missing values is superior to that of SVM. A main advantage of the RF classifier is that it ranks feature importance during the classification process, which can be used for feature selection (Gislason, Benediktsson & Sveinsson 2006; Pal 2005).

The classifiers described above can also be used to classify hyperspectral data; however, some of the classifiers may have limitations when working with a high number of input variables (e.g. hyperspectral imagery), reducing their potential to identify certain features. Consequently, a number of classifiers have been designed specifically for hyperspectral data. For instance, spectral mixture analysis (SMA) evaluates hyperspectral data and extracts specific endmembers (spectral signatures) and its fractional abundance within each pixel (Foody, Warner & Nellis 2009). This is particularly useful for hyperspectral imagery with a coarse spatial resolution. Spectral angle mapper (SAM) uses the angular distance between a reference spectrum and a target. SAM measures similarity between spectra by calculating the spectral contrast instead of the absolute difference, making it insensitive to different illumination conditions (Chuvieco & Huete 2010). Spectral feature fitting (SFF) matches absorption features in the spectra by using a least squares technique with continuum removed data (Dehaan & Taylor 2002).

Image classifiers can be employed within the pixel or object spatial domain, as outlined in the following section.

2.1.5.4 Spatial domains: Object-based vs pixel-based image analysis

The pixel-based spatial domain refers to individual pixels, not taking into account the spatial or contextual information related to each pixel (Weih & Riggan 2010). The first decade of remote sensing research focused on the spectral analysis of image pixels (Addink, Van Coillie & De Jong 2012). This led to the development of many sophisticated and well-established pixel-based techniques that can successfully classify remotely sensed imagery. With the increase of spatial resolution, the within class spectral variability also increased (causing the so-called “salt and pepper effect”). This phenomenon has a detrimental effect on the accuracies of pixel-based classifiers (Blaschke et al. 2014) and has resulted in an increased research interest in object-based solutions around 2000. This new paradigm in remote sensing was further supported by increased computer processing power and the realization that pixels are no longer the optimal spatial unit for mapping landscape elements (Addink, Van Coillie & De Jong 2012; Blaschke 2010). The resulting new approach, called geographic object-based image analysis (GEOBIA), is a process that mimics higher order logic, similar to human interpretation (human eye-brain combination), to identify and group useful shapes, sizes and textures within image data (pixels) (Campbell 2007; Hay & Castilla 2008). GEOBIA starts with a segmentation process that divides a high resolution image into segments of spatially continuous and homogenous regions, called objects. Image segmentation algorithms are commonly based on one of the two basic properties of the pixel’s grey level values – discontinuity and similarity. The discontinuity (abrupt changes in pixel levels) principle is used to partition the image into several non-overlapping objects, while the similarity principle is used for methods like region growing and merging (Addink, Van Coillie & De Jong 2012; Haralick & Shapiro 1985). Objects hold key advantages over pixels, in particular, an increase in the number of available spectral variables (e.g. mean, median, maximum, minimum and variance) and spatial features (e.g. distances, neighbourhood, topologies and hierarchical properties) (Blaschke & Strobl 2001; Flanders, Hall-Beyer & Pereverzoff 2003; Hay & Castilla 2008). The use of spatial information in object-based methods also allows for the integration of vector and raster data, enabling a GIS-like functionality for classification (Blaschke et al. 2014).

2.2 SALINITY DETECTION USING REMOTE SENSING

Given that remote sensing has the ability to capture data at both a temporal and spatial scale, it has the potential for identifying the dynamic accumulation of salts. When attempting to detect salt accumulation with remote sensing there are two main approaches. One approach is to detect salt accumulation directly on bare ground, exploiting the spectral characteristics of salt-affected soils (e.g. its mineralogy and the presence of salt crusts). Another approach is to detect salt accumulation indirectly by studying secondary manifestations of salt accumulation (Bastiaanssen 1998; Mougenot, Pouget & Epema 1993). The following subsections explain these two approaches in more detail.

2.2.1 Direct detection of salt-affected soils

To identify salt accumulation directly, it is necessary to understand the spectral behaviour of salt crusts within the electromagnetic spectrum. The main factors affecting the reflectance of salts, as determined by ground observations and radiometric measurements, are the quantity and mineralogy of salts, soil moisture, colour and roughness (Metternicht & Zinck 2003). Previous studies showed that salt-affected soils have higher reflectance in the visible and near to mid-infrared (NIR/SWIR) regions of the spectrum compared to unaffected soils (Abood, Maclean & Falkowski 2011; Dwivedi & Sreenivas 1998; Elnaggar & Noller 2010; Iqbal 2011; Khan et al. 2005; Metternicht & Zinck 2003; Rao et al. 1995; Setia et al. 2013; Sidike, Zhao & Wen 2014).

The direct spectral behaviour of commonly-occurring salts (chlorides, sulphates, carbonates and bicarbonates) was studied by Metternicht & Zinck (2009). They found that the mineralogy of these salts determines the presence or absence of certain absorption and reflection features in the EM spectrum. Under laboratory conditions, Csillag, Pasztor & Biehl (1993) identified six spectral ranges where the salinity status of soil are best characterized. This included the visible region (550–770 nm), two in the near-infrared region (900–1030 nm and 1270–1520 nm) and three in the middle infrared region (1940–2150 nm, 2150–2310 nm and 2330–2400 nm). Rao et al. (1995) similarly found that including a middle infrared band (1550 nm–1720 nm) in a false colour composite (FCC) display improved the identification of salt-affected soils. Likewise, Howari (2003) identified five wavelengths in the electromagnetic spectrum, namely 1000, 1400, 1900, 2200 and 2300 nm, in which distinct absorption features and high variability among salt crusts can be detected.

Studying the dielectric properties of salt-affected soils and crusts in the microwave region of the spectrum is also considered a direct approach. Although relatively few studies investigating the use of air and space-borne microwave sensors for salinity detection exist, microwave data has the

advantage of actively gathering data independent of atmosphere conditions (Metternicht & Zinck 2003). According to Shao et al. (2003), both soil water content and salinity are positively correlated with the dielectric constant. Del Valle et al. (2009) stated that using radar imagery from more than one satellite system is highly desirable for salinity detection because each might have different identification capabilities. They observed that one of the major factors influencing the scattering properties of salt-affected areas is surface roughness. In general, the microwave C and L bands can be used for salinity detection (Archer & Wadge 2001; Sreenivas, Venkataratnam & Rao 1995; Taylor et al. 1996; Del Valle et al. 2009).

A number of limitations of the direct approach are highlighted in the comprehensive reviews of Metternicht & Zinck (2003, 2009). The spectral behaviour of salt crusts is highly variable, mostly owing to a difference in quantity, mineralogy, soil moisture, colour (white to dark) and roughness (smooth to rough). Surface roughness is also highly variable in agricultural areas, especially were ploughing frequently occurs. The spatial pattern of salt accumulation is also constantly changing, which means that it often occurs in small patches, leading to mixed pixels. These temporal changes are dependent on seasonal rainfall, which can alter the spectral properties of salt-affected areas. In addition, the occurrence of vegetation (e.g. halophytic plants and weeds) in salt-affected areas can cause spectral confusion. This is exacerbated by other features with similar reflectance properties to saline soils (e.g. loose sand, eroded surfaces and non-saline structural crusts). The fact that the direct approach is confined to monitoring surface conditions when using satellite sensors is another limitation. Salt accumulation in early stages do not necessarily form a crust and, therefore, is not visible on the earth's surface.

The direct approach has proven to be effective at identifying salt accumulation with unique spectral signatures, especially in the near to mid-infrared regions. However, in South African irrigation schemes, ploughing and tillage is a frequent occurrence and crops are grown throughout the year. To prevent erosion, fallow fields are usually covered by dry plant material remains of the previous harvest. Since the soils are only fully exposed for a short period (i.e. after ploughing and before vegetation growth occurs) and tillage causes a variation in surface roughness, the direct approach will be less effective in these areas. In contrast, the indirect approach can overcome some of the limitations of the direct approach because it is independent of the spectral characteristics of soils or salt crust and can account for sub-surface salt accumulation to a certain extent.

2.2.2 Monitoring vegetation by remote sensing

Monitoring vegetation condition with remote sensing requires an understanding of how vegetation reacts to electromagnetic radiation. To use the indirect approach for detecting salt accumulation, it is necessary to understand how it affects vegetation condition. The next section explains how remote sensing can be used to monitor vegetation conditions and how salt accumulation affects vegetation condition.

2.2.2.1 Methods for monitoring vegetation condition

The spectral characteristics of plant leaves are very prominent and enable the establishment of strong relationships with selected spectral bands of multispectral imagery. Chlorophyll is the green substance in plant leaves that enables the plant to absorb sunlight, making photosynthesis possible. However, chlorophyll does not absorb all sunlight equally, resulting in its distinct spectral characteristics (Campbell 2007). EM energy in the VIS spectrum is mostly absorbed by the plant chlorophyll. More of the red and blue band are absorbed compared to the green band, which has slightly higher reflectance at roughly 10 to 15% (Gibson 2000) (Figure 2.3). This gives the green appearance of healthy vegetation in the VIS spectrum. A sharp contrast in absorption/reflective properties occur in the wavelengths between the red and NIR region of the EM spectrum. Close to 50% of the NIR EM energy, which is not visible to the human eye, is reflected from healthy plant leaves (Figure 2.3). The reflectance of the NIR energy occurs as a result of the mesophyll layer, situated deeper in the leaf structure below the chlorophyll layer. The mesophyll tissue is where the leaf's oxygen and CO_2 exchange, necessary for photosynthesis and respiration, takes place (Campbell 2007). Many plant stresses alter (decrease) the reflectance in the NIR region and sensors operating in this spectral range can be used for plant stress detection (Lillesand, Kiefer & Chipman 2004).

The band ratios used in VIs are particularly efficient due to the inverse relationship between the absorption of the red light by the chlorophyll and the reflectance of the NIR radiation by the mesophyll. Owing to the efficiency of VIs, earth observation and remote sensing have played a vital role in the agriculture sector. Agricultural applications of remote sensing include biomass and yield estimation; vegetation vigour and drought stress monitoring; assessment of crop phenological development; crop acreage estimation and cropland mapping; and precision agriculture (Atzberger 2013).

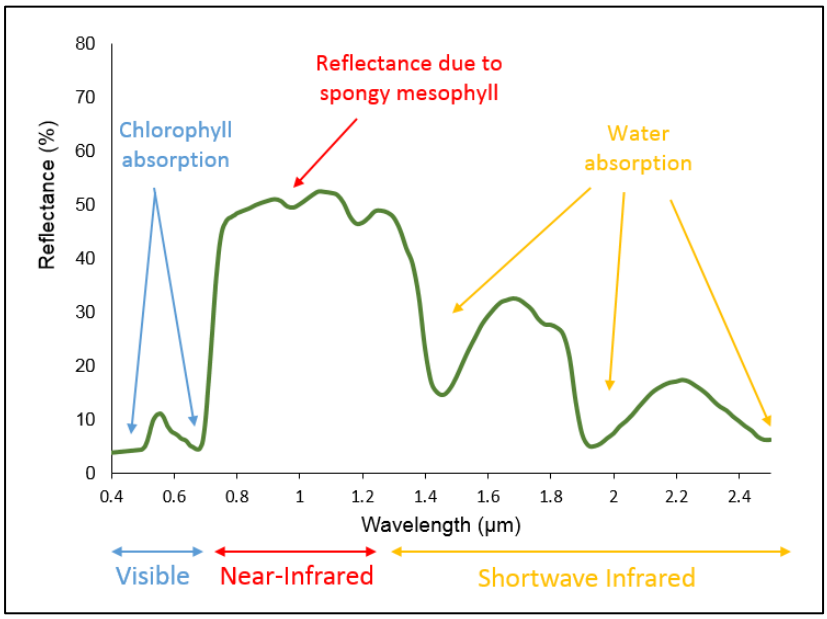

Source: HSU (2016)

Figure 2.3 Spectral reflectance of healthy vegetation

2.2.2.2 Effect of salt accumulation on vegetation

Excessive accumulation of salts in the root zone leads to a decreased ability of the plant to take up water. This “osmotic effect” causes the plant to use more metabolic energy in an attempt to take up more water, which leads to dehydration and wilting (McGhie & Ryan 2005). An excess of salt in the root zone may also lead to the absorption of dangerously high quantities of salts which, over time, becomes toxic. The toxicity leads to internal structural damage such as leaf injury symptoms and wilting (Hillel 2000; McGhie & Ryan 2005). Physiological plant stress and a deteriorating vegetation condition are thus closely linked to the accumulation of salts in the root zone. In some cases, the accumulation of salts leads to the invasion of salt tolerant weeds (halophytic vegetation). By adapting to saline conditions over time, halophytic vegetation has developed distinctive leaf and stem structures, making it an indirect indicator of salt accumulation (Dehaan & Taylor 2002). The next section summarizes research on indirect salinity detection using remote sensing methods.

2.2.3 Indirect remote sensing methods for monitoring salt accumulation

Indirect approaches that emerged in the literature review are discussed in the next section. A summary of satellite imagery and image classification techniques used for the indirect detection of salt accumulation is then given, followed by a general evaluation of the literature.

2.2.3.1 Detecting salt induced vegetation stress

The most common indirect remote sensing approach involves identifying physiological vegetation stress that relates to salt accumulation. Although this approach is applied in various ways, the methodology is mostly centred around the use of VIs for vegetation stress detection. A wide range of VIs for detecting salt accumulation has been evaluated and includes NDVI (Abood, Maclean & Falkowski 2011; Aldakheel 2011; Bouaziz, Gloaguen & Samir 2011; Fernández-Buces et al. 2009; Fernández-Buces et al. 2006; Golovina et al. 1992; Hamzeh et al. 2012a; Hamzeh et al. 2012b; Iqbal 2011; Khan et al. 2001; Lenney et al. 1996; Leone et al. 2007; Lobell et al. 2010; Naumann, Young & Anderson 2009; Peñuelas et al. 1997; Sidike, Zhao & Wen 2014; Stals 2007; Turhan et al. 2008; Wiegand et al. 1994; Wu et al. 2008), SAVI (Abood, Maclean & Falkowski 2011; Alhammadi & Glenn 2008; Allbed, Kumar & Aldakheel 2014; Bouaziz, Gloaguen & Samir 2011; Hamzeh et al. 2012a; Zhang et al. 2011), EVI (Bouaziz, Gloaguen & Samir 2011; Lobell et al. 2010), the combined spectral response index (COSRI) (Fernández-Buces et al. 2006), the moisture stress index (Iqbal 2011), the narrow band indices, the water index (WI) (Leone et al. 2007; Naumann, Young & Anderson 2009), the physiological reflectance index (PRI) (Hamzeh et al. 2012a; Naumann, Young & Anderson 2009) and the chlorophyll index (Naumann, Young & Anderson 2009). Modifications of VIs included that of Abood, Maclean & Falkowski (2011), who substituted the yellow band with the red band in the NDVI and SAVI; Zhang et al. (2011), who created a number of narrow band modifications of the SAVI; and Hamzeh et al. (2012a), who similarly created narrow band indices based on the SAVI and water indices. In each case, the modified indices slightly improved the accuracy for the identification of salts. Al-Khaier (2003) incorporated a biophysical approach (surface balance algorithm for land (SEBAL) (Bastiaanssen et al. 1998)) to successfully identify salt induced vegetation stress, but concluded that this approach is too reliant on highly detailed information (e.g. land surface and climate parameters) often not available. Zhang et al. (2011) suggested that the narrow wavelengths of 395–410; 483–507; 632–697; 731–762; 812–868; 884–909 and 918–930 nm are most sensitive to salt-affected vegetation response.

According to the literature, the success rate of the identification of vegetation stress due to salt accumulation both on a field level (Eldiery, Garcia & Reich 2005; Hamzeh et al. 2012a; Platonov, Noble & Kuziev 2013) and for larger areas (Abbas et al. 2013; Abood, Maclean & Falkowski 2011; Lobell et al. 2010) is high. Trends that surfaced within this approach are set out below.

- When using vegetation response for detecting salt accumulation, the time of peak vegetation growth is preferred (Allbed, Kumar & Aldakheel 2014; Hick & Russell 1990;

Johnstone & Barson 1990; Lobell et al. 2010). Sparse vegetation introduces soil background noise that reduces VIs' effective detection of vegetation stress (Aldakheel 2011; Alhammadi & Glenn 2008; Douaoui, Nicolas & Walter 2006).

- Confusion between salt induced vegetation stress and vegetation stress caused by other factors is more likely to occur when single date imagery is used (Mashimbye 2005; Stals 2007). Other factors that lead to poor vegetation response include rainfall variation, poor farming practices and other soil conditions (e.g. compaction). When a scene is observed at multiple dates, certain characteristics of salt accumulation become more apparent (Lenney et al. 1996). It is assumed that if a specific area experiences poor vegetation growth throughout multiple seasons, it is more likely to be salt-affected (Furby et al. 1995). Lobell et al. (2010) and Platonov, Noble & Kuziev (2013) used a multi-temporal, indirect approach to detect accumulated salts to good effect.
- Different crop types and growing phases have varying salt tolerances (Hanson, Grattan & Fulton 2006; Zhang et al. 2011). This phenomenon often leads to spectral confusion when using vegetation response as an indirect indictor for salt accumulation (Aldakheel 2011; Zhang et al. 2011). Zhang et al. (2011) stressed that a single vegetation index might not be sufficient to monitor the salt accumulation of a variety of crop species.

2.2.3.2 Methods unrelated to vegetation stress

Another indirect remote sensing approach is based on the concept that certain distinctive vegetation types (halophytes) often occur in salt-affected areas. Contrary to the first approach, this approach tries to identify healthy vegetation that can be linked to the occurrence of salt accumulation. Since this approach requires vegetation type identification, it is largely confined to hyperspectral studies, which includes matching spectral reflectance through narrow spectral bands to certain vegetation types (Dehaan & Taylor 2002; Dehaan & Taylor 2003; Dutkiewicz, Lewis & Ostendorf 2009a).

Other indirect indicators unrelated to vegetation response include ground water modelling and elevation derivatives such as water accumulation models, slope gradient, slope aspect, hilltops, upper slopes, lower slopes and valleys (Caccetta, Allen & Watson 2000; Elnaggar & Noller 2010; Fraser 2009; Furby, Caccetta & Wallace 2010; Stals 2007). These indirect indicators mainly serve as supplementary information for the direct or indirect approach in detecting salt accumulation.

2.2.3.3 Satellite imagery and image classification techniques

The majority of the literature related to the indirect approach focuses on medium resolution satellite imagery, for example 30 m Landsat (Abdelfattah, Shahid & Othman 2009; Aldakheel 2011; Al-Khaier 2003; Caccetta, Allen & Watson 2000; Dehni & Lounis 2012; Elnaggar & Noller 2010; Fernández-Buces et al. 2006; Furby, Caccetta & Wallace 2010; Gao & Liu 2008; García Rodríguez, Pérez González & Guerra Zaballos 2007; Howari 2003; Lenney et al. 1996; Mohamed, Morgun & Goma Bothina 2011); 23 m IRS (Abbas et al. 2013; Dwivedi et al. 2001; Dwivedi & Sreenivas 1998; Eldiery, Garcia & Reich 2005; Khan et al. 2001; Koshal 2010) and 250 m MODIS (Lobell et al. 2010), with some notable exceptions of IKONOS (Allbed, Kumar & Aldakheel 2014; Eldiery, Garcia & Reich 2005), QuickBird (Sidike, Zhao & Wen 2014) and WV2 (Abood, Maclean & Falkowski 2011). The reason for the relatively few studies involving very high resolution imagery is that most case studies focus on areas where salt accumulation occurs on a grand scale, such as Australia (Caccetta, Allen & Watson 2000; Dehaan & Taylor 2002; Dehaan & Taylor 2003; Dutkiewicz, Lewis & Ostendorf 2009b; Fraser 2009), USA (Elnaggar & Noller 2010; Howari 2003; Lobell et al. 2010; Naumann, Young & Anderson 2009), Northern Africa (Douaoui, Nicolas & Walter 2006; Lenney et al. 1996), Arabian regions (Alhammadi & Glenn 2008; Al-Khaier 2003; Koshal 2010; Tajgardan, Shataee & Ayoubi 2007) and Pakistan and India (Abbas et al. 2013; Khan et al. 2001; Koshal 2010).

Image classification and statistical analysis techniques are commonly used to evaluate the ability of vegetation response to detect salt accumulation. Examples of unsupervised classification (Khan et al. 2001; Lenney et al. 1996; Mashimbye 2005; Wiegand et al. 1994; Wu et al. 2008) and supervised classification (Howari 2003; Iqbal 2011) exist. Specific supervised classification techniques include MinD (Douaoui, Nicolas & Walter 2006; Hamzeh et al. 2012b), ML (Abbas et al. 2013; Hamzeh et al. 2012b; Wu et al. 2008), SVM (Hamzeh et al. 2012b), RF (Abood, Maclean & Falkowski 2011), SAM (Hamzeh et al. 2012b), while Stals (2007) employed a rule-based classification approach. Statistical techniques include correlation analysis (Allbed, Kumar & Aldakheel 2014; Peñuelas et al. 1997; Tajgardan, Shataee & Ayoubi 2007; Turhan et al. 2008), regression analysis (Douaoui, Nicolas & Walter 2006; Hamzeh et al. 2012a; Leone et al. 2007; Lobell et al. 2010; Tajgardan, Shataee & Ayoubi 2007; Wiegand et al. 1994), ordinary least square regression (Eldiery, Garcia & Reich 2005), partial least square regression (Sidike, Zhao & Wen 2014; Zhang et al. 2011), analysis of variance (ANOVA) (Naumann, Young & Anderson 2009) and kriging (Aldakheel 2011; Douaoui, Nicolas & Walter 2006). Hyperspectral specific classification techniques such as SAM, SFF, matched filtering and mixture tuned

matched filtering were successfully used to identify halophytic vegetation (Dehaan & Taylor 2002; Dehaan & Taylor 2003; Dutkiewicz, Lewis & Ostendorf 2009b).

2.2.3.4 Literature evaluation

According to the literature, the indirect approach has great potential for detecting salt accumulation and seems to be more effective than the direct approach. In the context of this study, methods identified in the literature still present some challenges. With the perspective of developing a large scale transferable salinity monitoring system, hyperspectral imagery will not provide a cost-effective solution. Without hyperspectral imagery, the identified narrow band VIs would not be useful, as upscaling them to multispectral bands would negate its advantage. The identification of halophytic vegetation also relies heavily on hyperspectral imagery and therefore would not be useful in the context of this study.

Since the mean field size of South African irrigation schemes are relatively small compared to study areas mentioned in literature and the occurrence of soil salinity is mainly confined to small localized patches across these fields, medium to low resolution satellite imagery would not be effective for identifying these areas. The wide range of identified image classification techniques also present a challenge, as it suggests that each technique might only be applicable to its respective study area and may not be transferable.

Apart from these challenges, multispectral-based VIs show great potential for indirectly identifying salt accumulation by monitoring vegetation stress. However, little is known about the optimal combinations of image transformations and classification techniques for detecting salt accumulation using VHR imagery. Identifying these combinations is vital in the context of finding a transferable approach for monitoring salt accumulation on over large areas. This study therefore sets out to identify suitable spatial and spectral resolutions for detecting salt accumulation in a South African irrigation scheme; test whether there are particular image transformations or classification techniques that can consistently identify salt accumulation; assess the effect of different crop types and their salinity tolerances; and determine at what spatial level salt accumulation is best detected in South Africa. The next chapter presents the first of two experiments and aims to identify the optimal spectral and spatial factors for indirectly detecting salt accumulation in cultivated fields.

CHAPTER 3: IDENTIFICATION OF WORLDVIEW-2 SPECTRAL AND SPATIAL FACTORS IN DETECTING SALT ACCUMULATION IN CULTIVATED FIELDS[1]

3.1 ABSTRACT

Soil salinity is a global threat to agricultural production and necessitates the monitoring thereof. Saline conditions in South African irrigation schemes generally occur in small patches (some only a few metres in diameter) and this study, which forms part of a Water Research Commission (WRC) project, evaluates the use of very high resolution (VHR) satellite imagery, in particular those produced by the WoldView-2 (WV2) sensor, for the detection of salt accumulation in irrigated areas. A range of features derived from the WV2 image was evaluated, namely eight WV2 bands, ten vegetation indices (VIs), 25 texture measures and two principal component analysis (PCA) components. These features were generated at six spatial resolutions (0.5 m, 2 m, 6 m, 10 m, 15 m and 20 m) to investigate the value of high spatial resolution for detecting affected areas. The relationships between the image features and electric conductivity measurements of 30 soil samples were studied by means of regression analysis and classification and regression tree (CART) modelling. The regression analysis results showed that a spatial resolution of 6 m or higher is ideal when VIs are used as input. When texture measures are used, higher spatial resolution (0.5 m) produced better models. The regression results also showed that the relatively high spectral resolution of the WV2 sensor (compared to other VHR sensors) did not provide a significant improvement in accuracy. The CART results provided a categorical quantification of salt accumulation and showed that VIs generated at 0.5 m resolution were the best features to use. Because the use of WV2 images is not financially viable for operational use in very large irrigation schemes, the study concludes with some guidelines on the spectral and spatial requirements of images for monitoring salt accumulation in irrigation schemes with similar conditions.

3.2 INTRODUCTION

Soil salinity refers to the accumulation of soluble salts in soils (Al-Khaier 2003). Salt accumulation in soils is a naturally occurring process, but can be induced by human interference, known as secondary salinity. Factors such as vegetation clearing, landscape reshaping through earthworks, and irrigation can lead to an increase of water and salt in soils and change where they accumulate (McGhie & Ryan 2005). About 77 million ha of the estimated one billion ha

[1] This chapter was published in Geoderma Journal and consequently conforms to the prescribed structure of that journal

associated with salt accumulation is caused by secondary salinity, of which irrigation has the largest impact (Ghassemi, Jakeman & Nix 1995; Metternicht & Zinck 2003).

A plant's ability to take up water is reduced when an excess of salt is present in the root zone. The salts reduce the osmotic potential of water and hinder its movement from the soil into the roots and is known as the osmotic effect. When saline conditions persist, a toxic effect can occur, caused by the continuous accumulation of salts in the plant through the process of water absorption (Hillel 2000; McGhie & Ryan 2005). The osmotic and toxic effects lead to visible indicators such as spotty/uneven growth of vegetation, plant wilting, a blue-green tinge and moisture stress. Depending on the quantity and mineralogy of salt accumulation, it can also result in the formation of white salt crusts, puffy soil, dark greasy surfaces, dehydrated cracks and coarser topsoil (Ghassemi, Jakeman & Nix 1995; McGhie & Ryan 2005; Metternicht & Zinck 2003).

Soil salinity can be detected using remotely sensed data either directly, by attempting to identify indicators of salt accumulation on the bare soil, or indirectly, by monitoring vegetation responses to saline conditions (Bastiaanssen 1998; Mougenot, Pouget & Epema 1993). Challenges in identifying salt accumulation through direct indicators include spectral ambiguity caused by variance in salt mineralogy, quantity, soil moisture, colour and surface roughness, which is exacerbated by farming practices such as tillage and irrigation(Metternicht & Zinck 2003; Zhang et al. 2011). Different vegetation types also respond differently to salt accumulation due to their varying tolerances to saline conditions (Zhang et al. 2011). This is particularly problematic in highly dynamic irrigation schemes where multiple crops can be planted per season. Temporal variability within irrigation schemes is less of a problem when an indirect approach is used. Several authors have successfully applied the indirect approach to monitor plant stress caused by salt accumulation (Abood, Maclean & Falkowski 2011; Fernández-Buces et al. 2006; Lenney et al. 1996; Lobell et al. 2010; Peñuelas et al. 1997; Wiegand et al. 1994; Zhang et al. 2011). All of these studies relied on vegetation indices (VIs) (e.g. NDVI, EVI, and SAVI). However, poor farming practices and soil preparation can also lead to poor VI responses, which can easily be mistaken for saline conditions (Furby, Caccetta & Wallace 2010). Further limitations of the use of VIs for detecting areas affected by salt accumulation includes the negative impact of bare ground backscatter/noise, especially during the early stages of growth (Dehni & Lounis 2012; Douaoui, Nicolas & Walter 2006) and the varying salinity tolerances of vegetation types (Zhang et al. 2011). Other indirect indicators of salt accumulation can include soil properties, terrain characteristics, and surface texture features (Caccetta, Allen & Watson 2000; Furby, Caccetta & Wallace 2010; García Rodríguez, Pérez González & Guerra Zaballos 2007; Howari 2003; Jenkin

1981; Metternicht & Zinck 2003). Data related to these indirect indicators can be sourced from previous soil surveys, digital elevation models (DEMs) and image texture information respectively.

An estimated 10% to 18% of irrigated areas in South Africa are affected by waterlogging, sodicity or salinity (Backeberg et al. 1996). Ghassemi, Jakeman & Nix (1995) observed that, in general, the extent of salt accumulation and waterlogging in South Africa is less than in many other countries and seem to be largely under control. This is perceived to be due to sound planning in the selection of irrigated soils, good drainage and the fact that the irrigated areas of South African are generally small (Ghassemi, Jakeman & Nix 1995). Consequently, salt accumulation often occurs in small patches of a few metres in diameter.

Although the extent of salt accumulation in South Africa is relatively small compared to many other countries (e.g. Egypt, Iran, and Argentina) (Ghassemi, Jakeman & Nix 1995), proactive monitoring is needed to keep track of the negative effects of salt accumulation and to determine if it is adequately managed.

From the literature, it is apparent that the majority of remote sensing applications for salt accumulation monitoring are focused on areas where salinity occurs on a grand scale in relatively large cultivated fields. As a result, medium to low resolution satellite imagery is often favoured with Landsat (30 m) (Abdelfattah, Shahid & Othman 2009; Aldakheel 2011; Al-Khaier 2003; Caccetta, Allen & Watson 2000; Dehni & Lounis 2012; Elnaggar & Noller 2010; Fernández-Buces et al. 2006; Furby, Caccetta & Wallace 2010; Gao & Liu 2008; García Rodríguez, Pérez González & Guerra Zaballos 2007; Howari 2003; Lenney et al. 1996; Mohamed, Morgun & Goma Bothina 2011) and IRS (20 m) (Abbas et al. 2013; Dwivedi et al. 2001; Dwivedi & Sreenivas 1998; Eldiery, Garcia & Reich 2005; Khan et al. 2001; Koshal 2010) being the most popular. Given that the mean field sizes are relatively small (e.g. 2 ha) in some of South Africa's irrigation schemes, medium to low resolution imagery will have little value, particularly when fields are elongated. Salt-affected areas in South Africa are also generally much smaller than what can be detected with medium resolution imagery (Nell & Van Niekerk 2014).

Very few applications of VHR imagery for salt accumulation monitoring exist. Notable exceptions are Abood, Maclean & Falkowski (2011) and Douaoui & Yahiaoui (2015) who used 2 m resolution WoldView-2 (WV2) imagery; and Eldiery, Garcia & Reich (2005) who used 4 m resolution IKONOS imagery. However, none of these studies investigated the value of spatial features (such as texture measures) for the identification of salt-affected areas. Also, VHR imagery has, to our knowledge, never been used for monitoring salt accumulation in South Africa. The primary aim of this study, which forms part of a WRC project, is therefore to

evaluate the use of VHR satellite imagery, specifically WV2, to identify suitable spectral and spatial features for the identification of salt accumulation in a cultivated field. A secondary aim is to improve the understanding of the importance of spatial resolution for detecting salt-affected areas with small spatial extents. Several fields in this study area have been abandoned due to uncontrolled salt accumulation. Proactively identifying salt-affected areas while they are still relatively small in size will improve rehabilitation strategies. In South Africa, soils with electroconductivity (EC) values of 4.0 dS/m (deci-siemens per metre) are considered as being salt-affected (Bresler, McNeal & Carter 1982; SASA 2007). This corresponds to the USDA classification of slightly, moderately and strongly saline (USADA 2015).

These objectives will be evaluated by analysing the WV2 derived features at six different spatial resolutions. Regression modelling and CART analysis will be used. The results are interpreted in the context of finding the best image features and optimal spatial resolution for predicting/identifying salt-affected areas in a South African irrigation system.

3.3 METHODS

3.3.1 Study area

A 2.8 ha irrigated lucerne (alfalfa) field in the Vaalharts irrigation scheme was chosen as the study site (Figure 3.1). The Vaalharts irrigation scheme is situated near the towns of Jan Kempdorp and Hartswater at the juncture of the Northern Cape, North West and the Freestate provinces. The scheme is drained by the low gradient, non-incising Harts River and consequently, has very limited topographical variance (Gombar & Erasmus 1976; Liebenberg 1977). The irrigation scheme has a semi-arid climate with cold, dry winters (June to August) and long warm summers (December to February) with a mean annual temperature of 19°C (Schulze 2006). It receives a mean annual rainfall of 400 mm (mostly during late summer) which necessitates irrigation (Schulze 2006). The irrigation methods applied in the scheme comprises roughly 70% flood irrigation and 30% pivot irrigation (Maisela 2007). The principal cash crops of the scheme are maize, wheat, barley, lucerne and groundnuts (Kruger, Van Rensburg & Van den Berg 2009).

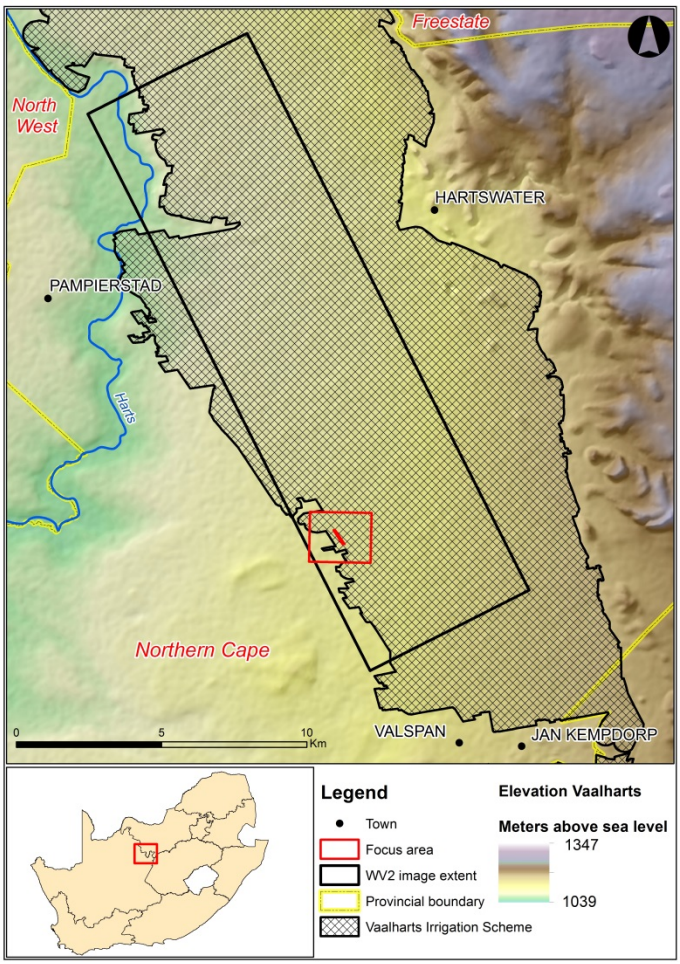

Figure 3.1 Study site location within the Vaalharts irrigation scheme

The selected lucerne field is supplied with flood irrigation to supplement the rainfall. Lucerne was targeted for this study because it is moderately sensitive to saline conditions and starts wilting at EC levels of 2.0 dS/m and above (at root zone level) (Hanson, Grattan & Fulton 2006). For this study, a single crop was selected so as to eliminate the complexities associated with multiple crop types that have varied spectral properties and tolerances to salt accumulation (Hanson, Grattan & Fulton 2006; Zhang et al. 2011).

3.3.2 Data acquisition and preparation

The timing of image acquisition is important for discriminating between saline and non-saline conditions. When using features like VIs, image data from the time of maximum growth (i.e. the end of a wet season) should ideally be used (Furby, Caccetta & Wallace 2010; Hick & Russell 1990). Since crop production and irrigation occurs almost continuously throughout the year in Vaalharts, the timing of image acquisition was less critical. A WV2 image covering a 100 km^2 section (Figure 3.1) of the Vaalharts irrigation scheme captured on 23 May 2012 was acquired. At the time of capture, the WV2 sensor offered higher spectral and spatial resolution compared

to other VHR sensors, with eight 2 m resolution relatively narrow bands in the visible and near-infrared spectral range (Table 3.1).

Table 3.1 WV2 bands and spatial resolution

Band number	Band description (WV2)	Wavelength (nm) (WV2)	Resolution(WV2)
1	Coastal blue (CB)	400-450	2 m
2	Blue	450-510	2 m
3	Green	510-580	2 m
4	Yellow	585-625	2 m
5	Red	630-690	2 m
6	Red Edge (RE)	705-745	2 m
7	Near-Infrared1 (NIR1)	770-895	2 m
8	Near Infrared2 (NIR2)	860-1040	2 m
9\Pan	Panchromatic	450-800	0.5 m

Geometric corrections were carried out on the image using PCI Geomatica (version 2013 Service Pack 2). A north-oriented implementation of the Gauss conform coordinate system (also known as the LO coordinate system) was used with central meridian set to 25 °E. Nearest neighbour (NN) resampling was selected during orthorectification to preserve the original digital numbers (DN) (Campbell 2007; Lillesand, Kiefer & Chipman 2004). Radiometric corrections were carried out using the ATCOR-2 model which converted the DNs into percentage reflectance.

The fusion of multispectral and panchromatic images is an effective technique for optimizing the spatial and spectral resolution of images (González-Audícana et al. 2004). The *Pansharp* algorithm as implemented in PCI Geomatica software was used to increase the 2 m spatial resolution of the multispectral data to 0.5 m. The *Pansharp* algorithm has been shown to preserve most of the spectral characteristics of the multispectral data in the resulting pansharpened image (Nikolakopoulos 2008; Zhang 2002).

To evaluate the effect of spatial resolution on the identification of salt-affected areas, the original 2 m multispectral bands were down-sampled to even 6, 10, 14, 16 and 20 m resolution using the mean aggregate function in ArcMap 10.1. The original 2 m multispectral image was used as a snap raster in the down-sampling process so as to eliminate any chance of misalignment and blurring. The 0.5-20 m resolution range was chosen as it covers the resolutions of common sensors indicated in Table 3.2 (RapidEye, LISS IV, SPOT-6/7, CBERS-4, SENTINEL-2, and ASTER).

Table 3.2 Relevant spectral and spatial resolutions of common satellite sensors

Satellite	Bands (resolution)
RapidEye	Blue(5 m), Green(5 m), Red(5 m), Red Edge(5 m), NIR (5 m)
LISS IV (IRS)	Green (6 m); Red (6 m); NIR (6 m)
SPOT 6, 7	Blue (6 m), Green (6 m), Red(6m, NIR (6 m)
CBERS 4	Green (10 m), Red(10 m), NIR (10 m)
SENTINEL-2	Blue(10 m), Green(10 m), Red(10 m), NIR(10 m)
ASTER	Green(15 m), Red(15 m, NIR(15 m)

A field survey was carried out to collect suitable training and reference data. Salinity occurrences are highly dynamic and can change within months. To get a true representation of the relationship between remotely sensed features and salt accumulation, it was vital that the captured image date corresponded closely with the field surveyed date. The survey was consequently conducted from 5 to 8 June 2012, less than two weeks after the image was acquired. A grid-based sampling approach was used to effectively capture the transition between salt-affected and unaffected areas (Figure 3.2). A total of 30 samples were collected by means of a soil auger at a depth of 15 cm (i.e. topsoil). The soils were characterized as being orthic and were classified as being from the Kimberly soil group (Macvicar et al. 1977). Differential GPS coordinates (10 cm accuracy), notes on the visual appearance and photographs of vegetation condition relative to the rest of the field were also recorded. Severe physiological stress was noted in salt-affected areas, while unaffected areas were generally characterized by normal vegetation growth. The EC of the soil samples were determined in a laboratory using the saturated paste technique. Soil samples with EC values of 4.0 dS/m or higher were regarded as being salt-affected, while all samples with EC values below 4.0 dS/m were regarded as being unaffected (Nell & Van Niekerk 2014; SASA 2007).

Figure 3.2 Surveyed points of the grid-based sampling approach. The adjacent field consists similarly of lucerne and orthic Kimberly soil

3.3.3 Image features

Vegetation indices (VIs)

VIs are the most popular and scientifically-proven remote sensing features for monitoring biomass and vegetation vigour (Campbell 2007). VIs that have been successfully used for mapping salt-affected areas include the normalized difference vegetation index (NDVI) (Abood, Maclean & Falkowski 2011; Dehni & Lounis 2012; Fernández-Buces et al. 2006; Koshal 2010; Lenney et al. 1996; Leone et al. 2007; Lobell et al. 2010; Peñuelas et al. 1997; Turhan et al. 2008; Wiegand et al. 1994; Wu et al. 2008; Zhang et al. 2011), soil-adjusted vegetation index (SAVI) (Abood, Maclean & Falkowski 2011; Alhammadi & Glenn 2008; Allbed, Kumar & Aldakheel 2014; Koshal 2010; Zhang et al. 2011) and enhanced vegetation index (EVI) (Lobell et al. 2010). NDVI is defined as:

Equation 3.1

$$\mathrm{NDVI} = (N - R)/(N + R)$$

where N is the reflectance in the near-infrared (NIR) band and R is the reflectance in the red band. Although NDVI is useful for a wide range of applications, it is very sensitive to soil background brightness (Bausch 1993; Huete 1988). Huete (1988) proposed using a soil-adjustment factor (L) to reduce soil background brightness. This factor accounts for first-order, non-linear, differential NIR and red radiative transfer through a canopy (Jiang et al. 2008). The resulting SAVI is defined as:

Equation 3.2

$$\text{SAVI} = (1 + L)((N - R)/(N + R + L))$$

where N is the reflectance in the NIR band, R is the reflectance in the red band and L is the soil-adjustment factor. L can vary from 0 to 1 depending on the amount of visible soil. Lower L values with increases in vegetation cover are needed as less soil is exposed. A value of 0.5 is a reasonable approximation for L when the amount of visible soil is unknown (Koshal 2010). SAVI provides better results at low vegetation cover than NDVI because of its ability to reduce the soil background effect (Koshal 2010).

The relatively low spectral resolution of VHR sensors has limited the development of other salt-affected soil detection VIs (Metternicht & Zinck 2003). Abood, Maclean & Falkowski (2011) took advantage of the additional spectral bands and high spatial resolution of the WV2 imagery to evaluate six adaptations of the NDVI and SAVI indices. The indices that proved to be the most successful in distinguishing salt-affected areas utilized the yellow band, specifically NDVI no. 3 (Equation 3.3) and SAVI no.2 (Equation 3.4).

Equation 3.3

$$\text{NDVI no. } 3 = (NIR1 - Y)/(NIR1 + Y)$$

where NIR1 is the reflectance of the WoldView-2's first near-infrared band and Y is the reflectance of the WoldView-2's yellow band.

Equation 3.4

$$\text{SAVI no. } 2 = 1.5((NIR1 - Y)/(NIR1 + Y + 0.5))$$

where NIR1 is the reflectance of the WoldView-2's first near-infrared band and Y is the reflectance of the WoldView-2's yellow band. The EVI was developed to optimize the vegetation signal with improved sensitivity in high biomass regions. It also improves vegetation monitoring by separating the canopy background signal and reducing atmospheric influences (Jiang et al. 2008). EVI is defined as:

Equation 3.5

$$\text{EVI} = G((N - R)/(N + C_1R - C_2B + L))$$

where N is the reflectance in the NIR band, R is the reflectance in the red band, B is the reflectance in the blue band, G is a gain factor, L is the soil-adjustment factor and C1 and C2 are aerosol resistance coefficients. The parameters, as adopted in the MODIS EVI algorithm, are L =1; C1 = 6; C2 = 7.5 and G = 2.5, and are used as a de facto standard for other sensors. All WV2 derived VIs were produced by performing raster calculations in ArcMap (10.1).

Image texture

There is no consensus on a definition for image texture as the meaning seems to vary according to the particular application. For the purposes of this study, it is defined as the variation in reflectance from pixel to pixel in a small neighbourhood (Russ 1999). The observation of image texture is determined by two factors, namely the scale of variation and the scale of observation (Mather & Magaly 2011). Howari (2003) noted that salt-affected soils tend to have uneven ('spotty') vegetation growth, which suggests a scale of variation. In this study, we manipulated the scale of observation by resampling the WV2 image to seven spatial resolution levels (0.5 m, 2 m, 6 m, 10 m, 14 m, 16 m and 20 m).

A total of 25 texture measurements were considered in this study (Table 3.3). The measurements were based on relative frequency distribution statistics (Conners & Harlow 1980; Haralick 1979; Haralick, Shanmugam & Dinstein 1973) and histogram statistics (Dekker 2003). The red and NIR bands, on each of the seven spatial scales, together with the original panchromatic band were used as input for the 25 texture algorithms considered, resulting in a total of 375 texture features. The panchromatic band was selected because it provides the highest resolution (0.5 m), while the red and NIR1 bands were selected because of its well-known sensitivity to vegetation variations.

Table 3.3 Algorithms used for texture feature generation

#	Neighbourhood-based texture algorithms (A)	Histogram-based texture algorithms (B)
1.	Homogeneity	Mean
2.	Contrast	Median
3.	Dissimilarity	Mean deviation from mean
4.	Mean	Mean deviation from median
5.	Variance	Mean Euclidean distance
6.	Entropy	Variance
7.	Angular second moment	Coefficient of variation
8.	Correlation	Skewness
9.	GLDV[a] angular second moment	Kurtosis
10.	GLDV entropy	Energy
11.	GLDV mean	Entropy
12.	GLDV contrast	Weighted-rank fill ratio
13.	Inverse difference	

[a] GLDV = Grey level difference vector.

PCA image transform

Campbell (2007) describes PCA as the process of identifying the optimum linear combinations of the original image layers that account for most of the variation in pixel values. PCA is widely used in salinity detection (Abbas et al. 2013; Dehni & Lounis 2012; Dwivedi et al. 2001; Eldiery, Garcia & Reich 2005; Khan et al. 2001; Tajgardan, Shataee & Ayoubi 2007). In this study only the first two components were included in the feature dataset as it accounted for more than 99% of the variation. These components were generated for all seven spatial levels resulting in a total of 14 features.

Table 3.4 provides a summary of the 515 features that were considered in the regression and CART analyses. The feature set consists of the eight WV2 bands, ten VIs, 25 texture features (Table 3.3; Neighbourhood and Histogram-based textures) and two PCA components for each of the seven spatial resolution sets.

Table 3.4 Summary of features considered for each of the six feature sets (spatial resolution scenarios)

Type	Feature	Total
Bands	Coastal Blue	56
	Blue	
	Green	
	Yellow	
	Red	
	Read Edge	
	NIR1	
	NIR2	
VIs	NDVI & NDVI[b]	70
	SAVI & SAVI[b]	
	EVI & EVI[b]	
	NDVI no 3 & NDVI[b] no3	
	SAVI no 2 & SAVI[b] no 2	
PCA	PCA band 1	14
	PCA band2	
Texture	Homogeneity (A)	375
	Contrast (A)	
	Dissimilarity (A)	
	Mean (A)	
	Variance (A)	
	Entropy (A)	
	Angular second moment (A)	
	Correlation (A)	
	GLDV angular second moment (A)	
	GLDV entropy (A)	
	GLDV mean (A)	
	GLDV contrast (A)	
	Inverse difference (A)	
	Mean (B)	
	Median (B)	
	Mean deviation from mean (B)	
	Mean deviation from median(B)	
	Mean Euclidean distance (B)	
	Variance (B)	
	Coefficient of variation (B)	
	Skewness (B)	
	Kurtosis (B)	
	Energy (B)	
	Entropy (B)	
	Weighted-rank fill ratio (B)	
	Total number of features:	**515**

[b] with NIR2 band

3.3.4 Spectral, statistical and CART analysis

According to Hick & Russell (1990) and Zhang et al. (2011), vegetated salt-affected areas have a higher reflectance in the red band and a lower reflectance in the NIR region. This is due to the decline in vegetation vigour in the presence of high levels of salts. A spectral analysis was carried out to investigate to what extent salt-affected areas can be differentiated using the bands of the WV2 image. The first step was to plot the spectral responses of vegetation in salt-affected and unaffected areas on a graph to allow a visual interpretation of the two profiles. The original 2 m multispectral bands were used as input in the spectral analysis.

The statistical relationships between the image features and salt-affected areas were then explored by modelling EC values through regression analyses. The WV2-derived features were specified as independent variables, while the measured EC values were specified as the dependent variable. Stepwise linear regression, partial least squares (PLS) regression and curve estimation regression were carried out in IBM SPSS (version 21) software. The curve estimations tested the fit between the EC values and the independent variables for various models (linear, logarithmic, inverse, quadratic, cubic, compound, power, s-curve, growth, exponential and logistic). The R^2 values produced by the regression analyses were used to compare the models as they quantify the variation explained by the model and consequently provide a good estimate of the overall predictive power of the model and the nature of the relationship between the input variables (Field 2006).

A CART, as implemented in the Salford Predictive Modeller software suite, was carried out to better understand the relationships between measured EC and the image features. CART has been shown to be a robust decision tree (DT) classifier and was designed for data mining and predictive modelling purposes (Laliberte, Fredrickson & Rango 2007; Myburgh & Van Niekerk 2013; Steinberg & Golovnya 2007; Yu et al. 2006). CART produces a number of classification trees from which it generates a variable importance list (VIL) based on best relative errors and receiver operating characteristics (ROC) values (a.k.a. area under the curve or AUC). The best relative error (BRE) describes the relationship between classification errors and tree size with zero representing no error and one indicating random guessing. A tree with an ROC value of 0.5 and lower is considered to have poor predictive power, while a tree with an ROC value of 0.7 or higher is likely to produce a good classification (Fawcett 2006; Steinberg & Golovnya 2007). The VIL summarizes the contribution of a specific feature to the overall tree when all nodes are examined. It contains the primary splitters (the feature that was used to split a node) and surrogate splitters (a backup feature that could be used when a primary splitter is missing). The VIL, therefore, acknowledges the influence of variables whose significance is hidden by other variables in the process of tree building (Steinberg & Golovnya 2007). In contrast to regression analysis, which investigates the continuous relationships between variables, CART can examine both continuous and categorical data. CART results in a crisp classification (e.g. salt-affected or unaffected) rather than a continuous regression model that is fuzzy in nature and difficult to interpret.

Unlike many other “black box” supervised classifiers, CART is transparent as the contribution of specific features to the classification result can be visualized and inspected. In addition, the DT that CART produces can be used to generate a ruleset that can be manipulated or modified as

needed. This DT also has great transferability potential, which makes it ideal for developing a salt accumulation monitoring solution.

3.4 RESULTS AND DISCUSSION

The spectral responses of vegetation in salt-affected and unaffected areas based on the WV2 bands are shown in Figure 3.3. The reflectance of the salt-affected areas in the red band is higher than that of unaffected areas. This suggests that the vegetation in salt-affected areas is growing less vigorously.

The difference between salt-affected and unaffected vegetation responses in the NIR band was found to be marginal. This contradicts studies done by Peñuelas et al. (1997), Wang et al. (2002), Tilley et al. (2007) and Zhang et al. (2011) who showed that when studying vegetation cover, a more substantial spectral difference between salt-affected and unaffected areas exists in the NIR region. A likely explanation for the smaller than expected differences in NIR reflectance in our study is the influence of background soil reflection. During the field surveys, it was noted that affected areas generally had incomplete vegetation canopy cover. Due to the compromised canopy cover, background features (e.g. bare ground and salt encrustations) are more likely to be exposed when plant wilting occurs. Salt encrustations, depending on the salt type, generally have higher reflectance in the NIR spectrum compared to unaffected soil (Abood, Maclean & Falkowski 2011; Elnaggar & Noller 2010; Iqbal 2011; Khan et al. 2005; Metternicht & Zinck 2003; Setia et al. 2013; Sidike, Zhao & Wen 2014) and this could have contributed to the relatively high reflectance in the NIR band.

Nevertheless, the relatively large difference in reflectance in the red band suggests that a VI that makes use of the ratio between the red and NIR bands has the potential to distinguish between salt-affected and unaffected areas. However, the fairly high standard deviations (as indicated by the error bars in Figure 3.3) show that such an approach will not be successful in all cases.

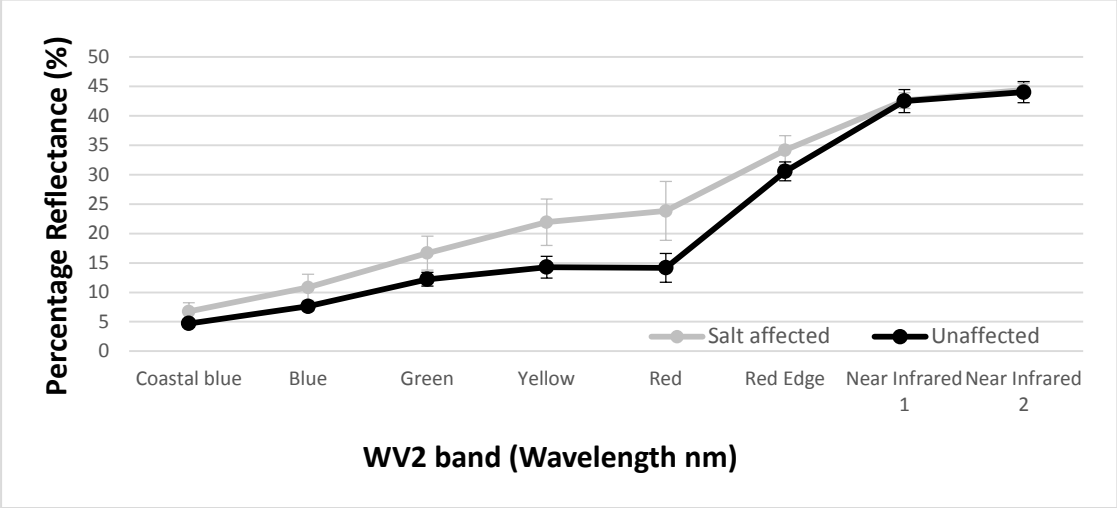

Figure 3.3 Spectral profile of salt-affected and unaffected vegetation. The series represents the mean response of the surveyed points where 4.0 dS/m separates salt-affected vegetation from unaffected vegetation (error bars represent one standard deviation)

Table 3.5 summarizes the regression results of models that produced the best R^2 values for each spatial resolution scenario. A strong relationship between the yellow band and the topsoil EC values was observed, with R^2 values of 0.7261, 0.6915 and 0.7311 at 0.5 m, 2 m and 6 m resolutions respectively. This is attributed to the absorption of yellow light by vegetation (Zhang et al. 2011) and the high reflectance of yellow wavelengths by salt efflorescence on exposed soils (Abood, Maclean & Falkowski 2011; Elnaggar & Noller 2010; Iqbal 2011; Khan et al. 2005; Metternicht & Zinck 2003; Setia et al. 2013; Sidike, Zhao & Wen 2014). The S-curve that models this relationship is shown in Figure 3.4a. Despite the high R^2, it is clear from Figure 3.4a, that the model becomes less reliable as EC increases. Considering the variability in radiance between images, it is also unlikely that the use of a model based on a single band will be robust enough for the operational identification of salt-affected areas in large irrigation schemes covered by multiple images. The transferability of this model to other areas is consequently questionable. VIs have been shown to be more robust and transferable as it makes use of relative measures such as band ratios (Asrar et al. 1984; Bannari et al. 1995). Table 3.5 shows that some of the VIs that were considered in the regression analyses also produced relatively strong models. Figure 3.4b, for instance, shows that the relationship between EVI (with the NIR2 band) and EC at 6 m resolution can be described using a compound curve with relatively strong predictive power ($R^2 = 0.7045$).

The VIs that make use of the yellow band (Equations 3.3 and 3.4) generally performed best when compared with the normal NDVI and SAVI indices (Equations 3.1 and 3.2). This is consistent with Abood, Maclean & Falkowski (2011) who found that the detection of salt-affected areas improved when the WV2 red band was substituted with the yellow band in the

generation of VIs. The differences in R^2 between the yellow and second NIR band indices compared to the standard VIs, however, were statistically insignificant in this study. This suggests that the greater spectral resolution of the WV2 image is superfluous in the creation of VIs. Only minor differences in R^2 values of the VI-based models were observed between 0.5 m and 6 m spatial resolutions after which the R^2 value dropped significantly (Table 3.5).

Table 3.5 Significant regression results from all spatial resolutions

	Bands			VIs			Texture			
Resolution	R^2	Feature	model	R^2	Feature	Model	R^2	Feature	model	Mean R^2
0.5 m	0.7261	Yellow	S	0.6680	EVI[c]	Compound	0.7661	B12 (red band)	S	0.720
2 m	0.6915	Yellow	S	0.6782	SAVI[c] no2	Compound	0.7169	B2 (red band)	S	0.6955
6 m	0.7311	Yellow	S	0.7045	EVI	Compound	0.6780	A4 (red band)	S	0.7045
10 m	0.5872	Red	S	0.5561	EVI	Compound	0.6590	B2 (red band)	S	0.6007
14 m	0.5123	Yellow	S	0.4429	EVI[c]	Compound	0.5111	B8 (red band)	Compound	0.4887
16 m	0.5430	Yellow	S	0.4901	EVI[c]	Compound	0.5219	B2 (red band)	Power	0.5183
20 m	0.4400	Red Edge	Compound	0.2240	EVI[c]	Compound	0.3760	B10 (red band)	Cubic	0.3467

[c] with NIR2 band

Of all the texture features evaluated, B12 (Table 3.3) together with the red band produced the strongest model at 0.5 m (R^2 = 0.766). The texture-based regression model outperformed the spectral-based models at all resolution scenarios except at 6 m. Figure 3.4c plots the relationship between the texture measure B12 and measured EC at 0.5 m resolution. This result is encouraging as texture measures are spatial measurements relative to the size of its kernel only and thus, theoretically less affected by radiometric variations. Texture should, therefore, produce models that are more robust and transferable.

The reduction of spatial resolution generally had a detrimental effect on the regression models, with most significant decreases between 6 m and 10 m resolutions (mean R^2 of 0.7045 and 0.6007 respectively) and between 10 m and 14 m resolutions (mean R^2 of 0.6007 and 0.4887 respectively). The pansharpening of the 2 m multispectral bands to 0.5 m improved the models based on the textural features, while the spectral and VI-based models were highly comparable to those generated from the original 2 m multispectral data.

The relatively poor performance of the models generated from 10m and lower resolutions is attributed to the limited extents of salt-affected areas, as observed during the field surveys. This finding suggests that spatial resolutions of 6 m or higher are required. For texture-based models, the highest possible resolution should be used (preferably 0.5 m). These resolutions are however subjected to the degree of salt accumulation.

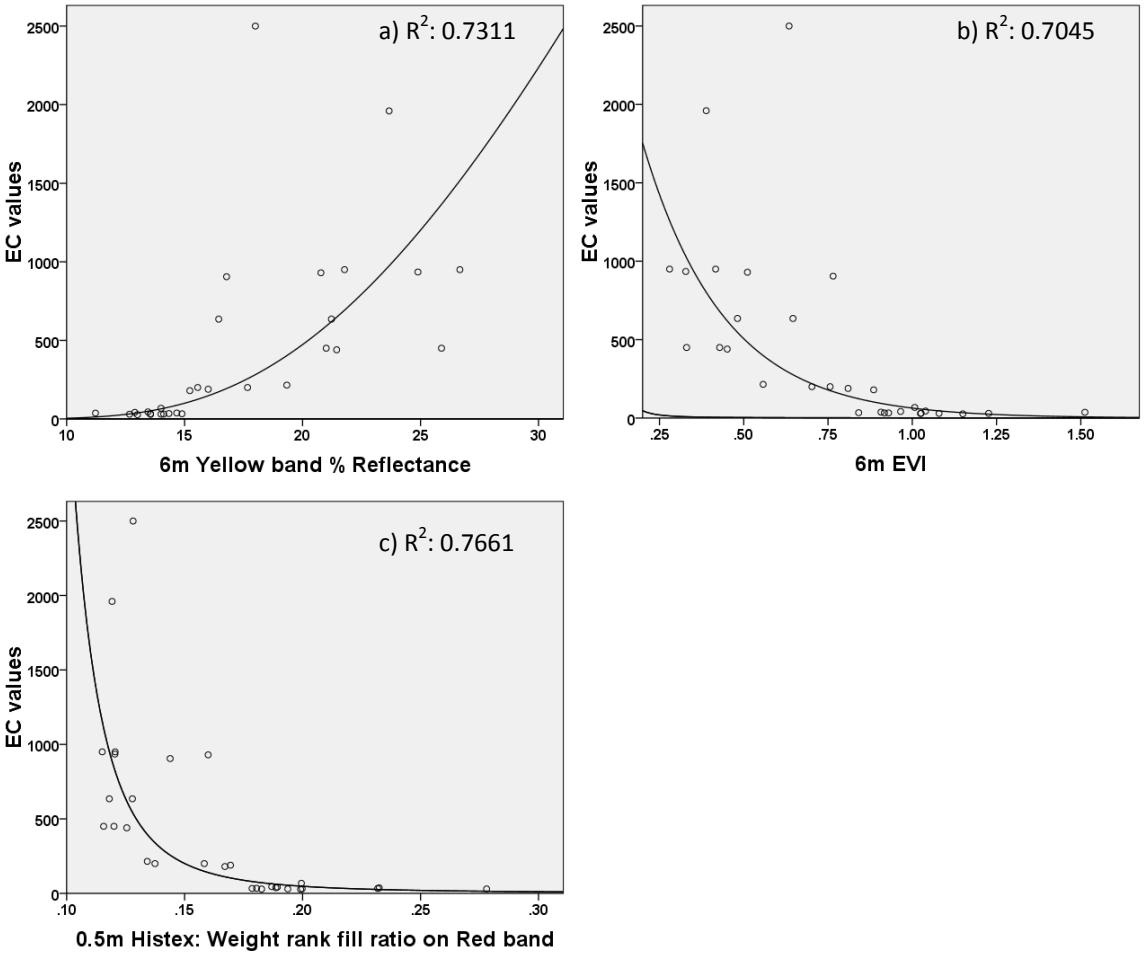

Figure 3.4 a) S-curve regression model (6 m yellow band) b) Compound regression model (6 m EVI) c) S-curve regression model (0.5 m B12)

Figure 3.5 is the resulting classification tree produced by CART and shows a relatively good classification (ROC = 0.875; BRE = 0.278) although the tree only has one main splitter (NDVI no. 3 at 0.5 m resolution). The VIL results, as determined by CART, are summarized in Table 3.6. Of the 515 features, the VIs dominated the classification tree and, in contrast to the regression analysis, the texture features had no significant influence. Based on the VIL results, any of the VIs with 100% variable importance can be used with their specified split value to reproduce the same result (Table 3.6). Band 5 (red) at 0.5 m resolution was also listed in the VIL. This corresponds with Figure 3.3 which indicates that maximum spectral separation between salt-affected and unaffected vegetation occurs in the red portion of the electromagnetic spectrum. This is attributed to the relatively high absorption of red light by healthy vegetation and its contrastingly strong reflection by bare soils and soils covered by salt encrustations (depending on the salt type). The red band was consequently of great value for salt accumulation detection in the study area.

The features identified in Table 3.6 are all of 0.5 m spatial resolution indicating the positive influence of pansharpening on the results. This result suggests that, when a more precise (crisp) delineation between unaffected and salt-affected areas is needed, the higher resolution VIs are most effective. This is likely because a VI at 0.5 m resolution can accommodate a finer delineating line than, for instance, a VI at 6 m.

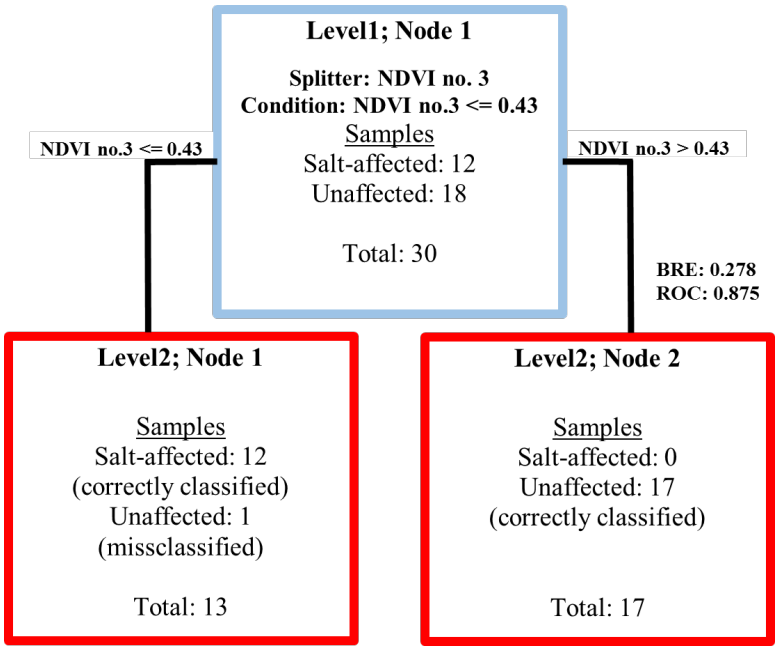

Figure 3.5 CART classification tree and descriptive statistics

Table 3.6 VIL of 445 features and split values

Feature	% importance	Split values
EVI** 0.5 m	100	0.31630
SAVI** 0.5 m	100	0.64892
NDVI** 0.5 m	100	0.43633
SAVI no2 0.5 m	100	0.63730
NDVI no3 0.5 m	100	0.428574
Band 5 0.5 m	89.4118	16.39065

More work is needed to determine to what extent the CART models can be transferred to other areas, as “overfitting” (i.e. producing high accuracies on specific training data while failing to produce similar accuracies on other data) is a well-known limitation of DT classifiers (Schaffer 1993). The performance of other machine learning classifiers such as k-nearest neighbour (k-NN), support vector machines (SVM), and random forests (RF) should also be investigated.

3.5 CONCLUSION

In this study 515 WV2-derived spectral and spatial (texture) features were analysed at 0.5 m, 2 m, 6 m, 10 m, 14 m, 16 m and 20 m resolutions to evaluate their potential for distinguishing between salt-affected and unaffected soils in an irrigated lucerne field.

Regression analyses were carried out to investigate the relationships between the image features and EC values of 30 soil samples collected in the study area. The results showed that there are significant and strong continuous relationships between EC and several of the features considered and that the yellow band, as well as a number of VIs and texture features, produced the strongest models. Generally, the strength of these relationships diminished as the spatial resolution was reduced.

CART was used to better understand the importance of specific features for producing a categorical (i.e. crisp) output. The CART analysis identified VIs as the most important variables at the highest resolution of 0.5 m. Although there is inherently a compromise of spectral information when pansharpening is performed (in this case from 2 m to 0.5 m), this result seems to agree with those of Zhang (2002) and Nikolakopoulos (2008) who showed that pansharpening can have a positive effect in some applications.

Overall, the regression analysis and CART results are very promising as they show that VIs generated at 6 m and higher resolution can potentially be used for the identification of salt accumulation in South African irrigation schemes. The results also suggest that high resolution texture features can potentially be used together with VIs for the indirect monitoring of salt-affected soils. Furthermore, the relatively high spectral resolution of the WV2 imagery is not critical, as the VIs (based on red and NIR wavelengths only) performed relatively well compared to the performance of the individual bands.

The results show that slightly lower spatial and spectral resolution imagery might produce comparable results. Notable candidates are SPOT-5 (2.5 m panchromatic; 10 m multispectral), SPOT-6 (1.5 m panchromatic; 6 m multispectral), RapidEye (5m multispectral) and Sentinel-2 (10 m multispectral) data. However, more work is needed to determine whether similar results will be obtained from using such imagery.

The models generated in this study only considered soil samples collected in a cultivated field with a single crop. It is well-known that crops differ in their response to saline conditions and more work is needed to investigate how these variations will affect remote sensing methods. Plant stress observed with satellite imagery might also be the result of factors unrelated to salt accumulation (e.g. irrigation and fertilisation). Such factors will have to be taken into

consideration in a monitoring system. One possible solution is to make use of multi-temporal imagery to identify areas within fields that are consistently under stress. More work is, however, needed to investigate the value of such approaches for the identification of salt-affected areas in irrigation schemes.

CHAPTER 4: AN EVALUATION OF SUPERVISED CLASSIFIERS FOR INDIRECTLY DETECTING SALT-AFFECTED AREAS AT IRRIGATION SCHEME LEVEL[1]

4.1 ABSTRACT

Soil salinity often leads to reduced crop yield and quality and can render soils barren. Irrigated areas are particularly at risk due to intensive cultivation and secondary salinization caused by waterlogging. Regular monitoring of salt accumulation in irrigation schemes is needed to keep its negative effects under control. The dynamic spatial and temporal characteristics of remote sensing can provide a cost-effective solution for monitoring salt accumulation at irrigation scheme level. This study evaluated a range of pan-fused SPOT-5 derived features (spectral bands, vegetation indices, image textures and image transformations) for classifying salt-affected areas in two distinctly different irrigation schemes in South Africa, namely Vaalharts and Breede River. The relationship between the input features and electroconductivity measurements were investigated using regression modelling (stepwise linear regression, partial least squares regression, curve fit regression modelling) and supervised classification (maximum likelihood (ML), nearest neighbour (NN), decision tree (DT) analysis, support vector machine (SVM) and random forests (RF)). Classification and regression trees (CART) and RF were used to select the most important features for differentiating salt-affected and unaffected areas. The results showed that the regression analyses produced weak models (< 0.4 R-squared). Better results were achieved using the supervised classifiers, but the algorithms tend to over-estimate salt-affected areas. A key finding was that none of the feature sets or classification algorithms stood out as being superior for monitoring salt accumulation at irrigation scheme level. This was attributed to the large variations in the spectral responses of different crops types at different growing stages, coupled with their individual tolerances to saline conditions.

4.2 INTRODUCTION

The term salinity is used to describe the processes and impacts of salt and water, while also being a measure of the amount of salt in soil or water (McGhie & Ryan 2005). Soil salinity is defined as the accumulation of soluble salts in the soil (Al-Khaier 2003). Salt accumulation can occur naturally (primary salinity) or as a result of human interference (secondary salinity). Human activities such as vegetation clearing, irrigation, and landscape reshaping through

[1] This chapter is published in the International Journal of Applied Earth Observation and Geoinformation and consequently conforms to the prescribed structure of that journal

earthworks can, for example, increase the volume of water and salt in the soil and change how they move and where they accumulate (Ghassemi, Jakeman & Nix 1995; McGhie & Ryan 2005; Metternicht & Zinck 2009). Determining salinity risk goes hand in hand with the understanding of groundwater movement since this controls the mobility and transfer of salt deposits, among other landscape factors (Spies & Woodgate 2005).

According to Hillel (2000), soil salinity is a severe environmental hazard that affects the growth of various crops. Although salinity might not be as dramatic or damaging as earthquakes or landslides, it is an environmental hazard that greatly reduces crop yields and agricultural production (Ghassemi, Jakeman & Nix 1995; Metternicht & Zinck 2009; Umali 1993; Zinck 2000). Salt accumulation also has additional secondary negative impacts, such as the devaluation of farm properties, land degradation, eutrophication of rivers, damage to infrastructure, increased soil erosion and engineering difficulties (Metternicht & Zinck 2003).

It is estimated that nearly one billion hectares (ha), which is equivalent to about 7% of the earth's continental extent, is associated with salt-affected areas (Ghassemi, Jakeman & Nix 1995). According to the Food and Agriculture Organization of the United Nations (FAO), of the 230 million ha land available for irrigation, 45 million ha (19.5%) are salt-affected (FAO 2016). Most of these affected areas are the consequence of human activities, in particular, irrigation (Metternicht & Zinck 2003). This is an alarming statistic and Abbas et al. (2013) estimate that, at a global scale, soil salinization is increasing at a rate of up to 2 million ha per annum.

Proactive monitoring of salt accumulation is needed to keep its negative effects under control. Salinity monitoring involves the identification of areas where salts concentrate and the detection of temporal and spatial changes in this occurrence (Zinck 2000). Remotely sensed data can contribute a great deal to monitoring these processes because of its ability to capture information in both spatial and temporal scales (Abbas et al. 2013). Bastiaanssen, Molden & Makin (2000) state that remote sensing has the potential to predict soil salinity, perform diagnosis and assess its impact. Compared to solely relying on regular field surveys for monitoring salt accumulation, the synthesis of remote sensing with field surveys can potentially save labour, time, and effort (Eldiery, Garcia & Reich 2005; Metternicht 1996).

Soil salinity can be detected from remotely sensed data either directly or indirectly (Bastiaanssen 1998; Mougenot, Pouget & Epema 1993). When studying the spectral properties of bare soil directly, indicators of salt accumulation includes white salt crusts, puffy soil, dark greasy surfaces, dehydrated cracks and coarser topsoil (Goodall, North & Glennie 2000; McGhie & Ryan 2005; Metternicht & Zinck 2003). The main limitation of the direct approach is that farming practices such as tillage and irrigation compromise the spectral properties of soils

(Metternicht & Zinck 2003; Zhang et al. 2011), particularly in highly dynamic irrigation schemes.

Techniques other than the direct approach are considered indirect methods for detecting salt accumulation. The aim of the indirect approach is to map the effect that salt accumulation has on land cover. Most indirect indicators are related to vegetation types and growth. An excess of salt in a plant's root environment leads to a reduced ability to take up water. The salts reduce the osmotic potential of water and hinder the movement of water from the soil into the root. If saline conditions persist, the small amount of salt that enters a plant along with water accumulates over time and becomes toxic (Hillel 2000; McGhie & Ryan 2005). These effects lead to spotty/uneven growth, plant wilting, blue-green tinge and moisture stress.

Several authors have successfully applied the indirect approach to identify plant stress caused by salt accumulation (Abood, Maclean & Falkowski 2011; Fernández-Buces et al. 2006; Koshal 2010; Lenney et al. 1996; Lobell et al. 2010; Peñuelas et al. 1997; Wiegand et al. 1994; Zhang et al. 2011). In all of these cases, vegetation indices (VIs) (e.g. NDVI, EVI and SAVI) were employed. The use of VIs is, however, not without complications. Plant species with a high salt tolerance can lead to ambiguity in the response of vegetation indices (Aldakheel 2011); poor farming practices and soil preparation can lead to poor vegetation responses which can be misinterpreted as being caused by salinity conditions (Furby et al. 1995); and using VIs in study areas with a high bare ground backscatter/noise can influence some of the vegetation indices negatively (Dehni & Lounis 2012; Douaoui, Nicolas & Walter 2006). Other indirect indicators of salt accumulation include soil types (García Rodríguez, Pérez González & Guerra Zaballos 2007) elevation and terrain data (Caccetta, Allen & Watson 2000; Farifteha, Farshada & Georgeb 2006; Furby et al. 1995; Jenkin 1981; McFarlane, George & Caccetta 2004) and image texture (Metternicht & Zinck 2003).

Most applications of remote sensing for monitoring salt accumulation have been carried out in areas where salt accumulation occurs on a grand scale. As a result, the majority of the satellite imagery used for the identification of salt accumulation has medium to low resolutions. Landsat (30 m) (Abdelfattah, Shahid & Othman 2009; Aldakheel 2011; Al-Khaier 2003; Caccetta, Allen & Watson 2000; Dehni & Lounis 2012; Elnaggar & Noller 2010; Fernández-Buces et al. 2006; Furby et al. 1995; Gao & Liu 2008; García Rodríguez, Pérez González & Guerra Zaballos 2007; Howari 2003; Lenney et al. 1996; Mohamed, Morgun & Goma Bothina 2011); IRS (20 m) (Abbas et al. 2013; Abbas & Khan 2007; Dwivedi et al. 2001; Dwivedi & Sreenivas 1998; Eldiery, Garcia & Reich 2005; Khan et al. 2001; Koshal 2010) and MODIS (250 m) (Lobell et al. 2010) are most commonly used. However, agricultural activities in irrigation schemes are

normally diverse in nature as many different crops are usually planted, often on a rotational basis. This poses a unique challenge for detecting salt accumulation, especially if it occurs in small patches within relatively small fields. Such areas will be difficult to detect using medium to low resolution (e.g. 20 to 250 m) satellite images. Few studies on the use of very high resolution (VHR) imagery for indirect salt accumulation monitoring exist. Exceptions include Douaoui & Yahiaoui (2015), and the unpublished work of Abood, Maclean & Falkowski (2011) who used WorldView-2 (WV2) (2 m) imagery; as well as Howari & Goodell (2009), Eldiery, Garcia & Reich (2005), Dwivedi, Kothapalli & Singh (2009) and Allbed, Kumar & Aldakheel (2014) who used IKONOS (4 m) imagery. Other high resolution imagery used for detecting soil salinity include airborne multispectral (Hick & Russell 1990; Howari 2003; Wiegand et al. 1994) and hyperspectral imagery (Dehaan & Taylor 2002; Dehaan & Taylor 2003; Dutkiewicz, Lewis & Ostendorf 2009b; Farifteh 2009; Naumann, Young & Anderson 2009; Schmid, Magaly & Gumuzzio 2009). Hyperspectral imagery in particular holds key advantages over standard multispectral imagery due to its rich spectral information (Metternicht & Zinck 2009). Due to limited coverage and low availability of these images, they were not considered for this study.

Supervised classification is a proven tool for successfully identifying salt accumulation. The ML classification is the most commonly applied supervised method for the identification of salt accumulation. Its application stretches across various satellite platforms, namely Landsat (Abbas et al. 2013; Castaneda & Herrero 2009; García Rodríguez, Pérez González & Guerra Zaballos 2007; Howari 2003; Iqbal 2011; Wu et al. 2008), LISS-II (Abbas et al. 2013) and IKONOS (Dwivedi, Kothapalli & Singh 2009; Howari & Goodell 2009). To our knowledge, however, no research has been done to evaluate the ability of different supervised classifiers for detecting salt-affected areas using VHR imagery in highly complex and dynamic irrigated areas.

The aim of this paper, which forms part of a Water Research Commission (WRC) project (WRC 2010), is thus to evaluate a range of indirect indicators – derived from SPOT-5 imagery – for detecting and classifying salt-affected areas at irrigation scheme level. Several supervised image classification techniques are evaluated, namely ML, SVM, NN, DT, and random forest (RF). The techniques are evaluated on two contrasting irrigation schemes in South Africa (Vaalharts and Breede River) to determine whether any of the classifiers consistently produce superior results and to identify the indirect indicators that can reliably be used to detect salt accumulation. The results are discussed and interpreted in the context of finding operational solutions for salt accumulation monitoring at irrigation scheme level.

4.3 METHODS

4.3.1 Study area

The Vaalharts irrigation scheme, situated on the borders of the Northern Cape, North West and the Free State provinces, near the towns of Jan Kempdorp, Hartswater, and Pampierstad, was selected as the first study area (Figure 4.1). The scheme covers 29181 ha and is one of the largest irrigation schemes in South Africa (Van Rensburg et al. 2012). The area borders two plateaus on the east and west of the Harts River Valley. The valley slopes towards the south with very little topographical changes due to the low gradient of the non-incising Harts River (Gombar & Erasmus 1976; Liebenberg 1977). Vaalharts is known for its sandy soils, which are prone to waterlogging and salt accumulation. This is exacerbated by insufficient natural drainage and soil compaction (Maisela 2007). Typically the soils consist of 8% clay, 2% silt, 68% fine sand and 22% medium and coarse sand (Streutker 1997). The scheme is located at an altitude of 1175 m above sea level and is known for its cold winters and long warm summers (Maisela 2007). The area receives a mean annual rainfall of 400 mm with a mean annual temperature of 19°C (Schulze 2006).

Due to its semi-arid climate, irrigation is required for crop production (Van Rensburg et al. 2012). Vaalharts receives its irrigation water from the Vaal and Harts rivers. Approximately 70% of the irrigation infrastructure comprises of flood irrigation, while pivot irrigation contributes to the remainder (Maisela 2007). The principal crops planted are maize, wheat, barley, lucerne, groundnuts and increasingly pecan nuts (Barnard 2013; Kruger, Van Rensburg & Van den Berg 2009). In addition to the high variation in crop type, most of the annual cash crops are subjected to a double cropping rotation system, which involves the planting and harvesting of two successive crops per year (Barnard 2013). This crop system implies that most crops are at different growing phases at any given time, which contributes to a high variation in vegetation responses observed with remote sensing.

The Breede River irrigation scheme was selected as the second study area (Figure 4.1). The Breede River originates in the Ceres Valley +- 100 km North West of Cape Town and flows 320 km in a south easterly direction where it reaches the Indian Ocean at Witsand (Kirchner 1995). The river drains a catchment of about 1.26 million ha. About a 100 000 ha is used for agriculture in the middle parts of the greater catchment, between Worcester and Robertson,. This intensively cultivated region was chosen as the focus area as it is a good representation of the larger irrigation scheme. The focus area has a gentle hilly relief defined with high mountain ranges north (Langeberg Mountain) and south (Riviersonderend Mountain) parallel to the river. These

mountain ranges are formed by resistant quartzite and sandstones, reaching heights of up to 1800 m in the north west of the catchment (Ghassemi, Jakeman & Nix 1995). The valleys are mainly underlined with shale and siltstone from the Malmesbury and Bokkeveld basements (Beuster, Shand & Carter 2003). The focus area is located at a mean altitude of 233 m above sea level and has a Mediterranean climate with dry and hot summers and moderately warm wet winters (Flügel & Kienzle 1989). It receives an annual rainfall of 290 mm mainly during the winter rainfall season (May to October), and is thus classified as semi-arid (Schulze 2006). The annual mean temperature for the area is 17°C (Schulze 2006).

The Greater Bandvlei Dam supplies the irrigation scheme with water in the dry season. The majority of the farm irrigation infrastructure comprises of drip and microjet systems (Beuster, Shand & Carter 2003). The crop mix in the Breede River irrigation scheme is less diverse compared to the Vaalharts scheme with wine grape variations being the primary (65%) crop. Other crops include peaches and apricots (13%), vegetables, mainly tomatoes (3%) and irrigated pastures (7%) (Moolman et al. 1999). In contrast to Vaalharts, the crops in the Breede River are generally not planted in an annual rotation, resulting in their growing phases being more harmonized (seasonal).

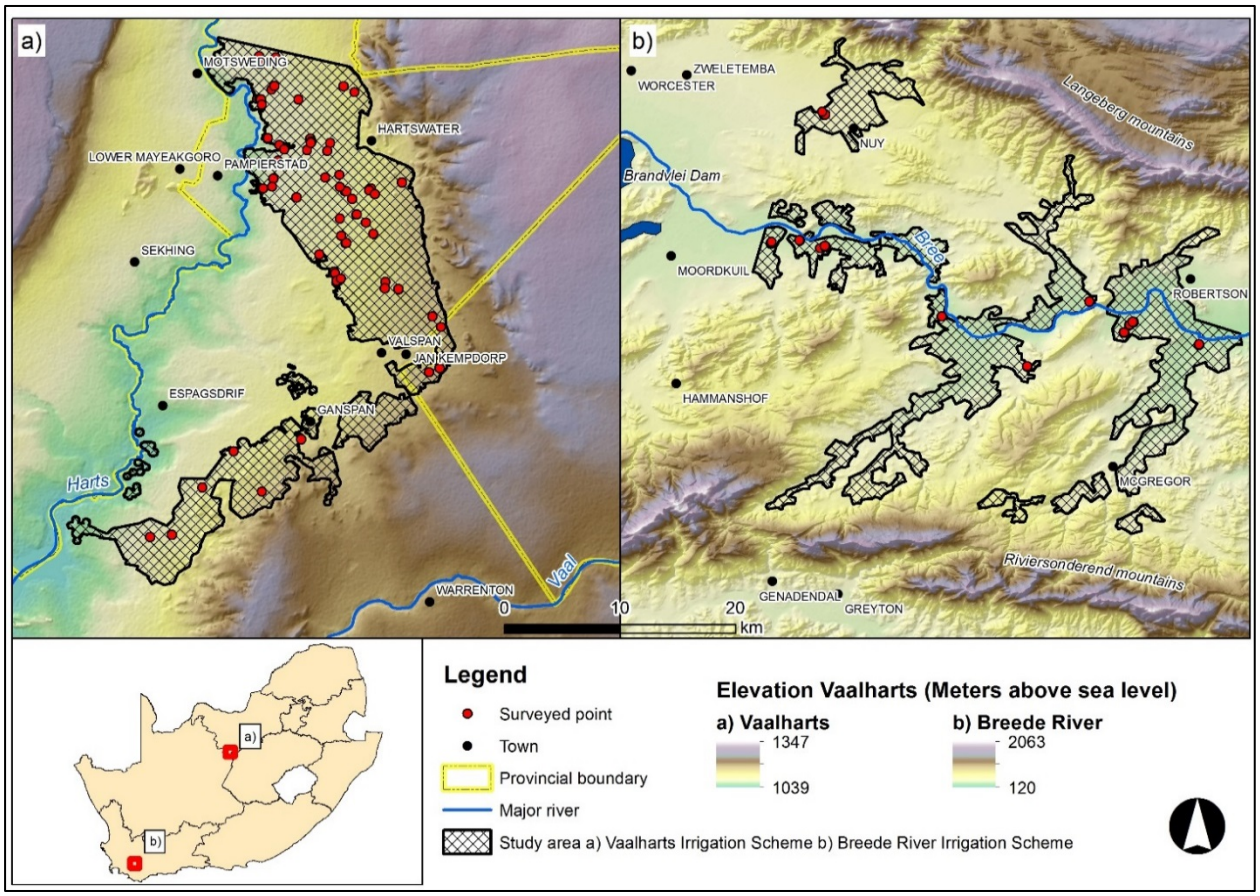

Figure 4.1 Study area map

Hanson, Grattan & Fulton (2006) compiled a database of crop types and their "maximum root zone salinity at which 100% yield occurs" (Threshold A) and a "reduction in relative yield per increase in soil salinity" (Slope B) rates. The figures of A and B for the dominant crops planted in the two selected irrigation schemes are listed in Table 4.1. The table also includes a qualitative rating for each crop type, based on the interpretation of A and B. Apricots are the most intolerant to high levels of salt accumulation, with a relatively low threshold value (A = 1.60) and steep slope (B = 24), while barley is the least sensitive to saline conditions (A = 8.00; B = 5). In general, the tolerances of the dominant crops produced in Vaalharts are more variable, with A having a standard deviation of 2.44 dS/m compared to 0.40 dS/m in Breede River. There is consequently a substantial difference in salt tolerance levels of the crops produced in two irrigation schemes.

Table 4.1 Salinity tolerances of dominant crops in the Vaalharts and Breede River irrigation schemes. Threshold A is the maximum root zone salinity at which 100% yield occurs. Slope B is the reduction in relative yield per increase in soil salinity.

	Crop type	Threshold (*A*) *dS/m*	Slope (*B*)	Qualification
Vaalharts	Maize\corn	1.70	12	Moderately intolerant
	Wheat	6.00	7.1	Moderately tolerant
	Barley	8.00	5	Tolerant
	Lucerne \ alfalfa	2.00	7.3	Moderately intolerant
	Groundnuts	3.20	29	Moderately intolerant
Breede River	Grapes	1.50	9.6	Moderately intolerant
	Peaches	1.70	21	Intolerant
	Apricots	1.60	24	Intolerant
	Tomatoes	2.50	9.9	Moderately intolerant

According to Backeberg et al. (1996) between 10% and 18% of irrigated areas in South Africa are affected by waterlogging, salinity, and sodicity. Ghassemi, Jakeman & Nix (1995) observed that, in general, the extent of salt-affected and waterlogged areas in South Africa is less than in many other countries and seems to be largely under control. This is due to sound planning in the selection of irrigated soils, good drainage and the fact that South African irrigated areas are generally smaller in size. It is mainly due to this favourable status why there are no programmes in place to monitor the extent of waterlogging and salt accumulation in South African irrigation schemes. However, salinity and waterlogging in the Vaalharts and Breede River irrigation schemes has increased to such an extent that some fields can no longer be cultivated, thereby reducing production and contributing to the loss of high potential agricultural land. The

underlying processes contributing to salinity in these areas are the artificial rise of the water table through leaky canal systems and over irrigation. Furthermore, since both areas have semi-arid climates, the rainfall necessary to sufficiently flush away these salts is often not enough. Considering that there are no programmes in place to monitor salt-affected areas in South Africa (De Villiers et al. 2003), remote sensing offers a promising support structure to optimize and improve otherwise costly field-based surveys.

4.3.2 Data collection and preparation

Image data from the time of maximum growth is optimal for indirectly discriminating between saline and non-saline conditions (Furby et al. 1995; Furby, Caccetta & Wallace 2010; Hick & Russell 1990). SPOT-5 imagery was preferred for this study since it offers superior ground coverage relative to cost compared to other VHR satellite imagery, making it more viable for national monitoring application. Two SPOT-5 satellite images, dated 27 April 2012 (Vaalharts) and 16 January 2013 (Breede River), were acquired from the South African National Space Agency (SANSA). Although SPOT-5 imagery has limited spectral resolution (Table 4.2) it contains the red and near-infrared (NIR) bands required for the generation of most VIs. Based on field observations of the extents of salt-affected areas in the two study areas, the 2.5 m and 10 m spatial resolutions of the SPOT-5 panchromatic and multispectral bands respectively, were considered to be adequate, particularly if the multispectral images are pansharpened (fused) to 2.5 m. The fusion of multispectral and panchromatic images has been shown to be an effective technique to optimize the spatial resolution of the coarser multispectral image (González-Audícana et al. 2004).

Table 4.2 SPOT-5 bands and spatial resolution

Band number	Band description (SPOT-5)	Wavelength (nm) (SPOT-5)	Resolution (SPOT-5)
1	Green	500-590	10 m
2	Red	610-680	10 m
3	Near-Infrared (NIR)	790-890	10 m
4	Short Wave Infrared (SWIR)	1580-1750	20 m
5\Pan	Panchromatic	450-690	2.5 m

Geometric and radiometric correction of all images were done using the software package PCI Geomatica (version 2013 SP2). A north-oriented implementation of the Gauss conform coordinate system (also known as the LO coordinate system), with central meridians 25ºE and 19ºE for Vaalharts and Breede River respectively, was used in the orthorectification process. NN resampling was employed during orthorectification to preserve the original digital numbers (DN)

(Campbell 2007; Lillesand, Kiefer & Chipman 2004). Radiometric corrections were carried out using the ATCOR-2 model, which resulted in images representing percentage surface reflectance. The Pansharp algorithm, as implemented in Geomatica, has been shown to preserve most of the spectral characteristics of the multispectral data in the resulting pansharpened image (Zhang 2002; Nikolakopoulos 2008) and was used to increase the 10 m resolution SPOT-5 multispectral data to 2.5 m.

A number of field surveys were carried out to collect suitable in situ data. Due to cloud cover, time of maximum vegetation growth prioritization and the temporal resolution of SPOT-5, the field surveys were contemporaneous with the image data on a scale of a year. Seasonality between the field surveys and images were kept constant as far as possible due to the characteristic changes of salt accumulation in different seasons (Metternicht & Zinck 2003). An indirect study of salt accumulation would, however, minimize this effect to some extent. Different sampling approaches were used to accommodate accessibility restrictions (e.g. canal systems and fencing). An attempt was made to include sites that represented as much as possible variation in terms of salt accumulation, soil types and crop types (Figure 4.1). A total of 69 and 48 samples were collected for Vaalharts and Breede River respectively. Soil samples were collected by means of a soil auger at a constant depth of 15 to 20 cm (topsoil) and analysed for the electroconductivity (EC) in a laboratory using the saturated paste technique. Differential GPS coordinates (10 cm accuracy), notes on the visual appearance of the immediate area, and in some cases, photographs were also captured.

4.3.3 Indirect indicator features

Features derived from the pansharpened SPOT-5 imagery included vegetation indices (VIs), image transformations and image texture. These features were analysed, together with the EC values, for its capability to indirectly classify salt accumulation.

Vegetation indices

VIs are the most popular and scientifically-proven tools for monitoring biomass and vegetative vigour (Campbell 2007). VIs that have been successfully used for mapping salt-affected areas include the normalized difference vegetation index (NDVI) (Abood, Maclean & Falkowski 2011; Dehni & Lounis 2012; Fernández-Buces et al. 2006; Koshal 2010; Lenney et al. 1996; Leone et al. 2007; Lobell et al. 2010; Peñuelas et al. 1997; Turhan et al. 2008; Wiegand et al. 1994; Wu et al. 2008; Zhang et al. 2011), soil-adjusted vegetation index (SAVI) (Abood, Maclean & Falkowski 2011; Alhammadi & Glenn 2008; Allbed, Kumar & Aldakheel 2014;

Koshal 2010; Zhang et al. 2011) and enhanced vegetation index (EVI) (Lobell et al. 2010). NDVI is defined as:

Equation 4.1

$$\text{NDVI} = (N - R)/(N + R)$$

where *N* is the reflectance in the NIR band and R is the reflectance in the red band. Although NDVI is useful for a wide range of applications, it is very sensitive to soil background brightness (Bausch 1993; Huete 1988). In order to adjust the soil background brightness constraint, Huete (1988) proposed using a soil-adjustment factor (L). This factor accounts for first-order, non-linear, differential NIR and red radiative transfer through a canopy (Jiang et al. 2008). The resulting SAVI is defined as:

Equation 4.2

$$\text{SAVI} = (1 + L)((N - R)/(N + R + L))$$

where *N* is the reflectance in the NIR band, *R* is the reflectance in the red and *L* is the soil-adjustment factor. *L* can vary from 0 to 1 depending on the amount of visible soil. Lower *L* values are needed as vegetation cover increases and less soil is exposed. However a value of 0.5 is a reasonable approximation for *L* when the amount of visible soil is unknown (Koshal 2010). SAVI provides better results than NDVI at low vegetation cover because of its ability to reduce the soil background effect (Koshal 2010).

The EVI was developed to optimize the vegetation signal with improved sensitivity in high biomass regions. It also improves vegetation monitoring by disconnecting the canopy background signal and reducing atmospheric influences (Jiang et al. 2008). EVI cannot be applied to SPOT-5 images as it requires a blue band. EVI-2 is a modification of EVI that does not require a blue band. Jiang et al. (2008) found that EVI-2 images show very similar patterns to EVI at a global scale with only minor differences. EVI-2, with optimal parameter values, is defined as:

Equation 4.3

$$EVI\ 2 = 2.5((N - R)/(N + \ 2.4R + 1))$$

where *N* is the reflectance in the NIR band and *R* is the reflectance in the red band. In addition to NDVI, SAVI, and EVI-2, the general vegetation moisture index (GVMI) was also considered in this study as it optimizes the retrieval of vegetation water content and minimizes the disturbing

effects of geophysical and atmospheric effects (Ceccato et al. 2002). GVMI makes use of the shortwave infrared band (SWIR), which distinguishes between variations in vegetation water content (Ceccato et al. 2002). GVMI is defined as:

Equation 4.4

$$GVMI = ((N + 0.1) - (S + 0.02))/(N + 0.1) + (S + 0.02)$$

where *N* is the reflectance in the NIR band and *S* is the reflectance in the SWIR band.

Image transformations

Two image transformations, namely principal component analysis (PCA) and intensity, hue and saturation (IHS) transformation, were considered in this study. Campbell (2007) describes PCA as the process of identifying the optimum linear combinations of the original image layers that account for most variation of pixel values within an image. PCA is widely used to aid in salinity detection (Abbas & Khan 2007; Dehni & Lounis 2012; Dwivedi et al. 2001; Eldiery, Garcia & Reich 2005; Khan et al. 2001; Tajgardan, Shataee & Ayoubi 2007). Only the first two principal components were included in the feature set as it accounted for more the 99% of the variation. The IHS (Carper 1990) transform is a spectral domain procedure that transforms three image bands to IHS space. The three bands chosen as input to the IHS transform were red, green and NIR.

Image texture features

Image texture – local brightness variation from pixel to pixel in a small neighbourhood (Russ 1999) – of the different spectral bands were considered as indirect indicators of salt accumulation. The observation of image texture is determined by two factors, namely the scale of variation and the scale of observation (Mather & Magaly 2011). Spotty growth of vegetation due to salt accumulation (Howari 2003) suggests a potential scale of variation. Given the relatively small extents of salt-affected areas in the study areas, the finest scale of observation (a 3x3 kernel) was used. Histex algorithms (Dekker 2003), as implemented in PCI Geomatica software, were implemented for processing first-order histogram-based texture layers for each of the four spectral bands and the first principal component (Table 4.3).

Table 4.3 Histex algorithms as implemented by the PCI software

Histex	Algorithm
Energy	*[SUM(i,j)(x_i,j)^2]*
Entropy	*-[SUM(i,j)(p_i,j * LOG2(p_i,j))]*
Kurtosis	*[SUM(i,j)(x_i,j - Mean)^4] / [(M - 1) * Var^2]*
Mean Deviance	*[SUM(i,j)(|x_i,j - Mean|)] / M*
Mean Deviance Median	*[SUM(i,j)(|x_i,j - Median|)] / M*
Mean Euclidean Distance	*([SUM (i,j)(x_i,j - x_c)^2]) / (M - 1)*
Mean	*[SUM(i,j)(x_i,j)] / M*
Median	*[SUM(i,j)(x_i,j)] / M*
Normalized Coefficient	*SQRT(Var) / Mean*
Skewness	*[SUM(i,j)(x_i,j - Mean)^3] / [(M - 1) * Var^(3/2)]*
Variance	*[SUM(i,j)(x_i,j - Mean)^2] / (M - 1)*
Weight Rank Fill	*[SUM(p% brightest pixels)] / [SUM(i,j)(x_i,j)]*

Where: *M* is the number of pixels in the window (K * L)
i = 0, …, K-1
j= 0, …, L-1
x_c is the value of the central pixel of the window
x_i,j is the value of a current pixel of the texture window centred on x_c

Source: Dekker (2003)

Table 4.4 provides a summary of the 73 indirect indicator features considered for analysis. The feature set consists of the four SPOT-5 bands; four VIs; 12 image texture measurements per spectral band, the first two principal components, and three IHS image transforms.

Table 4.4 Indirect indicator feature sets considered

Type	Feature	Total
Spectral bands:	Green	4
	Red	
	NIR	
	SWIR	
VIs:	NDVI	4
	SAVI	
	EVI2	
	GVMI	
Texture:	Energy	60
	Entropy	
	Kurtosis	
	Mean Deviance	
	Mean Deviance Median	
	Mean Euclidean distance	
	Mean	
	Median	
	Normalized Coefficient	
	Skewness	
	Variance	
	Weight rank fill	
Image transformations:	PCA band 1	5
	PCA band2	
	Intensity	
	Hue	
	Saturation	
	Total number of features	73

4.3.4 Model building

A land cover map and field boundary data were used to exclude non-cultivated areas (e.g. non-agricultural land uses and the fallow fields) from the analyses. Given that increased reflectance in the visible and reduced reflectance in the NIR spectra have been shown to be consistent in the vegetation responses to salt stress (Hick & Russell 1990; Tilley et al. 2007; Wang et al. 2002; Zhang et al. 2011), a spectral reflectance analysis was performed to better understand the effect of salt accumulation on vegetation growth in each study area. The samples collected during the field surveys were used to extract the reflectance values from the pansharpened image bands to create the profiles.

Regression analyses were carried out to investigate the continuous statistical relationships between the indirect indicator features and salt-affected areas, mainly to provide a basis for comparison with the supervised classification results. The regression analysis could also be used

as a feature selection platform should it produce sufficient results. To model EC values the indirect indicator features (Table 4.4) were used as the independent variables, while measured EC values were defined as the dependent variable. Stepwise linear regression (SLR) and curve estimation regressions were carried out using IBM SPSS (version 21) software (Table 4.5). Partial least squares (PLS) regression was carried out using XLSTAT (Table 4.5). The R-squared value was used to interpret the overall fit of the regression model and the size of the relationship between the two variables.

Table 4.5 Regression models and algorithms

Regression model (Curve Fit)	Equation	Multiple regression model	Equation
Linear	$E(Yt)=\beta0+\beta1t$	Partial least squares (PLS)	$Y = X.W_h(P_h'.W_h)^{-1}.C_h' + E_h$
Logarithmic	$E(Yt)=\beta0+\beta1\ln(t)$	Stepwise linear regression (SLR)	$E(Yt)=\beta0+\beta1t+\beta2t+\ldots\ \beta nt$
Inverse	$E(Yt)=\beta0+\beta1/t$		
Quadratic	$E(Yt)=\beta0+\beta1t+\beta2t2$		
Cubic	$E(Yt)=\beta0+\beta1t+\beta2t2+\beta3t3$		
Compound	$E(Yt)=\beta0\beta t1$		
Power	$E(Yt)=\beta0t\beta1$		
S	$E(Yt)=\exp(\beta0+\beta1/t)$		
Growth	$E(Yt)=\exp(\beta0+\beta1t)$		
Exponential	$E(Yt)=\beta0e\beta1t$		
Logistic	$E(Yt)=(1u+\beta0\beta t1)-1$		

Where: Yt is the observed series ($t = 1 \ldots n$)
$E(Yt)$ is the expected value of Yt
B_n is a constant value
$\beta0$ is an optional user defined constant value

Where (PLS): Y is the dependent variable
X is the independent variable
E_h is the matrix of residuals
W_h, P_h, W_h,C_h are matrices generated by PLS

The regression analyses were followed by a series of categorical (binary) supervised classifications using the indirect indicator features as input. For this purpose, the EC values of the samples were split into two distinct classes (salt-affected and unaffected) using a threshold of 4.0 dS/m in accordance with the Soil Science Society of America (Bresler, McNeal & Carter 1982; SASA 2007). Samples with EC values equal to or higher than this threshold were regarded as being salt-affected while all samples with lower EC values were classified as being unaffected.

Because it is known that some classifiers are sensitive to high feature dimensionality (Friedman 1997; Hughes 1968; Oommen et al. 2008), the CART and RF algorithms, as implemented in the Salford Predictive Modeller software suite, were used to identify the most important indirect indicators of salt accumulation at scheme level. CART is a robust DT classifier designed for data mining and predictive modelling (Steinberg & Golovnya 2007). RF as defined by Breiman (2001) is an ensemble of unpruned CART-like tree classifiers (Gislason, Benediktsson &

Sveinsson 2006; Pal 2005). Unlike CART and other common DT classifiers, RF is less sensitive to overfitting (Breiman 2001) and has been shown to be an effective feature selection tool (Cutler et al. 2007; Gislason, Benediktsson & Sveinsson 2006). Although its known that the use of CART and RF is not ideal for selecting features when dissimilar classifiers (e.g. ML, SVM, NN) are used, many examples exist where these algorithms have successfully been implemented for feature dimensionality reduction (Laliberte, Fredrickson & Rango 2007; Myburgh & Van Niekerk 2013; Yu et al. 2006).

All the features in Table 4.4 were used as predictor variables in the feature selection process. The resulting variable importance lists (VILs) summarize the contribution of a particular feature to the classification success and give recognition to the variables whose significance are hidden by other variables in the process of tree building (Steinberg & Golovnya 2007). The VIL's essential function is to reduce the feature dimensionality and the computational requirement, while preserving the overall accuracy of the classification (Laliberte, Fredrickson & Rango 2007; Yu et al. 2006).

Six supervised classification algorithms (Table 4.6) were evaluated. Customized software developed in C++ using libSVM and OpenCV libraries was used for this purpose (Myburgh & Van Niekerk 2014). SVM is known for its superior results in classification accuracy when compared to less sophisticated (e.g. ML and NN) classifiers (Mountrakis, Im & Ogole 2011; Myburgh & Van Niekerk 2013; Myburgh & Van Niekerk 2014; Pal & Mather 2005; Tzotsos & Argialas 2008). RF (aka Random Trees) is a relatively new classifier in the field of remote sensing and has been shown to compare well, and even outperform SVM (Bosch, Zisserman & Muoz 2007; Novack et al. 2011; Pal 2005).

Table 4.6 Supervised classifiers considered and their implementations

Classifier	Library
Support Vector Machine (SVM1)	Libsvm 3.2 (Chang & Lin 2011)
Support Vector Machine (SVM2)	OpenCV 2.4.10 (Bradski 2000)
Nearest Neighbour (NN)	OpenCV 2.4.10
Maximum likelihood classification (MLC)	OpenCV 2.4.10
Decision Trees (DT)	OpenCV 2.4.10
Random Forest (RF)	OpenCV 2.4.10

The supervised classifications were carried out in an object-based image analysis (OBIA) paradigm. The main advantage of an OBIA approach is that the feature values at each surveyed point and its immediate neighbourhood are considered during the training and classifying process (Blaschke & Strobl 2001; Flanders, Hall-Beyer & Pereverzoff 2003; Hay & Castilla 2008). Objects were generated using the multi-resolution image segmentation algorithm in the

eCognition software program. A scale parameter suitable for identifying salt-affected areas was determined through experimentation and visual interpretation. A scale parameter of two was found to produce objects that are sufficiently homogenous (i.e. slightly over-segmented). All four pansharpened SPOT-5 bands were used as input for the segmentation. The same set of objects was used for each supervised classification implementation. Each of the six supervised classifiers was trained separately using the different feature sets outlined in Table 4.4.

The classifiers were trained using 60% of the reference data, while the remaining 40% was used for accuracy assessment purposes. Error matrices representing the classified areas relative to the reference areas were produced for each classifier from which the overall accuracy and the kappa statistic was extracted (Congalton & Green 2009). The training and accuracy assessments sample sets were kept consistent for all the classifiers for comparison purposes.

4.4 RESULTS AND DISCUSSIONS

4.4.1 Spectral analysis

Figure 4.2 shows the spectral profiles of salt-affected (EC > 4.0 dS/m) and unaffected (EC < 4.0 dS/m) crops in the Vaalharts irrigation scheme. Compared to healthy crops, salt-affected crops generally have a higher reflectance in the blue to red region of the electromagnetic spectrum, while reflectance is lower in the near and shortwave infrared regions. This suggests that vegetation in salt-affected areas experience weaker growth (vegetation vigour) than in unaffected areas. This result is in accordance with the findings of Hick & Russell (1990), Tilley et al. (2007), Wang et al. (2002) and Zhang et al. (2011) and suggests that VIs that make use of the ratio between the red and NIR bands have the potential to distinguish between salt-affected and unaffected crops. However, the relatively high standard deviation in the NIR region (indicated by error bars in Figure 4.2) indicates that an approach using VIs only might not be successful in all cases. The high standard deviation can be attributed to the fact that not all vegetation stress is directly related to salt accumulation and that vegetation types differ in its sensitivity to salinity.

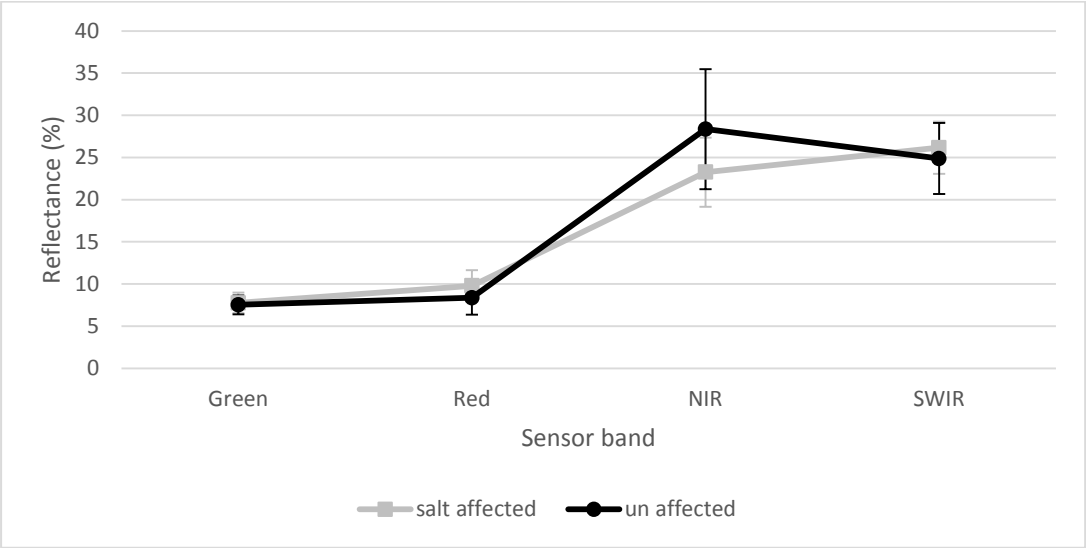

Figure 4.2 Spectral profiles of salt-affected (n = 19; EC >4.0 dS/m) and unaffected (n = 50; EC < 4.0 dS/m) vegetation as extracted from the SPOT-5 image of Vaalharts with error bars indicating one standard deviation

The spectral profiles of the samples taken in the Breede River irrigation scheme (Figure 4.3) differs from in the expected profile in that salt-affected samples generally have a higher reflectance in all the bands. This is most likely due to the presence of background soil reflectance, as the predominant crops in the Breede River area are wine grapes and pruning fruit trees, which are planted in rows and separated by bare soil for easy access during harvesting. In addition, visible salt encrustations on bare soil are known to have high reflectance in the visible and NIR regions (Abood, Maclean & Falkowski 2011; Elnaggar & Noller 2010; Iqbal 2011; Khan et al. 2005; Metternicht & Zinck 2009; Metternicht & Zinck 2003; Rao et al. 1995; Setia et al. 2013; Sidike, Zhao & Wen 2014), which may further contribute to the atypical shape of the salt-affected profile in Figure 4.3. This result suggests that VIs will be less effective for differentiating between salt-affected and unaffected crops in the Breede River irrigation scheme and that other image features such as intensity, image texture, principal components, or even the image bands themselves, may provide better discriminations of these classes.

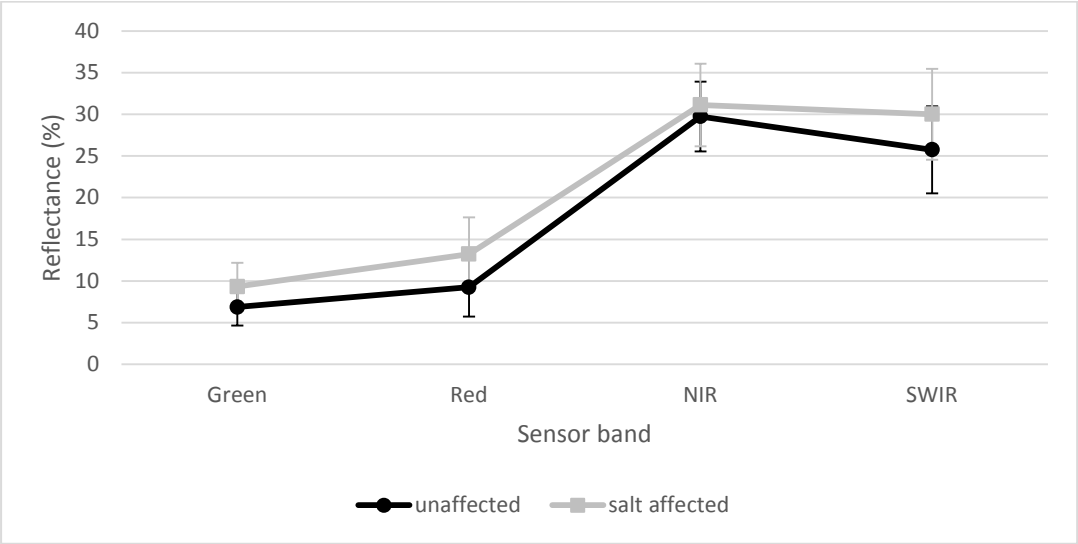

Figure 4.3 Spectral profiles of salt-affected (n = 23; EC > 4.0 dS/m) and unaffected (n = 25; EC < 4.0 dS/m) vegetation as extracted from the SPOT-5 image of the Breede River with error bars indicating one standard deviation

4.4.2 Regression modelling

A series of regression modelling procedures were carried out to identify the individual or combinations of image features that best relate to salinity levels (as represented by EC). For either study areas, none of the singular (curve fit) or multiple linear regression models (SLR, PLS) produced any significant results and none of the 78 features paired with the EC values produced a model with an R-squared value greater than 0.4. This result contradicts findings of Hamzeh et al. (2012a) and Leone et al. (2007) who showed that strong relationships (R-square values greater than 0.65) between soil salinity and vegetation response exist. However, these studies focused on a single crop type and a likely explanation for the poor performance of the regression modelling in this study might be that different crops with varying tolerances to saline conditions were considered (Hanson, Grattan & Fulton 2006; Zhang et al. 2011). Better results would likely have been obtained if each individual crop type were considered independently. However, this would require accurate crop type data, which was not available for the study areas and is often not routinely available at scheme level. Also, the different growth stages of crops (even of the same type) planted at different times and in separate fields is also a source of variation and probably had a negative impact on the success of regression models.

4.4.3 Feature selection

It is clear from the VILs in Table 4.7 that VIs played an important role in the CART and RF analyses of Vaalharts, confirming the observations made based on Figure 4.2. Texture measures also featured strongly in this irrigation scheme.

Table 4.7 Six most important variables in Vaalharts according to CART and RF respectively

CART		Random Forests	
Feature	**Variable Importance %**	**Feature**	**Variable Importance %**
EVI2	100.00	Histex, Variance algorithm; M = Red layer (Table 4.3)	100
Histex, Median algorithm; M = NIR layer (Table 4.3)	58.89	SAVI	89.6632
SAVI	51.63	Histex, Median algorithm, M = NIR layer (Table 4.3)	82.9395
NDVI	51.63	NDVI	81.7054
Histex, Energy algorithm; M = NIR layer (Table 4.3)	44.53	GVMI	76.9302
Histex, Mean algorithm; M = NIR layer (Table 4.3)	44.53	Histex, Mean deviation algorithm; M = Red layer (Table 4.3)	74.4403

All of the important indirect indicators of salt accumulation in the Breede River relate to texture measures (Table 4.8). Although it was expected (based on the spectral profiles in Figure 4.3) that VIs will not feature as strongly as in Vaalharts, the strong influence of texture over other features (e.g. intensity and principal components) was unforeseen. At closer inspection, it was determined that the importance of texture measures can be attributed to the woody vines and orchards that make up the majority of the crops in the Breede River. Because these crops are planted in rows, they are characterized by high levels of image texture. A reduction in biomass caused by saline conditions results in a dramatic reduction in texture as it increases reflectance from the soil background and thereby reduces the contrast between the planted and unplanted rows. This effect is amplified by the relatively low root zone salt tolerance threshold (*A*) and high deterioration slope (*B*) of these crops (Table 4.1) which can lead to rapid reductions in biomass under saline conditions.

Table 4.8 Six most important variables in Breede River according to CART and RF respectively

CART		Random Forests	
Feature	**Variable Importance %**	**Feature**	**Variable Importance %**
Histex, Mean Euclidean distance algorithm; M = PCA layer(Table 4.3)	100.00	Histex, Mean deviation algorithm; M = PCA layer (Table 4.3)	100
Histex, Mean Euclidean distance algorithm; M = Red layer (Table 4.3)	89.68	Histex, Variance algorithm; M = PCA layer (Table 4.3)	83.2958
Histex, Mean Euclidean distance algorithm; M = Green layer (Table 4.3)	88.98	Histex, Mean Euclidean distance algorithm; M = PCA layer (Table 4.3)	76.4266
Histex, Mean Euclidean distance algorithm; M = SWIR layer (Table 4.3)	80.17	Histex, Mean Euclidean distance algorithm; M = Green layer (Table 4.3)	72.194
Histex, Variance algorithm; M = Red layer (Table 4.3)	80.17	Histex, Mean Euclidean distance algorithm; M = Red layer (Table 4.3)	68.1412
Histex, Variance algorithm; M = Green layer (Table 4.3)	78.97	Histex, Mean deviation algorithm, M = Red layer (Table 4.3)	65.5552

4.4.4 Supervised Classification

4.4.4.1 Summary of error matrices

Each of the six supervised classifiers were applied to seven different sets of input features (Table 4.4) namely: all the features (Feature Set A, n = 73); only the spectral bands (Feature Set B, n = 4); only the VIs (Feature Set C, n = 4); only the texture measures (Feature Set D, n = 60); and a combination of the image transformations (PCA, IHS) (Feature Set E, n = 5). Two additional feature sets (F, n = 6 and G, n = 6), representing the first six features of the VILs generated by CART and RF respectively, were also used as separate inputs to the classifiers.

The overall accuracy (OA) and Kappa coefficient (KC) for each feature set and classifier, as extracted from the error matrices are listed in Table 4.9 and Table 4.10 for Vaalharts and Breede River respectively.

Table 4.9 Summary of average and individual classifiers for Vaalharts

Feature Set	**SVM 1**		**SVM 2**		**NN**		**ML**		**DT**		**RF**		***Mean***		***STDDEV***	
	OA	**KC**	**OA**	**KC**	**OA**	**KC**	**OA**	**KC**	**OA**	**KC**	**OA**	**KC**	***OA***	***KC***	***OA***	***KC***
All features (A)	76.5	0.50	78.9	0.54	79.8	0.60	73.7	0.38	86.9	0.72	85.8	0.70	***80.3***[a]	*0.58*	*4.73*	*0.12*
Bands (B)	70.6	0.39	68.7	0.36	79.6	0.58	69.4	0.40	64.6	0.20	77.3	0.53	*71.7*	*0.41*	*5.18*	*0.12*
VIs (C)	77.9	0.55	70.3	0.40	59.8	0.14	72.7	0.49	76.1	0.48	76.9	0.51	*72.3*	*0.43*	*6.15*	*0.14*
Texture (D)	82.5	0.62	82.0	0.60	79.8	0.60	62.9	0.06	81.4	0.60	77.3	0.50	*77.7*	*0.50*	*6.83*	*0.20*
Image transform (E)	76.3	0.51	83.4	0.65	73.8	0.48	77.6	0.57	56.8	0.04	78.4	0.56	74.4	0.47	*8.39*	*0.20*
CART VIL (F)	77.8	0.56	78.7	0.56	58.6	0.08	71.1	0.46	69.5	0.30	80.4	0.59	*72.7*	*0.42*	*7.44*	*0.18*
RF VIL (G)	69.3	0.34	70.0	0.38	78.8	0.57	63.8	0.23	**92.9**[c]	0.85	82.2	0.63	*76.2*	*0.50*	*9.67*	*0.21*
Mean	*75.8*	*0.50*	*76.0*	*0.50*	*72.9*	*0.43*	*70.2*	*0.37*	*72.6*	*0.46*	***79.8***[b]	*0.57*				
Standard deviation	*4.20*	*0.09*	*5.72*	*0.11*	*8.87*	*0.21*	*4.91*	*0.16*	*10.1*	*0.27*	*3.06*	*0.07*				

[a] Best feature set result; [b] Best classifier result; [c] Best classification resul

Table 4.10 Summary of average and individual classifiers for Breede River

Feature Set	SVM 1		SVM 2		NN		ML		DT		RF		*Mean*		*STDDEV*	
	OA	**KC**	**OA**	**KC**	**OA**	**KC**	**OA**	**KC**	**OA**	**KC**	**OA**	**KC**	***OA***	***KC***	***OA***	***KC***
All features (A)	88.4	0.76	83.2	0.64	86.9	0.74	88.4	0.76	72.5	0.49	72.5	0.49	*82.0*	*0.65*	*6.9*	*0.12*
Bands (B)	88.4	0.76	75.1	0.53	84.2	0.69	81.9	0.64	88.4	0.76	88.4	0.76	*84.4*	*0.69*	*4.9*	*0.09*
VIs (C)	79.3	0.60	79.3	0.60	72.0	0.48	74.8	0.53	70.5	0.46	70.5	0.46	*74.4*	*0.52*	*3.7*	*0.06*
Texture (D)	**91.6**[c]	0.81	91.3	0.80	86.9	0.74	88.4	0.76	72.5	0.49	76.8	0.56	***84.6***[a]	*0.69*	*7.3*	*0.12*
Image transform (E)	75.1	0.53	88.4	0.76	78.3	0.58	84.2	0.69	74.8	0.53	72.0	0.48	*78.8*	*0.60*	*5.7*	*0.10*
CART VIL (F)	83.1	0.61	83.1	0.61	84.9	0.64	83.6	0.62	79.8	0.54	78.5	0.48	*82.2*	*0.58*	*2.2*	*0.05*
RF VIL (G)	82.6	0.59	82.6	0.59	84.9	0.64	84.3	0.64	78.3	0.50	85.7	0.67	*83.1*	*0.61*	*2.4*	*0.06*
Mean	*82.8*	*0.67*	***83.3***[b]	*0.65*	*82.6*	*0.64*	***83.7***[b]	*0.66*	*76.7*	*0.54*	*77.8*	*0.56*				
Standard deviation	*4.73*	*0.10*	*4.98*	*0.09*	*5.08*	*0.08*	*4.26*	*0.08*	*5.68*	*0.10*	*6.45*	*0.11*				

[a] Best feature set result; [b] Best classifier result; [c] Best classification result

4.4.4.2 Vaalharts discussion

In Vaalharts Feature Set A produced the best classification result with a mean OA and KC of 80.3% and 0.58 respectively (Table 4.9). The relatively high accuracy achieved when using the full feature set supports the findings of Myburgh & Van Niekerk (2013) who showed that most of the classifiers considered (in particular SVM, DT and RF) are relatively insensitive to the so-called "curse of dimensionality". When mapping salinity stress Hamzeh et al. (2012b) similarly found that a larger feature set (multiple hyperspectral bands) performed similarly well or even outperformed smaller feature sets (VIs, PCA) when using the SVM classifier. The RF feature selection strategy produced comparable mean results (OA 76.2%; KC 0.50) while the CART feature selection generally produced lower accuracies. Generally, the mean OA of the features and classifiers are relatively high (72.7-80.3%), but the relatively low (0.42-0.58) mean KC values suggest only a fair to moderate agreement between modelled and observed salt accumulation when accounting for chance (Viera & Garrett 2005).

The relatively poor performances of the feature selection strategies suggest that the feature selection process was too aggressive. The inclusion of more than six features in the VILs might have provided better results. Nevertheless, the feature selection strategy resulted in very good classifications in some cases. For instance, the best classification result for Vaalharts was achieved when the DT classifier was applied to Feature Set G, which consisted of the six best features according to the RF VIL. This combination produced an OA of 92.9% and KC 0.85

which is much higher than when the full set of features was used for the same classifier (OA=86.9; KC=0.72) (Figure 4.4). Although Figure 4.4 illustrate a good agreement between the in situ data and the classification, it seems like the classifier overestimates salt-affected areas. These misclassifications are mainly attributed to the differences in vegetation response between different crop types and other factors such as poor farming practices or soil compaction.

On average, the most successful classifier in Vaalharts was RF, with a mean OA of 79.76% (Table 4.9). To our knowledge, RF has not been applied for identifying salt accumulation in published literature, and this result suggests that this classifier holds much potential for this purpose. The relatively good performance of RF is attributed to its ability to produce accurate classifications with limited training data (Ham et al. 2005; Mountrakis, Im & Ogole 2011). RF is also non-parametric and consequently has the capability to perform well with data that is not normally distributed, as was the case in this study.

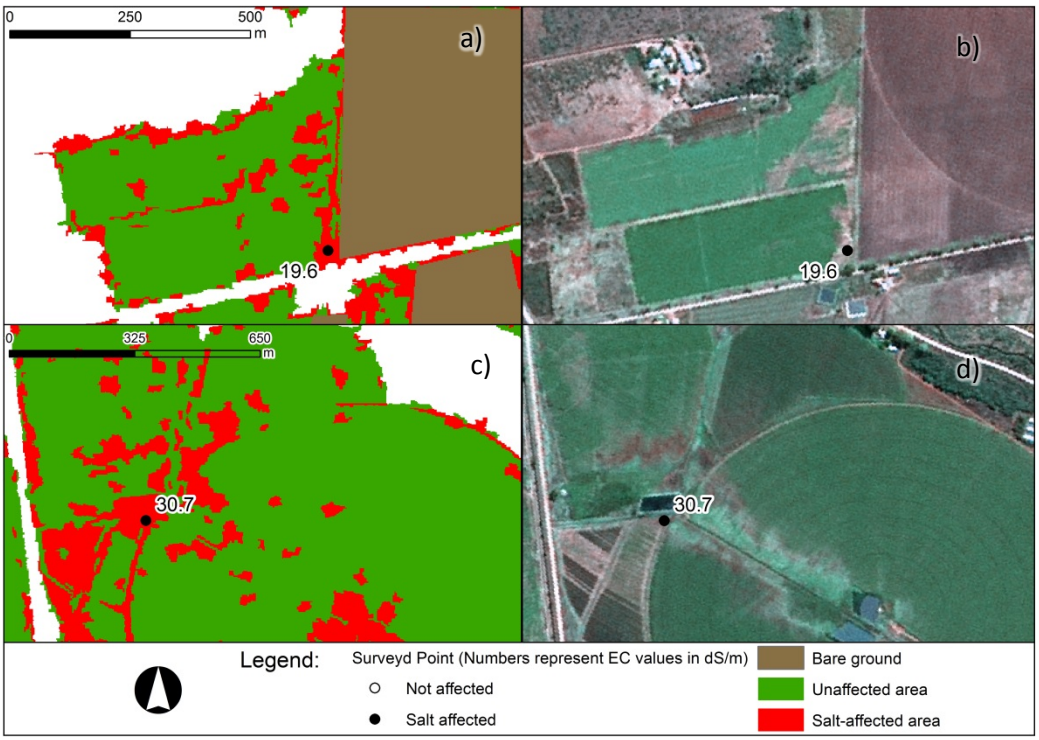

Figure 4.4 DT classification results (a and c) using Feature Set G in two detail areas within the Vaalharts irrigation scheme. On the right true colour images of the same areas are provided for comparison purposes (b and d).

4.4.4.3 Breede River discussion

Feature Set D (texture measures) was the most successful set of features in the Breede River study area, producing a mean OA and KC of 84.6% and 0.69 respectively (Table 4.10). The individual best-performing classification was with the SVM1 classifier using feature set D with a 91.6% OA and a KC value of 0.81 (Figure 4.5). Very similar accuracies were achieved when the original bands (Feature Set B) were used as input (OA=88.4; KC=0.76). Compared to

Vaalharts, the feature selection strategies were more successful in the Breede River, with both the CART (Feature Set F) and RF (Feature Set G) methods providing higher mean accuracies compared to when all the features were considered (Feature Set A). Feature Set C (VIs) produced the poorest classification results in the Breede River area. This result was anticipated given the spectral profiles of the classes shown in Figure 4.3. Feature Set E, containing the image transformation data (e.g. PCA and IHS), unexpectedly produced relatively poor results. Although Figure 4.3 shows that salt-affected areas generally have higher reflectance responses in all bands, it seems that this relationship is not consistent (supported by the large standard deviations in Figure 4.3 and that the classifiers were unable to successfully separate the classes using image transformation features such as intensity and the first principal component).

Overall, SVM2 and ML produced the best classifications with a mean OA of 83.29% and 83.66% respectively (Table 4.10). This result corresponds with the findings of Hamzeh et al. (2012b) and Bouaziz, Gloaguen & Samir (2011) in which SVM outperformed other classifiers (e.g. spectral angle mapper, minimum distance & ML) for detecting salt-affected areas. The good performance of the SVM classifier is attributed to its ability to find support vectors with limited training data (Pal & Mather 2005). SVM has the added advantage of being a binary (2-class) classifier, which is ideal for differentiating between salt-affected and unaffected areas. In spite of its sensitivity to high feature dimensionality, ML performed surprisingly well in the Breede River study area.

Generally, higher accuracies were achieved in Breede River compared to Vaalharts and the higher mean KC values (0.52-0.69) of Breede River suggest a fair to substantial agreement when chance is taken into consideration (Viera & Garrett 2005). The higher accuracies in the Breede River area are attributed to the lower variation in crop types (Table 4.1).

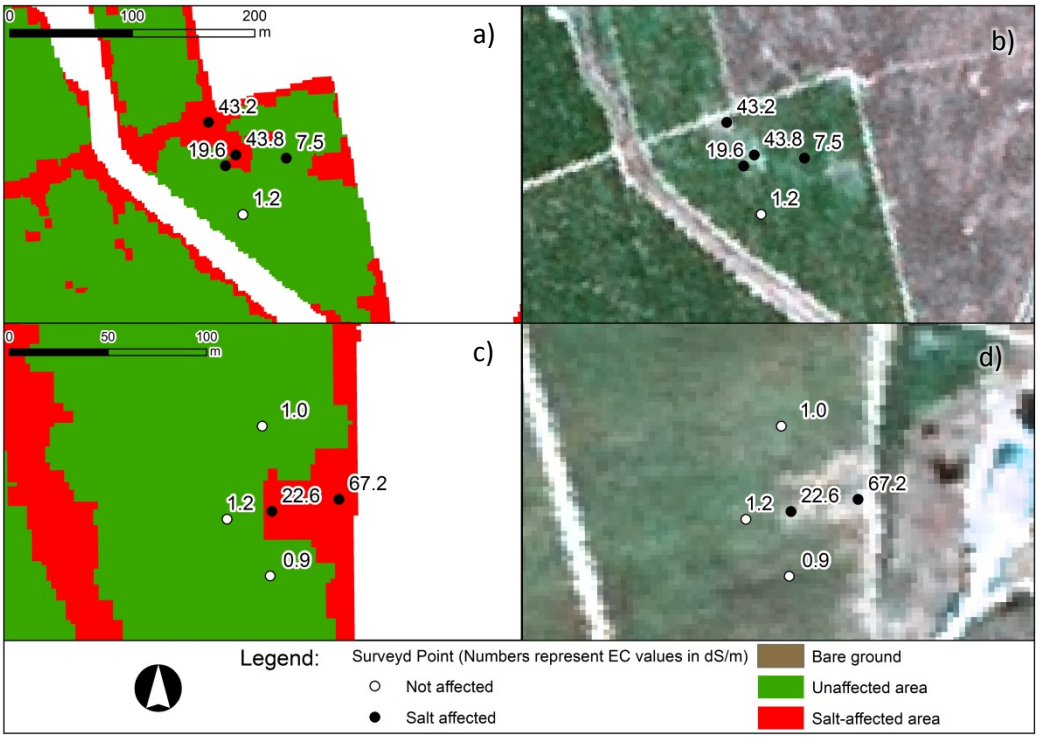

Figure 4.5 SVM classification result using Feature Set D in two detail areas within the Breede River irrigation scheme (a and c). On the right true colour image combination (b and d)

4.4.4.4 General discussion

A key finding of this study is that none of the feature sets and/or classification algorithms stood out as being superior for monitoring salt accumulation at irrigation scheme level. At best, the feature set which showed the most consistency in identifying salt accumulation on a scheme level was image texture (77.7% OA in Vaalharts and 84.6% OA in Breede River). This finding is notable as, to our knowledge, no published research on the use of image texture for indirectly classifying salt accumulation exists. Image texture has great potential for operational salt accumulation monitoring as it will likely be more stable and transferable than VIs at scheme level. However, more research is needed to test this hypothesis.

Due to the large variations in how different crops respond to saline conditions, the classifications in this study tended to produce many false positives (over-classification). This suggests, in agreement with Metternicht (1996), that supervised classification methods can be used as a scoping mechanism for identifying salt accumulation in cultivated fields and that the identified areas should be visited to determine the extent of accumulation. Supervised classification of remotely sensed imagery can consequently be used to reduce in situ monitoring, but more work is needed to find earth observation solutions that can be applied for operational monitoring of salt accumulation in large, complex irrigation schemes.

One approach to overcome some of the limitations of supervised classification is to shift the focus from scheme level to field level. An evaluation of each individual field (planted with a single crop type) relative to itself might reduce the temporal and spatial variances of crop types and their salinity tolerances. The use of multi-temporal imagery might help in determining whether an area within a field is consistently experiencing poor vegetation growth (Abdelfattah, Shahid & Othman 2009; Caccetta, Allen & Watson 2000; Furby et al. 1995; Lenney et al. 1996; Lobell et al. 2010). According to Furby et al. (1995), persistently poor vegetation cover over multiple growing seasons are more likely to be caused by salt accumulation than poor farming practices (Lenney et al. 1996). More work is needed to evaluate whether a field-based, multi-temporal approach will improve classification accuracies.

4.5 CONCLUSIONS

This study examined a number of indirect indicators for identifying salt-affected areas in cultivated fields at irrigation scheme level. Given that affected areas tend to occur in small patches within fields, 2.5 m pansharpened SPOT-5 high resolution satellite imagery was evaluated in two distinctly different South African irrigation schemes (Vaalharts and Breede River).

A series of regression analyses were carried out to evaluate the continuous relationships between the observed in situ salinity levels (represented by EC) and 78 different geospatial features. The results showed that all the regression models were insignificant, most likely due to the high levels of variation in the spectral responses of different crop types at different growing stages, coupled with their individual tolerances to saline conditions (Hanson, Grattan & Fulton 2006; Zhang et al. 2011).

A categorical, supervised classification approach to identifying salt-affected areas was also evaluated. CART and RF were used to reduce the dimensionality of the full feature set to two feature subsets, each containing the six most important features. Four other subsets of features (image bands; VIs; texture; image transformations) were also used as input to six different classification algorithms (ML, NN, RF, DT, and two implementations of SVM). The results showed that DT using the RF VIL as input (Feature Set H) produced the best result in Vaalharts (OA=92.9%; KC=0.85), while SVM1, using texture measures as input, produced the best result in Breede River (OA=91.6%; KC=0.81).

The high levels of accuracies achieved suggest that supervised classification of image features holds much potential for monitoring salt accumulation in agricultural areas. However, based on visual interpretations of the results and inputs from local experts it was determined that the

classifications tend to over-estimate salt-affected areas in both irrigation schemes and that the outputs can at best be used as a scoping mechanism for monitoring salt accumulation. More work, possibly using a multi-temporal approach at individual field level, is needed to find robust solutions for routine monitoring of salt accumulation in large complex irrigation schemes.

CHAPTER 5: QUANTIFICATION OF SALT-AFFECTED AND WATERLOGGED AREAS IN SELECTED SOUTH AFRICAN IRRIGATION SCHEMES USING A MULTI-TEMPORAL GEOBIA APPROACH[1]

5.1 INTRODUCTION

The complex nature of irrigation schemes poses a unique challenge for salt accumulation and waterlogging monitoring. The large variation in crop types and small field sizes, combined with the occurrence of salt accumulation and waterlogging in small patches, requires a transferable, robust methodology. In Chapter 3 a good relationship between image features and soil EC values was found at individual field level. Chapter 4 demonstrated that the use of a single classification technique or feature set at scheme level is not sufficiently transferable or accurate for quantifying and monitoring purposes. Seasonal variability of vegetated and fallow fields necessitates the combination of both the indirect and direct approach to provide useful information about the status of salt accumulation and waterlogging. Based on the experiments of Chapters 3 and 4, it seems that a field-based approach, where a crop would be evaluated relative to itself, would reduce the variances introduced by different crop types in different growing stages and with different salinity tolerances. A field-based approach would additionally enable the use of both direct and indirect indicators.

In this chapter, a rule-based classification approach, which delineates patches within each field with significantly different spectral properties compared to the rest of the field (i.e. anomalies), is proposed. The technique applies geographical object-based image analysis (GEOBIA) on multi-temporal SPOT-5 imagery. The methodology was applied to nine different irrigations schemes across South Africa. In contrast to Chapters 3 and 4, which focused exclusively on the identification of salt accumulation, both salt accumulation and waterlogging is targeted in this new approach as they are strongly related (Section 1.1.1). The results are discussed and interpreted in the context of finding an operational solution to salt accumulation and waterlogging in South Africa. The chapter concludes with an overview of remaining challenges and recommendations for further work are made.

[1] This chapter is structured as an article with the intention to submit it to a journal for publication. An in depth discussion of the rationale and literature is excluded to reduce duplication from previous chapters.

5.2 METHODS

5.2.1 Study areas

To represent the true variability of South African irrigation schemes, nine schemes across the country, namely Vaalharts, Loskop, Makhatini, Olifants River, Tugela River, Breede River, Sundays River, Pondrif and Douglas, were selected for analysis. Figure 5.1 shows the location of each scheme. A short description of each scheme follows. Overviews of Vaalharts and Breede River are excluded here as they were described in Section 4.3.1.

Loskop Irrigation Scheme

The Loskop irrigation scheme is located in the Limpopo province, intersecting the towns of Marblehall and Goblersdal. The scheme forms part of the Olifants River basin, where salinization has been identified as the main agricultural pollution problem (Aihoon, Groenewald & Sartorius Von Bach 1997). The area is situated at 916 m above sea level and the geography ranges from mountainous bushveld to undulating terrain with thorn trees (Tren & Schur 2000). The region comprises a mix of the central sandy bushveld region and the Springbokvlakte and Loskop thornveld regions (Mucina & Rutherford 2006). Loskop has a mean annual temperature of 20°C and a mean annual rainfall of 552 mm (Schulze 2006). The main crops grown in the scheme are citrus, table grapes, maize, wheat, soya bean, cotton, tobacco and groundnuts.

Makhatini Irrigation Scheme

The Makhatini irrigation scheme is situated in the KwaZulu-Natal (KZN) province east of the town Jozini and south of the Phongolo River. The scheme is situated 92 m above sea level in the Makhatini and Western Maputaland clay bushveld region (Mucina & Rutherford 2006) and has a humid subtropical climate with a mean annual temperature of 22°C and a mean annual rainfall of 577 mm (Schulze 2006). The majority of crops is sugar cane, while cotton and a variety of vegetables are also grown.

Tugela River Irrigation Scheme

Located 1104 m above sea level in the KZN province, the Tugela river irrigation scheme includes the towns Bergville and Winterton. Drained by the upper part of the Tugela River, the area falls within the moist grassland bioclimatic region of KZN (Mucina & Rutherford 2006). Over the past 30 years, the scheme has changed from furrow and overhead sprinkler irrigation to mainly centre pivot irrigation systems. The scheme has a mean annual temperature of 18°C and a mean annual rainfall of 745 mm (Schulze 2006). Crops grown in this area are mostly commodity

and industrial crops, mainly maize and winter wheat with soybeans as a rotational crop (Phipson 2012).

Olifants River Irrigation Scheme

The Olifants River irrigation scheme is located in the Western Cape and includes the towns of Lutzville and Vredendal. Irrigation water is provided by the Olifants River, which has the second largest catchment in South Africa. Bordering the Atlantic Ocean, the scheme has a mean elevation of 31 m above sea level and consists mainly of the Namaqualand Riviera region (Mucina & Rutherford 2006). The mean annual temperature of the area is 18.5°C, while the mean annual rainfall is 134 mm (Schulze 2006). Crops in this region are mostly grapes and citrus.

Sundays River Irrigation Scheme

The Sundays River irrigation scheme is located at 83 m above sea level at the foot of the Eastern Cape, bordering the Indian Ocean. Major settlements in the vicinity of the irrigation scheme are Addo and Kirkwood. The scheme is situated predominantly between two series of alluvial terraces, and according to Mucina & Rutherford (2006) forms mostly part of the Albany alluvial vegetation region. Sundays River has a mean annual temperature of 18.5°C and a mean annual rainfall of 380 mm (Schulze 2006). Citrus is the dominant crop in this irrigation scheme.

Pondrift Irrigation Scheme

The Pondrift irrigation scheme receives its water supply from the Limpopo River, which forms the boundary between the Limpopo province, Zimbabwe and Botswana. The scheme, located in the northern-most water management area near the town of Pondirft, has a mean height of 506 m above sea level. The area consists of alluvial deposits from the Quaternary system and forms part of the subtropical alluvial vegetation region (Mucina & Rutherford 2006). The mean annual temperature in the Pondirft irrigation scheme is 22°C and the mean annual rainfall is 314 mm (Schulze 2006). Cotton, grain sorghum and tobacco are the main crops in this region.

Douglas Irrigation Scheme

The Douglas irrigation scheme receives water from the Orange and Vaal rivers and is located in the eastern part of the Northern Cape near the towns of Douglas and Salt Lake. The irrigation scheme is located 1014 m above sea level and has a mean annual temperature of 19°C. The mean annual rainfall is 293 mm (Schulze 2006). Accoding to Armour (2002), 28% of the area is flood irrigated while 70% is sprinkler irrigated. The trend is, however, towards the conversion to centre pivots. The region comprises a combination of the upper Gariep alluvial vegetation and

the Kimberly thornveld regions (Mucina & Rutherford 2006). Main crops grown in this irrigation scheme are wheat, maize, lucerne, potatoes, cotton and groundnuts (Armour 2002).

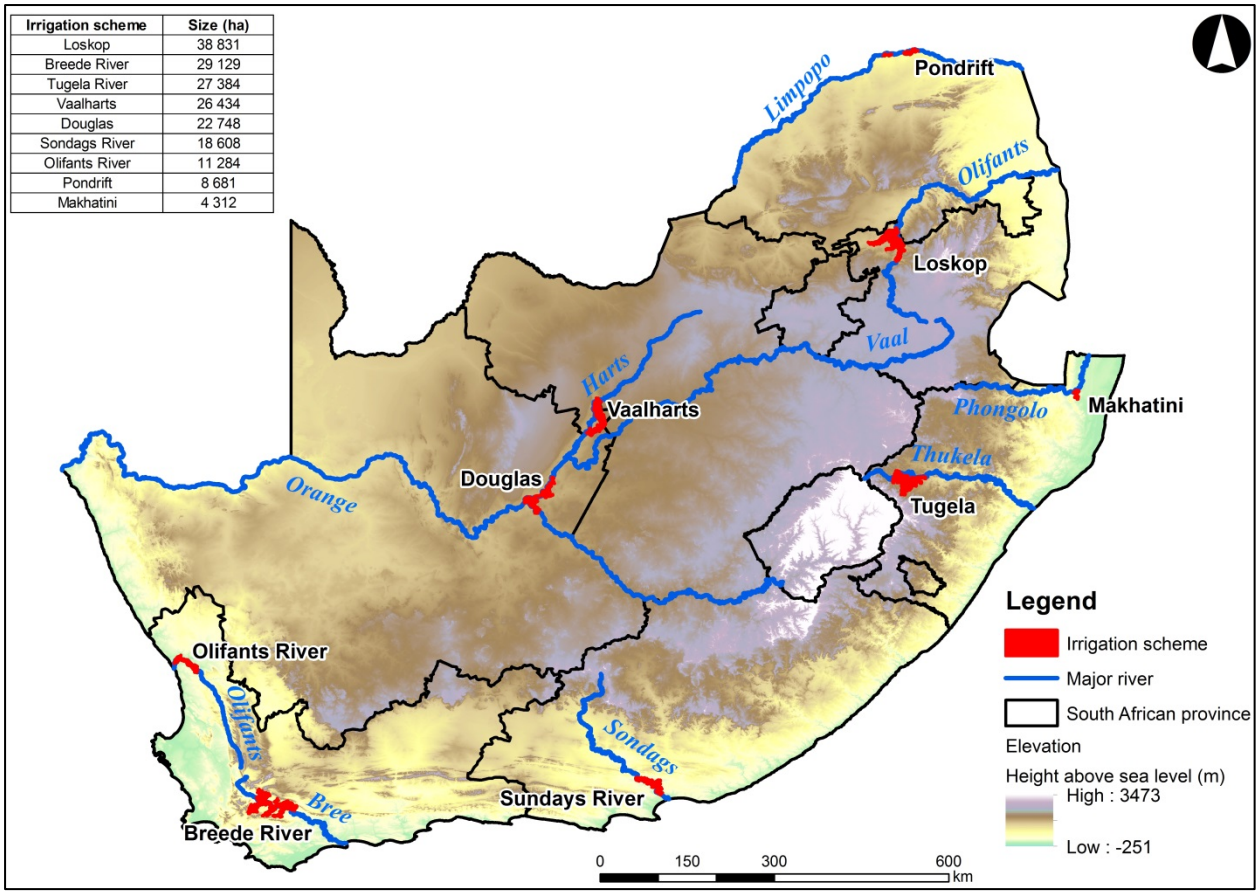

Figure 5.1 Geographical distribution of the nine irrigation schemes across South Africa, with elevation data as backdrop

5.2.2 Within-field anomaly detection (WFAD)

Vegetation response, as an indirect indicator of salt accumulation, is ambiguous because of varying tolerances of plants to saline or waterlogged conditions. This is exacerbated by crops being in different growing phases, as it confounds inter-field response comparisons (Hanson, Grattan & Fulton 2006; Zhang et al. 2011). Direct indicators are similarly ambiguous as they can vary from white salt crusts to greasy black surfaces and surface ponding (McGhie & Ryan 2005). To effectively quantify salt accumulation and waterlogging at a scheme level, each of these indicators needs to be considered. However, developing a methodology to identify each unique indicator separately will result in a highly complex system. Such an approach will likely not be robust as the indicators may vary from region to region.

The indicators of salt accumulation and waterlogging share a common characteristic that can be exploited for their detection and delimitation. If it can be assumed that a salt accumulation or waterlogging indicator only affects a part of a field (i.e. is spatially smaller than the entire field

in which it occurs), each indicator will appear as an area of abnormality (anomaly) in an otherwise spectrally homogenous field. When such an anomaly is compared to the average spectral response of the field in which it occurs, it becomes more apparent. Conceptually, this approach – called WFAD – would be ideal for the characteristically small and patchy nature of salt-affected and waterlogged areas in South African irrigation schemes (see Section 3.3, Figure 3.2) and would be applicable to both fallow and vegetated fields. Potentially, the WFAD should also accommodate the limitations posed by the spectral ambiguity of direct and indirect indicators of salt accumulation and waterlogging. For example, using this approach in a wheat field that has a relatively high root zone salinity tolerance (Section 4.3, Table 4.1), the anomaly would be compared to the wheat field itself and not to a more sensitive maize field. The following sections explain how the WFAD method was implemented and evaluated in the nine study areas.

5.2.3 Data collection and preparation

According to Lobell et al. (2010), the risk of producing poor results is high when single date remotely sensed imagery is used to identify salinity. When using multi-temporal remote sensing data, certain characteristic trends become more apparent, and if poor vegetation conditions persist throughout multiple growing seasons, they are more likely to be caused by salt accumulation (Furby et al. 1995; Lenney et al. 1996). Two-year multi-temporal SPOT-5 scenes covering most of the nine study areas were consequently acquired from the South African National Space Agency (SANSA). In some areas, multiple scenes were required as a single SPOT-5 scene did not cover the full extent of the study area (Table 5.1). With a relatively high temporal resolution and the capability of pan-fusing multispectral bands to 2.5 m, SPOT-5 imagery provides a cost-effective alternative to other VHR alternatives such as WorldView-2, QuickBird or IKONOS imagery.

Table 5.1 SPOT-5 scenes acquired for the study areas

Irrigation Scheme	Scene Date
Vaalharts	27 April 2012
	20 Feb 2011
Loskop	30 Sept 2012
	3 June 2012
	18 May 2012
	15 June 2011
	5 May 2011

	17 Aug 2011
Makhathini	26 July 2012
	2 Aug 2011
Tugela	22 March 2012
	1 Aug 2011
Olifants	26 Jan 2013
	10 April 2012
Breede	16 Jan 2013
	26 Feb 2013
	26 March 2012
	11 Dec 2012
Sundays	18 Feb 2013
	12 April 2012
Pondrift	23 Feb 2013
	12 March 2012
Douglas	13 Aug 2013
	16 April2013

Geometric and radiometric corrections of all images were done using the software package PCI Geomatica (v 2013 SP2), while the nearest neighbour method was used to do all necessary resampling during pre-processing in order to preserve the original digital numbers (DN) (Campbell 2007; Lillesand, Kiefer & Chipman 2004). A north-oriented implementation of the Gauss conform coordinate system (also known as the LO coordinate system), with the central meridian adjusted for each scheme, was used. The mathematical model ATCOR-2 was employed to convert the DN's into percentage reflectance, while the Pansharp algorithm was used to increase the resolution of all the 10 m and 20 m multispectral bands to 2.5 m.

To compare each field to itself, detailed field boundaries were needed for each study area. Field boundaries in GIS vector format were obtained from the Department of Agriculture, Forestry and Fisheries and refined and improved for each area using manual editing.

Field surveys were conducted from June 2012 to October 2014 to collect suitable reference data. Accessibility was often restricted by canal systems and fencing, but an attempt was made to include sites that represent great variation in terms of salt accumulation, waterlogging and unaffected areas. Surveyed points varied from being clustered to being randomly spaced across

each scheme. The location of the surveyed points was guided by an initial analysis of each area and expert knowledge of the scheme (i.e. areas known to be affected).

Soil samples were collected by means of a soil auger and analysed for its electroconductivity (EC) value using laboratory analyses (saturated paste technique). Soil samples with EC values of 4.0 dS/m or higher were regarded as being salt-affected. Some waterlogging were caused by shallow or rising water tables and do not necessarily result in surface ponding (Dwivedi, Sreenivas & Ramana 1999). Waterlogging status in such areas can only be established by analysing the vertical soil profile, therefore this analysis was carried out up until 1 m below the soil surface at each sample site. Saturation of the top soil was determined in situ to identify waterlogging status. All survey points were accompanied by a GPS coordinate, notes on the visual appearance of the immediate area and in some cases a photograph was also recorded.

5.2.4 Applied GEOBIA

Sophisticated and well-established pixel-based techniques that successfully classify lower resolution images exist (Blaschke et al. 2014). However, high resolution images often lead to a high within-class spectral variability that can decrease the accuracy of pixel-based approaches (Hay, Niemann & McLean 1996). In this study, the extent of salt-affected and waterlogged areas are greater than that of the image pixels of the pan-fused SPOT-5 imagery (2.5 m), making it susceptible to within class variabilities. As discussed in Section 2.1.5.4, GEOBIA mimics higher order logic, similar to human interpretation, for identifying useful shapes, sizes and textures from image data (Campbell 2007).

The WFAD technique was implemented in eCognition Developer 8 and 9. The first step in the WFAD process is to perform image segmentation. The implementation of the segmentation for each of the nine irrigation schemes was based on three SPOT-5 spectral bands as they have higher spatial resolutions (10 m) compared to the SWIR band (20 m). Segmentation was done on each SPOT-5 image for each year. The scale factor of the multi-resolution segmentation (MRS) algorithm, which determines the size of the objects, was adjusted individually (using visual interpretation) to produce meaningful objects that best represent the levels of homogeneity within a field for each irrigation scheme.

Hierarchical segmentation, one of the spatial features of GEOBIA, enables more than one level of segmentation sharing inherent properties (Campbell 2007). For each individual scheme, the vector layer delineating the fields was used for the first (*parent*) segmentation level. Below the *parent* level objects, MRS was used to populate the *parent* objects with smaller *child* level

objects (Figure 5.2). Each *child* object inherits all the properties (e.g. mean, median, mean ratio and variance per band) of its relative *parent* object.

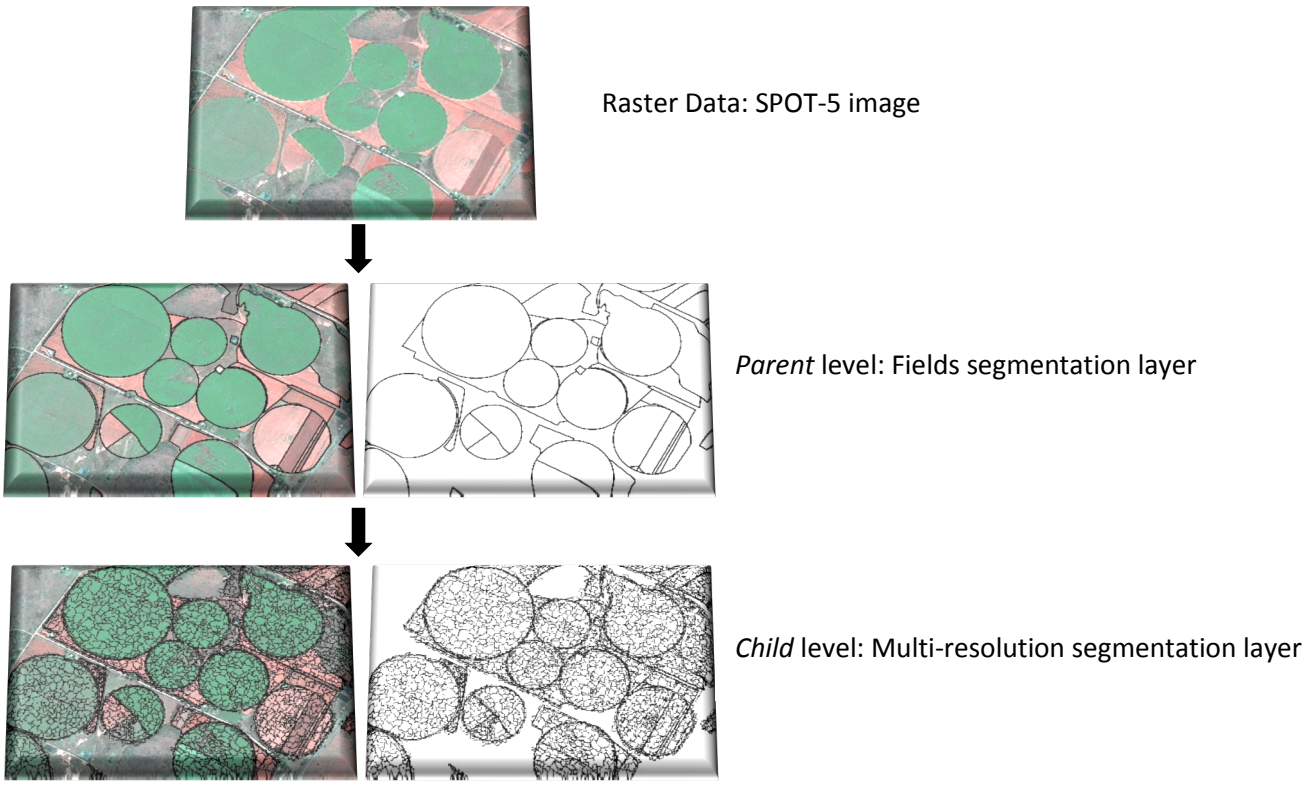

Figure 5.2 Hierarchical WFAD segmentation process

The second step in the WFAD process was to classify the image objects. Although a wide range of classification approaches and procedures to assign classes to the objects is available (see Section 2.1.5.3), a rule-based (expert system) classification approach was preferred as it has the ability to accommodate observable differences and changes within the data. A ruleset approach also does not require training data and the rules can progressively be applied and refined while maintaining full control of the classification process (Lucas et al. 2007).

Fields of each irrigation scheme were firstly classified as *vegetated* or *bare* on the *parent* level using the NDVI. Secondly, for the identification of anomalies, the spectral response of each *child* object was compared to the average spectral response of its relative *parent* object. If a substantial difference occurred between the *child* object and the relative *parent* object, the *child* objects were identified as an anomaly. This mean difference (MeaD) process is illustrated in Figure 5.3.

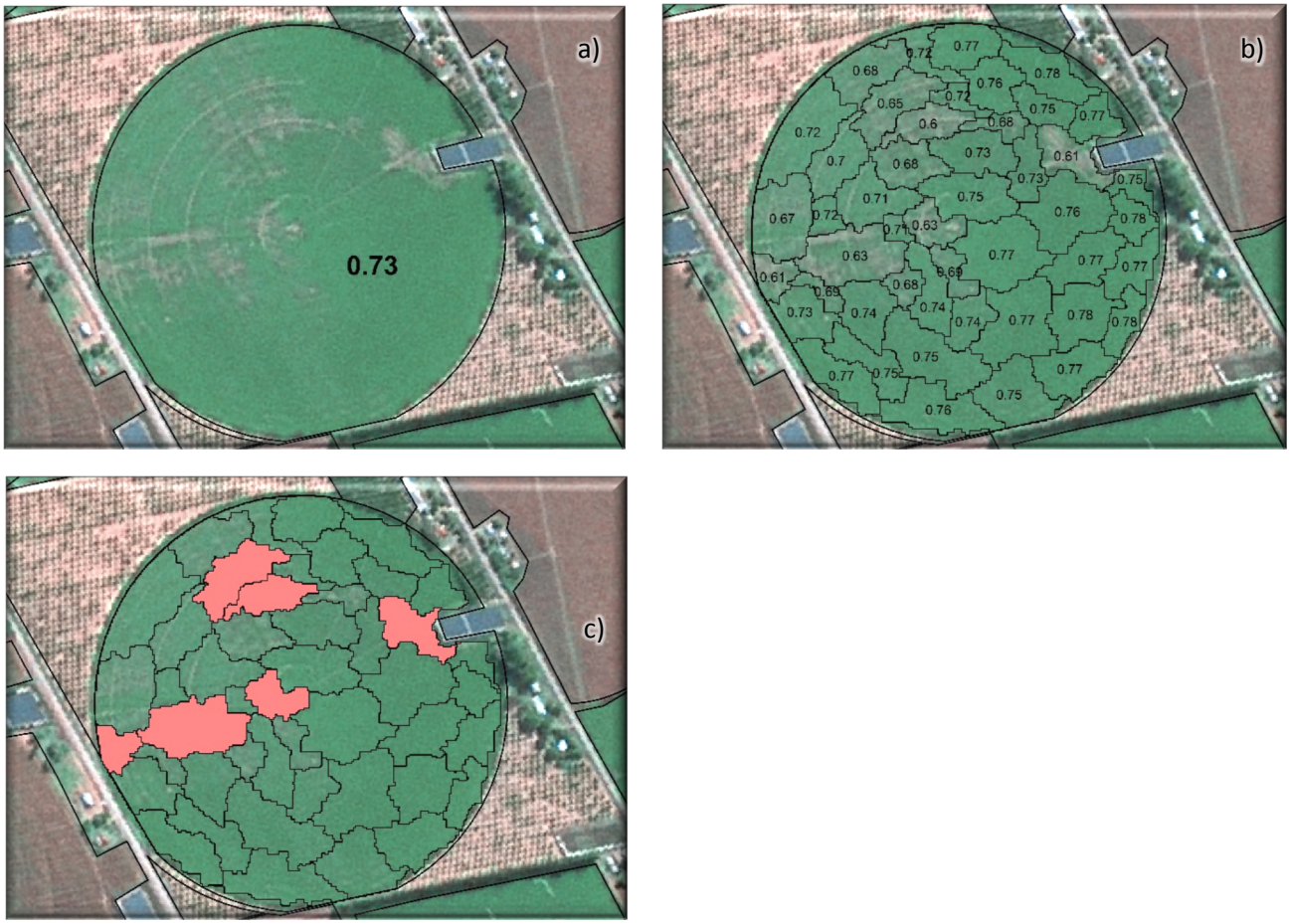

Figure 5.3 Mean difference threshold process. a) *Parent* level segmentation with mean NDVI value b) *Child* level segmentation with individual NDVI values c) Identified anomalies with MeaD equation when a threshold of -0.07 is applied.

A MeaD equation was used to identify threshold values that highlight anomalies with a substantially different spectral response. The equation is described as:

$$MeaD = SR_{Child\ object} - SR_{Relative\ Parent\ object} \quad \text{Equation 5.1}$$

where $SR_{Child\ object}$ is the mean spectral response of a child object; and

$SR_{Relative\ Parent\ object}$ is the mean spectral response of the relative parent object.

A positive MeaD threshold identifies a *child* object with a substantially higher spectral response compared to the relative *parent* object, while a negative MeaD threshold identifies a *child* object with a substantially lower spectral response compared to the relative *parent* object.

The spectral response used for comparing the *child* and *parent* objects differed for vegetated (indirect indicators) and fallow (direct indicators) fields to accommodate the different indicators for soil salinity and waterlogging.

The NDVI was used to identify anomalies in vegetated fields (Figure 5.3). Given that the main indicator of salt accumulation and waterlogging in vegetated fields is physiological stress (Abood, Maclean & Falkowski 2011; Fernández-Buces et al. 2006; Koshal 2010; Lenney et al. 1996; Lobell et al. 2010; Peñuelas et al. 1997; Wiegand et al. 1994; Zhang et al. 2011), only a negative MeaD threshold was implemented. Although halophytic vegetation can occur within vegetated fields, it was assumed that its vegetation response would be less than that of a commercially grown crop. Image texture was identified as a promising image transformation for indirect salinity detection (Chapter 3 and 4), but was not included in the implementation of the WFAD because it is still an unestablished method for salinity detection. Within the context of WFAD, image texture would only highlight the boundary between an affected and not-affected area due to brightness differences and as such is not of much use.

For fallow fields, the NDVI and a brightness band ratio (*Br*) (Equation 5.2) were used. A positive MeaD threshold was implemented for the NDVI on bare fields to identify potential halophytic plants (Dehaan & Taylor 2002; Dehaan & Taylor 2003; Dutkiewicz, Lewis & Ostendorf 2009a; Elnaggar & Noller 2010; García Rodríguez, Pérez González & Guerra Zaballos 2007). To detect salt encrustations, with generally high reflectance values in the visible and near-infrared regions, a positive MeaD threshold was used for the *Br* (Abood, Maclean & Falkowski 2011; Dwivedi & Sreenivas 1998; Elnaggar & Noller 2010; Iqbal 2011; Khan et al. 2005; Metternicht & Zinck 2003; Rao et al. 1995; Setia et al. 2013; Sidike, Zhao & Wen 2014). A negative MeaD threshold was used to accommodate the generally low reflectance values associated with waterlogging (ponding) (Dwivedi & Sreenivas 1998). The *Br* (brightness) can be defined as:

$$Br = (G + R + N)/3$$ Equation 5.2

where G is the reflectance in the green band;

R is the reflectance in the red band; and

N is the reflectance in the near-infrared band.

Because of its lower (20 m) resolution, the SWIR band was not included in the brightness ratio. The positive and negative MeaD threshold values were manually determined for each SPOT-5 image during analysis. To improve the automation of WFAD, further research should be directed towards achieving a higher level of image standardization in order to use single threshold values for all areas.

5.2.5 Multi-temporal analysis and quantification

A multi-temporal analysis was carried out for each scheme using the anomalies identified for both years. ArcGIS software was used for this purpose. Anomalies occurring in both years were exclusively considered as potential salt-affected or waterlogged areas. The multi-temporal analysis would potentially eliminate anomalies caused by factors unrelated to salt accumulation or waterlogging (Furby et al. 1995; Lenney et al. 1996; Lobell et al. 2010).

An anomaly ratio (*Ar*), describing the relationship between anomalies caused by salt accumulation and waterlogging and other non-related anomalies, was introduced to account for the likelihood of failing to completely eliminate all anomalies unrelated to salt accumulation or waterlogging. The *Ar* (Equation 5.3) was calculated using categories (A_{sw} and A_o) derived from the ground surveyed data of each scheme.

$$Ar = \frac{A_{sw}}{(A_{sw} + A_o)} \qquad \text{Equation 5.3}$$

where A_{sw} represents the anomalies related to salt accumulation or waterlogging; and

A_o represents anomalies related to other factors.

Final estimations of affected areas were calculated by using the *Ar* to alter the total percentage covered by the anomalies (Equation 5.4). The most recent extents of the anomalies were used for area calculations.

$$Quantification\ (\%) = ((Area_{anomalies}/Area_{total}) \times 100) \times Ar \qquad \text{Equation 5.4}$$

where $Area_{anomalies}$ represents the total area of anomalies in hectares; and

$Area_{total}$ represents the total area of fields in the relative irrigation scheme in hectares.

Because no training data was needed for the rule-based classification, the field surveyed points were exclusively used for testing the accuracy of the WFAD method. Accuracy assessment for each scheme was carried out to produce error matrices and the final quantification percentages.

5.3 RESULTS

Error matrices (also called confusion matrices) show the accuracies achieved by the WFAD method for each irrigation scheme (Table 5.2 to Table 5.10). The field verification columns represent three categories, namely *Salt-affected\Waterlogged*, *Stressed* and *Unaffected* areas. Anomalies that appear to be caused by salt accumulation and waterlogging (e.g. indicators such as plant stress and the occurrence of halophytic vegetation), but were found to show no sign thereof during the field surveys, are represented by the *Stressed* category. This category essentially represents anomalies unrelated to salt accumulation and waterlogging that the multi-temporal imagery was unable to eliminate. These observations were used to calculate *Ar*. Anomalies that were found to have been caused by salt accumulation and/or waterlogging were arbitrarily labelled "Anomaly1" in the error matrices, while the predicted observations that were verified to be caused by other factors were labelled as "Anomaly2". Given that the WFAD method does not differentiate between anomalies caused by salt accumulation and/or waterlogging, the User's Accuracy percentage for the two types of anomalies were combined for accuracy assessment purposes.

Table 5.2 Vaalharts irrigation scheme error matrix

Predicted data	Field verification data: Salt-affected/ Waterlogged	Stressed	Unaffected	Total	*User's Accuracy (%)*
Anomaly1	**18**	0	6	24	81.25
Anomaly2	0	**8**	0	8	
Not Anomaly	11	3	**24**	38	63.2
Totals	29	11	30	**70**	
Producer's Accuracy (%)	62.1	72.73	80		
Overall accuracy	**71.64**				
Kappa	**0.58**				

Table 5.3 Loskop irrigation scheme error matrix

Predicted data	Field verification data: Salt-affected/ Waterlogged	Stressed	Unaffected	Total	*User's Accuracy (%)*
Anomaly1	**35**	0	5	40	90.7
Anomaly2	0	**14**	0	14	
Not Anomaly	8	3	**25**	36	69.5
Totals	43	17	30	**90**	
Producer's Accuracy (%)	81.4	82.4	83.3		
Overall accuracy	**82.20**				
Kappa	**0.72**				

Table 5.4 Makhatini irrigation scheme error matrix

Predicted data	Field verification data: Salt-affected/ Waterlogged	Stressed	Unaffected	Total	*User's Accuracy (%)*
Anomaly1	**25**	0	6	31	86.04
Anomaly2	0	**12**	0	12	
Not Anomaly	5	0	**8**	13	61.54
Totals	30	12	14	**56**	
Producer's Accuracy (%)	83.3	100	57.14		
Overall accuracy	**80.4**				
Kappa	**0.672**				

Table 5.5 Tugela irrigation scheme error matrix

Predicted data	Field verification data: Salt-affected/ Waterlogged	Stressed	Unaffected	Total	*User's Accuracy (%)*
Anomaly1	**43**	0	10	53	85.3
Anomaly2	0	**15**	0	15	
Not Anomaly	5	3	**7**	15	46.67
Totals	48	18	17	**83**	
Producer's Accuracy (%)	89.58	83.33	41.18		
Overall accuracy	**78.3**				
Kappa	**0.6**				

Table 5.6 Olifants River irrigation scheme error matrix

Predicted data	Field verification data					
		Salt-affected/ Waterlogged	Stressed	Unaffected	Total	*User's Accuracy (%)*
	Anomaly1	**34**	0	13	47	79.7
	Anomaly2	0	**17**	0	17	
	Not Anomaly	6	0	**12**	18	66.67
	Totals	40	17	25	**82**	
	Producer's Accuracy (%)	85	100	48		
	Overall accuracy	**76.8**				
	Kappa	**0.6**				

Table 5.7 Breede River irrigation scheme error matrix

Predicted data	Field verification data					
		Salt-affected/ Waterlogged	Stressed	Unaffected	Total	*User's Accuracy (%)*
	Anomaly1	**26**	0	5	31	85.7
	Anomaly2	0	**4**	0	4	
	Not Anomaly	8	7	**35**	50	70
	Totals	34	11	40	**85**	
	Producer's Accuracy (%)	76.47	36.36	87.5		
	Overall accuracy	**76.5**				
	Kappa	**0.58**				

Table 5.8 Sondags River irrigation scheme error matrix

Predicted data	Field verification data					
		Salt-affected/ Waterlogged	Stressed	Unaffected	Total	*User's Accuracy (%)*
	Anomaly1	**15**	0	3	18	84.2
	Anomaly2	0	**1**	0	1	
	Not Anomaly	7	0	**25**	32	78.13
	Totals	22	1	28	**51**	
	Producer's Accuracy (%)	68.18	100	89.29		
	Overall accuracy	**80.4**				
	Kappa	**0.6**				

Table 5.9 Pondrift irrigation scheme error matrix

Predicted data	Field verification data					
		Salt-affected/ Waterlogged	Stressed	Unaffected	Total	*User's Accuracy (%)*
	Anomaly1	**14**	0	11	25	65.6
	Anomaly2	0	**7**	0	7	
	Not Anomaly	17	2	**26**	45	57.78
	Totals	31	9	37	**77**	
	Producer's Accuracy (%)	45.16	77.78	70.27		
	Overall accuracy	**61.0**				
	Kappa	**0.326**				

Table 5.10 Douglas irrigation scheme error matrix

Predicted data	Field verification data					
		Salt-affected/ Waterlogged	Stressed	Unaffected	Total	*User's Accuracy (%)*
	Anomaly1	**21**	0	9	30	72.7
	Anomaly2	0	**3**	0	3	
	Not Anomaly	13	0	**20**	33	60.61
	Totals	34	3	29	**66**	
	Producer's Accuracy (%)	61.76	100	68.97		
	Overall accuracy	**66.7**				
	Kappa	**0.387**				

Accurate delineation of salt-affected or waterlogged areas is vital for quantification purposes. Field survey points were used to visually verify the accuracy of the delineated areas (Figure 5.4). Hanson, Grattan & Fulton (2006) showed that crop types have a unique rate at which relative yield is reduced relative to soil salinity increases. The transition between affected and unaffected

areas will thus vary among different crop types and can have a significant effect on the delineated extent of an anomaly. Figure 5.4a and b indicate a highly accurate delineation of the extent of the affected areas, while Figure 5.4c and d show some inconsistencies.

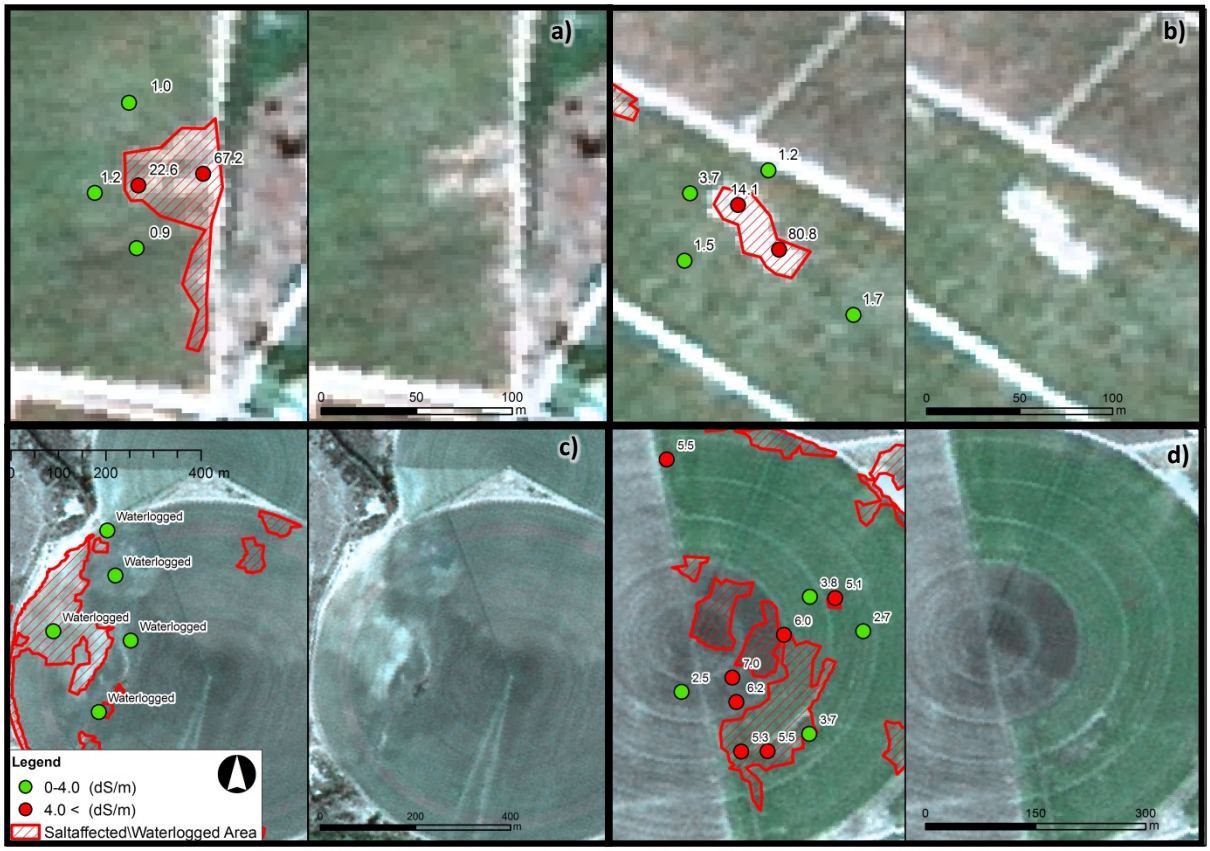

Figure 5.4 Indication of the extent of anomaly delineation for four areas, with a and b representing examples of good delineations and c and d highlighting some inconsistencies

The mean overall accuracy (OA) for the nine schemes is 75% with a mean kappa of 0.6. The error matrices (Table 5.2 to Table 5.10) aid in the interpretation of the salt-affected and waterlogging quantification percentage for each scheme in Table 5.11.

Table 5.11 Salt-affected and waterlogging quantification

Irrigation scheme	Total area considered (ha)	Anomalies (ha)	Ar	Estimated affected area (ha)	Estimated affected area (%)
Vaalharts	26434	572	0.725	414.7	1.57
Loskop	38831	1239	0.716	887.124	2.28
Makhatini	4312	194	0.714	138.516	3.21
Tugela River	27384	2032	0.727	1477.264	5.39
Olifants River	11284	320	0.702	224.64	1.99

Breede River	29129	1807	0.773	1396.811	4.80
Sondags River	18608	556	0.95	528.2	2.84
Pondrift	8681	604	0.775	468.1	5.39
Douglas	22748	1614	0.919	1483.3	6.52

5.4 DISCUSSION

The WFAD achieved a mean accuracy of 75% across the nine study areas, demonstrating its robustness and potential for monitoring salt-affected and waterlogged areas in South Africa. Producer's accuracies (PA) of salt-affected and waterlogged areas ranged from high (Tugela 89.6%; Olifants 85%; Makhatini 83.3%; Loskop 81.4%; Breede 76.5%), to medium (Sondags 68.2%; Vaalharts 62%, Douglas 61.8%) to low (Pondrift 45.16%). A likely explanation for the poor PA in the Pondrift and Douglas irrigation schemes is the occurrence of false positives due to recent flood damage. Flood damage leads to heterogeneous patches in fields unrelated to salt accumulation or waterlogging. During a flood, salts are temporarily flushed from the soil, only to return at a later stage. The rehabilitation period after a flood also varies. All of these factors highlight the importance of synchronizing the capture of satellite and field data. In some cases, the area of salt accumulation or waterlogging is greater than the area of normal growth in a field (often also related to flood damage). As a result, the MeaD algorithm highlights the areas of normal growth as anomalies and were consequently recorded as false positives.

Field digitizing errors also contributed to false positives. A common cause is when vector boundaries do not accurately delineate the true field boundary, especially when areas slightly outside a field is included. The spectral properties of these areas do not match the associated field and are consequently identified as anomalies by the MeaD equation. Using object relationships, the ruleset was modified to eliminate most of these errors, but some errors could not be avoided.

False positives may also occur when a fixed threshold value (e.g. 4.0 dS/m (EC) for salt accumulation) is used to verify if an area is affected or not. Even though the WFAD accommodates various crop sensitivities to salt accumulation and waterlogging, the accuracy of the method can be compromised if a salt tolerant crop displays no physiological stress at an EC level of 4.0 dS/m.

The two-year multi-temporal approach failed to effectively eliminate all anomalies not associated with salt accumulation or waterlogging. Anomalies caused by features such as ground compaction, drought stress and poor farming practices frequently occurred in both images. Increasing the period of analysis to 3 or 4 years may improve the elimination of non-related anomalies. The multi-temporal imagery did, however, eliminate most anomalies unrelated to salt accumulation and waterlogging. Harvesting remnants such as symmetrical tracks caused by harvesters and stacking of bales all lead to areas of high heterogeneity within a field, but were successfully eliminated by the multi-temporal approach.

Considering the false positives and varying anomaly extents, the quantification of salt-affected and waterlogged areas presented in this study should be considered as an estimation and not absolute figures (Table 5.11). The quantifications (Table 5.11) only represent the current active fields in each scheme and does not consider fields that were abandoned due to salt accumulation and/or waterlogging. If abandoned fields were to be included, the percentages will be higher. Some fields have been abandoned for an extended period of time and a much larger temporal analysis would be needed to credibly identify such cases. Nevertheless, the estimations based on the WFAD method is a good representation of the current status of each scheme and serves as a starting point for further monitoring. Apart from the abandoned areas, the percentages indicate that salt accumulation and waterlogging is under control, especially when compared to the percentages of other areas such as Egypt, Iran, and Argentina that have affected areas of 30% or more (Ghassemi, Jakeman & Nix 1995).

5.5 CONCLUSIONS

A robust WFAD approach to quantify salinity and waterlogging was applied to nine different irrigation systems in South Africa. The great variety of crop types, field size and different indirect and direct salinity indicators across the irrigation schemes posed a unique challenge. The WFAD method uses a GEOBIA approach with a rule-based classification scheme. MeaD thresholds were applied separately for vegetated and bare fields to accommodate the various salt accumulation and waterlogging indicators. The WFAD has various strengths and weaknesses. The weaknesses include:

- The manual delineation of field boundaries for a large irrigation scheme is a time-consuming process. Inaccuracies in delineations led to an increase in false positives.
- The multi-temporal approach does not eliminate all anomalies unrelated to salt accumulation and waterlogging. The addition of more seasons is suggested to remedy this.

- Currently, the approach cannot distinguish between salt-affected or waterlogged areas.

The strengths of the WFAD are:

- Unlike with supervised classification, training data is not necessary and ground truth data (where available) can thus be used exclusively for accuracy assessment.
- The technique is not restricted to only vegetated or only bare areas.
- Most of the known salinity and waterlogging indicators are accounted for by the various MeaD thresholds.
- The approach accounts for (at least to a certain extent) the different crop growing phases and sensitivities to salt accumulation and waterlogging by evaluating each field relative to itself.
- The approach is easily transferable across different irrigation schemes.
- Seasonal factors unrelated to salt accumulation and waterlogging are accounted for by using multi-temporal imagery.
- The approach produces a quantifiable result.

The monitoring of salt-affected and waterlogged areas is necessary for the mitigation of potential damage to agricultural areas (De Villiers et al. 2003). With a mean OA and kappa of 75% and 0.6 respectively, the WFAD presents a robust, systematic approach for keeping track of these areas. Recent satellite imagery can easily be incorporated to identify salt-affected and waterlogged areas and to monitor spatial and temporal changes.

More research is needed to automate the field boundary delineation, as the manual digitizing of fields is very time-consuming and error prone. Further analyses of the spectral properties of the anomalies could also help in distinguishing between salt-affected or waterlogged areas.

The next and final chapter provides a summary and a critical evaluation of the research. After reflecting on the research aims and objectives, recommendations for further research are presented and the value of the research is outlined.

CHAPTER 6: DISCUSSION AND CONCLUSIONS

This chapter presents a summary, discussion and critical evaluation of the collective results of the study. The specified aims and objectives are revisited, suggestions for future research are made and conclusions are drawn.

6.1 ASSESSING THE INDIRECT APPROACH FOR SALINITY DETECTION USING EARTH OBSERVATION TECHNIQUES

The primary aim of this study was to evaluate the capability of the indirect approach to detect salt accumulation in South African irrigation schemes, specifically within the context of developing a robust (transferable) salinity monitoring system. The research was motivated by the detrimental impact of high salinity levels on the agricultural sector and the absence of a monitoring system in South Africa.

The literature review presented in Chapter 2 related directly to Objective 1 of the study and provided an overview of earth observation and the various remote sensing approaches to mapping salt accumulation. The review highlighted the potential of the indirect approach to detect salt accumulation and identified vegetation deterioration as one of the key indicators. Most of the previous research on remotely sensed salinity detection was conducted with medium to low resolution satellite imagery in areas where salt accumulation occurs on a grand scale. The literature study helped to formulate the research questions and shaped the research approach to achieve the aims of this study.

Chapters 3 and 4 were dedicated to examining the capability of the indirect approach to identify salt accumulation at a field and scheme level respectively. For each of these experiments, appropriate in situ reference and remote sensing data were acquired, satisfying Objective 2. Experiments in Chapter 3 were aimed at identifying suitable spatial and spectral properties to effectively detect salt accumulation at a field level (Objective 3). Empirical data used for this experiment was a combination of WV2 derived image features and field surveyed EC values. The relationship between the two datasets was tested using quantitative analysis, specifically regression modelling and decision tree analysis (CART).

Chapter 3 showed that utilizing vegetation response for detecting salt accumulation at a field level is promising. Regression modelling results achieved R-squared values of 0.766, 0.704 and 0.731 for image texture, VIs, and spectral bands respectively, and CART produced an ROC value of 0.875 using VIs. Spatial resolutions of 6 m or below were found to be acceptable and a wider spectral resolution improved the results marginally (Research question 1). However, the

improvements of the wide spectral resolution (eight spectral bands) were insignificant, suggesting the use of more cost-effective, high resolution satellite imagery for a large scale implementation (Research question 2).

The experiments of Chapter 4 aimed to evaluate the capability of pan-fused 2.5 m SPOT-5 imagery (with relevant derived image features) to indirectly detect salt accumulation at an irrigation scheme level by using different classification techniques (Objective 4). The experiments were conducted on two distinctly different irrigation schemes. Continuous relationships between the two empirical datasets (image-derived features and EC values) were tested using regression modelling, while CART analyses and RF classifications were used for feature selection. Supervised classifiers (ML, NN, DT, SVM and RF) were tested for delineating areas of salt accumulation.

The regression modelling results showed poor continuous relationships between EC values and indirect indicators (< 0.4 R-squared). Although the supervised classifications produced high accuracies (92.9% and 91.6% OA for Vaalharts and Breede River respectively), the models overestimated the observed salt accumulation. No individual classification technique or set of image features performed consistently well across both study areas, which suggests that this approach is not sufficiently transferable for large scale monitoring purposes. These findings can largely be attributed to the variation in spectral responses between different crop types, growing stages and salinity tolerances in different irrigation schemes (Research question 3). For the supervised classification approach to be successful at a national level, extensive training data would be required for each scheme. This data would also have to be updated regularly to accommodate the dynamic nature of salt accumulation and waterlogging. This would negate some of the advantages of using remote sensing over traditional in situ monitoring methods.

The evaluation of the usefulness of the indirect approach to detect salt accumulation showed that its potential lies at field level (Research question 4). When a field is compared only to itself, different crop growing phases and varying salinity tolerances will have less of an effect and the distinct relationship between vegetation response and salt accumulation will become more apparent. Consequently, if a viable salinity monitoring approach is to be implemented, a field-based approach is proposed.

6.2 DEVELOPMENT AND EVALUATION OF AN EARTH OBSERVATION METHODOLOGY FOR MONITORING SALT ACCUMULATION

The secondary aim of the study was to develop and evaluate a transferable earth observation methodology for monitoring salt accumulation in South African irrigation schemes by taking the results of Chapters 3 and 4 into consideration. In Chapter 5, a semi-automated GEOBIA rule-based classification approach was presented (Objective 5).

Multi-temporal SPOT-5 images were acquired for nine irrigation schemes in South Africa and ground truth data was collected. The within-field anomaly detection (WFAD) method was implemented on a field level across each irrigation scheme. This was achieved through hierarchical segmentation using predefined field boundaries of the study areas. The rule-based classification system considered the spectral characteristics of all known salinity and waterlogging indicators, both direct and indirect. An equation that measured each object's mean spectral difference relative to the field in which it occurs was employed.

The mean OA and kappa values of 75% and 0.6 respectively across the nine irrigation schemes are very encouraging and demonstrate that the procedure is transferable (Research question 5). The key advantages of this approach are that it does not require training data; is able to deal with bare and vegetated areas; accommodates the variability in crop growing stages and salinity sensitivity by evaluating each field with itself; eliminates areas not related to salt accumulation and waterlogging by using multi-temporal imagery; and produces a quantifiable result.

The WFAD approach is, however, not without shortcomings: the manual field boundary delineation is time-consuming; it currently only uses imagery over two years for multi-temporal analysis; and it cannot distinguish between waterlogging or salt-affected areas.

6.3 FUTURE RESEARCH RECOMMENDATIONS

For further evaluation of the indirect approach, it is recommended that the use of image texture to monitor vegetation response to salt accumulation be more thoroughly investigated. Even though there was variation in the performance of different texture algorithms in Chapters 3 and 4, texture measures seem to be more transferable than VIs at scheme level. No published literature on the use of image texture for indirectly classifying salt accumulation were found, suggesting a gap in existing knowledge.

The automation of field boundary delineation would greatly benefit the WFAD method. This would require studying various edge detection algorithms and possibly considering hyperspectral and active remote sensing data. Research on the spectral characteristics of the areas identified as

anomalies can also be valuable for identifying the source of the anomaly. The spectral properties could, for example, indicate whether the anomaly was caused by waterlogging or by salt accumulation. For instance, if a salt crust is exposed, imagery with a wider spectral range (e.g. Sentinel-2) might be able to identify the type of salt compound (e.g. carbonates, sulphates or chlorides) (Metternicht & Zinck 2009). These salt types are characterized by their absorption and reflectance features in the visible, near and shortwave infrared regions. Being cognizant of the source of the anomaly would be of very helpful in designing rehabilitation activities.

6.4 CONCLUSIONS

Salt accumulation poses a threat to sustainable agriculture and can reduce crop yield – particularly in irrigation schemes. A need for systematic management of salt accumulation is needed to mitigate against further losses of agricultural land. To successfully manage salt accumulation, it is necessary to keep track of and monitor the changes thereof. Traditional salinity monitoring methods are laborious, necessitating alternative methods for monitoring salt accumulation over large areas.

This study contributed towards the use of VHR satellite imagery in indirectly identifying salt accumulation. Specifically, it identified optimal combinations of VHR imagery and image analysis techniques and answered several other key research questions in the field of remotely sensed salinity detection. The results provide a point of departure for future work on salt accumulation monitoring in irrigation schemes.

The experiments conducted in this study laid a foundation for the development of an earth observation salinity monitoring system. The WFAD approach presents a viable solution for delimiting salt-affected and waterlogged areas and implementing rehabilitation measures. Continuous monitoring and rehabilitation of salt accumulation and waterlogging in irrigation schemes will help to sustain agricultural production. In turn, this will contribute to improved food security for South Africa and its citizens.

REFERENCES

Abbas A & Khan S 2007. *Using remote sensing techniques for appraisal of irrigated soil salinity*. Proceedings of the International Congress on Modelling and Simulation MODSIM: Modelling and Simulation Society of Australia: 2632–2638.

Abbas A, Khan S, Hussain N, Hanjra MA, . & Akbar S 2013. Characterizing soil salinity in irrigated agriculture using a remote sensing approach. *Physics and Chemistry of the Earth* 55-57: 43–52.

Abdelfattah M, Shahid S & Othman Y 2009. Soil salinity mapping model developed using RS and GIS-a case study from Abu-Dhabi, United Arab Emirates. *European Journal of Scientific Research* 26, 3: 342–351.

Abood S, Maclean A & Falkowski M 2011. *Soil salinity detection in the Mesopotamian agricultural plain utilizing WorldView-2 imagery*. Houghton: Michigan Technological University.

Addink EA, Van Coillie FMB & De Jong SM 2012. Introduction to the GEOBIA 2010 special issue: From pixels to geographic objects in remote sensing image analysis. *International Journal of Applied Earth Observation and Geoinformation* 15, 1: 1–6.

Aihoon JK, Groenewald JA & Sartorius Von Bach HJ 1997. Agricultural salinization in the Olifants River at Loskop valley, Mpumalanga / Landbou-geïnduseerde versouting in die Olifantsrivier by die Loskopvallei, Mpumalanga. *Agrekon* 36, 3: 268–283.

Aldakheel YY 2011. Assessing NDVI spatial pattern as related to irrigation and soil salinity management in Al-Hassa oasis, Saudi Arabia. *Journal of the Indian Society of Remote Sensing* 39, 2: 171–180.

Alhammadi MS & Glenn EP 2008. Detecting date palm trees health and vegetation greenness change on the eastern coast of the United Arab Emirates using SAVI. *International Journal of Remote Sensing* 29, 6: 1745–1765.

Al-Khaier F 2003. Soil salinity detection using satellite remote sensing. Master's thesis. Enschede: ITC, International Institute for Geo-Information Science and Earth Observation.

Allbed A, Kumar L & Aldakheel YY 2014. Assessing soil salinity using soil salinity and vegetation indices derived from IKONOS high-spatial resolution imageries: Applications in a date palm dominated region. *Geoderma* 230-231: 1–8.

Archer DJ & Wadge G 2001. Modelling the backscatter response due to salt crust development. *IEEE Transactions on Geoscience and Remote sensing* 39, 10: 2307–

2310.

Armour RJ 2002. The economic effects of poor and fluctuating irrigation water salinity levels in the lower Vaal and Riet rivers. Master's thesis. Bloemfontein: University of the Free State, Department of Agriculturak Economics.

Armstrong W, Justin SHFW, Beckett PM & Lythe S 1991. Root adaptation to soil waterlogging. *Aquatic Botany* 39, 1-2: 57–73.

Asrar G, Fuchs M, Kanemasu E & Hatfield J 1984. Estimating absorbed photosynthetic radiation and leaf area index from spectral reflectance in wheat. *Agronomy journal* 76, 2: 300–306.

Atzberger C 2013. Advances in remote sensing of agriculture: Context description, existing operational monitoring systems and major information needs. *Remote Sensing* 5, 2: 949–981.

Backeberg G 2003. Water usage and irrigation policy. In the challenge of change: Agriculture, land and the South African economy. Pietermaritzburg: University of Natal Press.

Backeberg G, Bembridge TJ, Bennie ATP, Groenewald JA, Hammers PS, Pullen R. & Thompson H 1996. *Policy proposal for irrigated agriculture in South Africa*. Report No KV96/96. Pretoria: Water Research Commission.

Bannari A, Morin D, Bonn F & Huete AR 1995. A review of vegetation indices. *Remote Sensing Reviews* 13, 1-2: 95–120.

Barnard JH 2013. On-farm management of salinity associated with irrigation for the Orange-Riet and Vaalharts schemes. University of the Free State, Bloemfontein.

Barrett-Lennard EG 2003. The interaction between waterlogging and salinity in higher plants: Causes, consequences and implications. *Plant and Soil* 253, 1: 35–54.

Bastiaanssen WGM 1998. *Remote sensing in water resources management : The state of the art*. Colombo: International Irrigation Management Institute.

Bastiaanssen WGM, Meneti M, Feddes R & Holtslag A 1998. A remote sensing surface energy balance algorithm for land (SEBAL) 1.Formulation. *Journal of Hydrology* 212-213: 198–212.

Bastiaanssen WGM, Molden DJ & Makin IW 2000. Remote sensing for irrigated agriculture: Examples from research and possible applications. *Agricultural Water Management* 46, 2: 137–155.

Bausch WC 1993. Soil background effects on reflectance-based crop coefficients for corn. *Remote Sensing of Environment* 46, 2: 213–222.

Beuster H, Shand M. & Carter CA 2003. *Breede River basin study*. Report No PH 00/00/3102. Pretoria: Department of Water Affairs and Forestry.

Blaschke T & Strobl J 2001. Was ist mit den pixeln los? Neue entwicklungen zur integration von fernerkundung und GIS. *Geo-Informations-Systeme* 14, 6: 12–17.

Blaschke T 2010. Object based image analysis for remote sensing. *ISPRS Journal of Photogrammetry and Remote Sensing* 65, 1: 2–16.

Blaschke T, Hay GJ, Kelly M, Lang S, Hofmann P, Addink E, Queiroz Feitosa R, van der Meer F, van der Werff H, van Coillie F & Tiede D 2014. Geographic object-based image analysis - Towards a new paradigm. *ISPRS Journal of Photogrammetry and Remote Sensing* 87: 180–191.

Bosch A, Zisserman A & Muoz X 2007. *Image classification using random forests and ferns*. Proceedings of the 11th IEEE International Conference on Computer Vision. Rio de Janeiro: 1-8.

Bouaziz M, Gloaguen R & Samir B 2011. Remote mapping of susceptible areas to soil salinity, based on hyperspectral data and geochemical, in the southern part of Tunisia. In *Remote Sensing for Agriculture, Ecosystems, and Hydrology XIII*. Prague: SPIE.

Bouaziz M, Matschullat J & Gloaguen R 2011. Improved remote sensing detection of soil salinity from a semi-arid climate in northeast Brazil. *Comptes Rendus - Geoscience* 343, 11-12: 795–803.

Bradski G 2000. The OpenCV library. *Dr.Dobb's Journal of Software Tools* 25, 120: 122 – 125.

Breiman L 2001. Random forests. *Machine learning* 45: 5–32.

Bresler E, McNeal B & Carter D 1982. *Saline and sodic soils*. New York: Springer-Verlag.

Caccetta P, Allen A & Watson I 2000. *The land monitor project*. Proceedings of the 10th Australian Remote Sensing and Photogrammetry Conference. Adelaide: 21-25.

Campbell J 2007. *Introduction to remote sensing*. 4th ed. London: Taylor & Francis.

Carper WJ 1990. The use of intensity-hue-saturation transformations for merging SPOT panchromatic and multispectral image data. *Photogrammetric Engineering & Remote Sensing* 56, 4: 457–467.

Castaneda C & Herrero J 2009. Application of Landsat and ERS imagery to the study of saline wetlands in semiarid agricultural areas of northeast Spain. In Metternicht GI & Zinck J, (eds) *Remote sensing of soil salinization: Impact on land management*, 175-197. Boca Raton: CRC Press, Taylor & Francis Group.

Ceccato P, Gobron N, Flasse S, Pinty B & Tarantola S 2002. Designing a spectral index to

estimate vegetation water content from remote sensing data: Part 2. Validation and applications. *Remote Sensing of Environment* 82, 2-3: 198–207.

Chang C & Lin C 2011. LIBSVM: A library for support vector machines. *ACM Transactions on Intelligent Systems Technology* 2, 27:1-27

Chang KT 2010. *Introduction to geographic information systems*. 5th ed. Singapore: McGraw Hill.

Chuvieco E & Huete A 2010. *Fundamentals of satellite remote sensing*. Boca Raton: Taylor & Francis Group.

Congalton R & Green K 2009. *Assessing the accuracy of remotely sensed data*. 2nd ed. Boca Raton: CRC Press, Taylor & Francis Group.

Conners RW & Harlow CA 1980. A theoretical comparison of texture algorithms. *IEEE transactions on pattern analysis and machine intelligence* 2, 3: 204–222.

Csillag F, Pasztor L & Biehl L 1993. Spectral band selection for the characterization of salinity status of soils. *Remote Sensing of Environment* 43, 3: 231–242.

Cutler DR, Edwards TC, Beard KH, Cutler A, Hess KT, Gibson J & Lawler JJ 2007. Random forests for classification in ecology. *Ecology* 88, 11: 2783–2792.

Del Valle HF, Blanco PD, Sione W, Rostagno CM & Elissalde NO 2009. Assessment of salt-affected soils using multisensor radar data: A case study from northeastern Patagonia (Argentina). In Metternicht GI & Zinck J (eds) *Remote Sensing of Soil Salinization: Impact on Land Management*, 155-173. Boca Raton: CRC Press, Taylor & Francis Group.

De Villiers MC, Nell JP, Barnard RO & Henning A 2003. *Salt-affected soils : South Africa*. Report No PR 26879. Pretoria: Food Agricultural Organization.

Dehaan RL & Taylor GR 2002. Field-derived spectra of salinized soils and vegetation as indicators of irrigation-induced soil salinization. *Remote Sensing of Environment* 80, 3: 406–417.

Dehaan RL & Taylor GR 2003. Image-derived spectral endmembers as indicators of salinisation. *International Journal of Remote Sensing* 24, 4: 775–794.

Dehni A & Lounis M 2012. Remote sensing techniques for salt affected soil mapping: Application to the Oran region of Algeria. *Procedia Engineering* 33: 188–198.

Dekker RJ 2003. Texture analysis and classification of ERS SAR images for map updating of urban areas in the Netherlands. *IEEE Transactions on Geoscience and Remote Sensing* 41, 9: 1950–1958.

Douaoui A & Yahiaoui I 2015. Combination of remote sensing and kriging to improve soil

salinity mapping in the Hmadna plain (Algeria). *Soil-Water Journal*: 1–5.

Douaoui A, Nicolas H & Walter C 2006. Detecting salinity hazards within a semiarid context by means of combining soil and remote-sensing data. *Geoderma* 134, 1-2: 217–230.

Dutkiewicz A, Lewis M & Ostendorf B 2009a. Evaluation and comparison of hyperspectral imagery for mapping surface symptoms of dryland salinity. *International Journal of Remote Sensing* 30, 3: 693–719.

Dutkiewicz A, Lewis M & Ostendorf B 2009b. The suitability of airborne hyperspectral imagery for mapping surface indicators of salinity in dryland farming areas. In Metternicht GI & Zinck J (eds) *Remote sensing of soil salinization: Impact on land management*, 91-112. Boca Raton: CRC Press, Taylor & Francis Group.

Dwivedi RS & Sreenivas K 1998. Delineation of salt-affected soils and waterlogged areas in the Indo-Gangetic plains using IRS-1C LISS-III data. *International Journal of Remote Sensing* 19, 14: 2739–2751.

Dwivedi RS, Kothapalli R & Singh AN 2009. Generation of farm-level information on salt-affected soils using IKONOS-II multispectral data. In Metternicht GI & Zinck J (eds) *Remote sensing of soil salinization: Impact on land management*, 73-89. Boca Raton: CRC Press, Taylor & Francis Group.

Dwivedi RS, Ramana KV, Thammappa SS & Singh A 2001. The utility of IRS-1C LISS-III and PAN-merged data for mapping salt-affected soils. *Photogrammetric Engineering and Remote Sensing* 67, 10: 1167–1175.

Dwivedi RS, Sreenivas K & Ramana KV 1999. Inventory of salt-affected soils and waterlogged areas: A remote sensing approach. *International Journal of Remote Sensing* 20, 8: 1589–1599.

Eldiery A, Garcia LA & Reich RM 2005. Estimating soil salinity from remote sensing data in corn fields. *Hydrology Days* 970: 31–42.

Elnaggar AA & Noller JS 2010. Application of remote-sensing data and decision-tree analysis to mapping salt-affected soils over large areas. *Remote Sensing* 2, 1: 151–165.

FAO 2016. Extent of salt-affected soils [online]. Available from: http://www.fao.org/soils-portal/soil-management/management-of-some-problem-soils/salt-affected-soils/more-information-on-salt-affected-soils/en/ [Accessed 5 January 2016].

Farifteh J 2009. Model-based integrated methods for quantitative estimaton of soil salinity from hyperspectral remote sensing data. In Metternicht GI & ZinckJ (eds) *Remote*

sensing of soil salinization: Impact on land management, 305-340. Boca Raton: CRC Press, Taylor & Francis Group.

Farifteha J, Farshada TA & Georgeb R 2006. Assessing salt-affected soils using remote sensing, solute modelling, and geophysics. *Geoderma* 130: 191 – 206.

Fawcett T 2006. An introduction to ROC analysis. *Pattern Recognition Letters* 27, 8: 861–874.

Fernández-Buces N, Siebe C, Cram S & Palacio JL 2006. Mapping soil salinity using a combined spectral response index for bare soil and vegetation: A case study in the former lake Texcoco, Mexico. *Journal of Arid Environments* 65, 4: 644–667.

Fernández-Buces N, Siebe C, Prieto JLP & Webster R 2009. Mapping soil salinity from samples data and remote sensing in the former Lake Texcoco, central Mexico. In Metternicht GI & Zinck J (eds) *Remote sensing of soil salinization: Impact on land management*, 291-304. Boca Raton: CRC Press, Taylor & Francis Group.

Field A 2006. *Discovering statistics using SPSS*. 2nd ed. London: SAGE Publications Ltd.

Fischer WA, Hemphill WR & Kover A 1976. Progress in remote sensing (1972–1976). *Photogrammetria* 32, 2: 33–72.

Flanders D, Hall-Beyer M & Pereverzoff J 2003. Preliminary evaluation of eCognition object-based software for cut block delineation and feature extraction. *Canadian Journal of Remote Sensing* 29, 4: 441–452.

Flügel W-A & Kienzle S 1989. *Hydrology and salinity dynamics of the Breede River, Western Cape Province, Republic of South Africa*. Report No. 182. Baltimore: International Association of Hydrological Sciences.

Foody GM, Warner T a & Nellis MD 2009. *The SAGE handbook of remote sensing*. London: SAGE Publications Ltd.

Fraser D 2009. Mapping areas susceptible to soil salinity in the irrigation region of southern New South Wales, Australia. In Metternicht GI & Zinck J (eds) *Remote sensing of soil salinization: Impact on land management*, 63-72. Boca Raton: CRC Press, Taylor & Francis Group.

Friedman JH 1997. On bias, variance, 0/1—loss, and the curse-of-dimensionality. *Data mining and knowledge discovery* 77, 1: 55–77.

Furby S, Caccetta P & Wallace J 2010. Salinity monitoring in western Australia using remotely sensed and other spatial data. *Journal of Environment Quality* 39, 1: 16 –25.

Furby S, Wallace J, Caccetta P & Wheaton G 1995. *Detecting and monitoring salt-affected land*. Canberra: Land and Water Resources Research and Development Corporation,

Canberra ACT.

Gao J & Liu Y 2008. Mapping of land degradation from space: a comparative study of Landsat ETM+ and ASTER data. *International Journal of Remote Sensing* 29, 14: 4029–4043.

García Rodríguez P, Pérez González ME & Guerra Zaballos A 2007. Mapping of salt-affected soils using TM images. *International Journal of Remote Sensing* 28, 12: 2713–2722.

Ghassemi F, Jakeman AJ & Nix HA 1995. *Salinisation of land and water resources: human causes, extent, management and case studies*. Wallingford: CAB international.

Gibson PJ 2000. *Introductory remote sensing: Principals and concepts*. London: Routledge.

Gislason PO, Benediktsson JA & Sveinsson JR 2006. Random forests for land cover classification. *Pattern Recognition Letters* 27, 4: 294–300.

Golovina N, Minskiy D, Pankova Y & Solov'yev D 1992. Automated air photo interpretation in the mapping of soil salinization in cotton-growing zones. *Mapping Sciences and remote Sensing* 29, 3: 262–268.

Gombar O & Erasmus C 1976. *Vaalharts ontwateringsprojek.* Report No GH2897. Pretoria: Department of Water Affairs.

González-Audícana M, Saleta JL, Catalán RG & García R 2004. Fusion of multispectral and panchromatic images using improved IHS and PCA mergers based on wavelet decomposition. *IEEE Transactions on Geoscience and Remote Sensing* 42, 6: 1291–1299.

Goodall TM, North CP & Glennie KW 2000. Surface and subsurface sedimentary structures produced by salt crusts. *Sedimentology* 47, 1: 99–118.

Gould PR 1967. On the geographical interpretation of eigenvalues. *Transactions of the Institute of British Geographers* 42, 42: 53.

Ham J, Chen Y, Crawford MM & Ghosh J 2005. Investigation of the random forest framework for classification of hyperspectral data. *IEEE Transactions on Geoscience and Remote Sensing* 43, 3: 492–501.

Hamzeh S, Naseri A, AlaviPanah S, Mojaradi B, Bartholomeus H, Clevers JPW & Behzad M 2012a. Estimating salinity stress in sugarcane fields with spaceborne hyperspectral: Vegetation indices. *International Journal of Applied Earth Observation and Geoinformation* 21, 1: 282–290.

Hamzeh S, Naseri A, AlaviPanah S, Mojaradi B, Bartholomeus H & Herlod M 2012b.

Mapping salinity stress in sugarcane fields with hyperspectral satellite imagery. In Remote Sensing for Agriculture, Ecosystems, and Hydrology XIV. Edinburgh: SPIE.

Hanson BR, Grattan SR & Fulton A 2006. *Agricultural salinity and drainage*. 2nd ed. California: Department of Land, Air and Water Resources, University of California.

Haralick RM & Shapiro LG 1985. Image segmentation techniques. *Computer Vision, Graphics, and Image Processing* 29, 1: 100–132.

Haralick RM 1979. Statistical and structural approach to texture. *Proceeding of IEEE* 67, 5: 786–804.

Haralick RM, Shanmugam K & Dinstein I 1973. Textural features for image classification. *IEEE Transactions on Systems, Man, and Cybernetics* 3, 6: 610 – 621.

Hay GJ & Castilla G 2008. Geographic object-based image analysis (GEOBIA): A new name for a new discipline. In Blaschke T, Lang S & Hay G (eds) *Object-Based Image Analysis*, 75 - 89. Berlin: Springer.

Hay GJ, Niemann KO & McLean GF 1996. An object-specific image-texture analysis of H-resolution forest imagery. *Remote Sensing of Environment* 55, 2: 108–122.

Hick PT & Russell WGR 1990. Some spectral considerations for remote sensing of soil salinity. *Australian Journal of Soil Research* 28: 417 – 431.

Hillel D & Vlek P 2005. The sustainability of irrigation. *Advances in Agronomy* 87, 05: 55–84.

Hillel D 2000. *Salinity management for sustainable irrigation*. Washington: The International Bank for Reconstruction.

Howari FM & Goodell PC 2009. Characterization of salt-crust build-up and soil salinization in the United Arab Emirates by means of field and remote sensing techniques. In Metternicht GI & Zinck J (eds) *Remote sensing of soil salinization: Impact on land management*, 141-154. Boca Raton: CRC Press, Taylor & Francis Group.

Howari FM 2003. The use of remote sensing data to extract information from agricultural land with emphasis on soil salinity. *Australian Journal of Soil Research* 41, 7: 1243–1253.

HSU 2016. Vegetation spectral reflectance curves. Available from [online]: http://gsp.humboldt.edu/olm_2015/Courses/GSP_216_Online/lesson2-1/vegetation.html [Accessed 25 June 2016].

Huete AR 1988. A soil-adjusted vegetation index (SAVI). *Remote Sensing of Environment* 25, 3: 295–309.

Hughes G 1968. On the mean accuracy of statistical pattern recognizers. *IEEE Transactions on Information Theory* 14, 1: 55 – 63.

Iqbal F 2011. Detection of salt affected soil in rice-wheat area using satellite image. *African Journal of Agriculture Research* 6, 21: 4973–4982.

Jenkin JJ 1981. Terrain, groundwater and secondary salinity in Victoria, Australia. *Agricultural Water Management* 4: 143 – 171.

Jiang Z, Huete AR, Didan K & Miura T 2008. Development of a two-band enhanced vegetation index without a blue band. *Remote Sensing of Environment* 112, 10: 3833–3845.

Johnstone R & Barson M 1990. *An assessment of the use of remote sensing techniques in land degradation studies*. Canberra: Australian Department of Primary Industries and Energy, Bureau of Rural Resources.

Khan NM, Rastoskuev VV, Sato Y & Shiozawa S 2005. Assessment of hydrosaline land degradation by using a simple approach of remote sensing indicators. *Agricultural Water Management* 77, 1-3: 96–109.

Khan NM, Rastoskuev VV, Shalina EV & Sato Y 2001. *Mapping salt-affected soils using remote sensing indicators - A simple approach with the use of GIS IDRISI*. Proceedings of the 22nd Asian Conference on Remote Sensing. Signapore.

Kirchner J 1995. *Investigation into the contribution of groundwater to the salt load of the Breede river, using isotopes and chemical tracers.* Report No 344/1/95. Pretoria: Water research Commission.

Koshal AK 2010. *Indices based salinity areas detection through remote sensing & GIS in parts of South West Punjab*. Proceedings of the 13th Annual International Conference and Exhibition on Geospatial Information Technology and Applications. Gurgaon: 1–11.

Kruger M, Van Rensburg JBJ & Van den Berg J 2009. Perspective on the development of stem borer resistance to Bt maize and refuge compliance at the Vaalharts irrigation scheme in South Africa. *Crop Protection* 28, 8: 684–689.

Laliberte AS, Fredrickson EL & Rango A 2007. Combining decision trees with hierarchical object-oriented image analysis for mapping arid rangelands. *Photogrammetric Engineering & Remote Sensing* 73, 2: 197–207.

Lenney MP, Woodcock CE, Collins JB & Hamdi H 1996. The status of agricultural lands in Egypt: The use of multitemporal NDVI features derived from Landsat TM. *Remote Sensing of Environment* 56, 1: 8–20.

Leone AP, Menenti M, Buondonno A, Letizia A, Maffei C & Sorrentino G 2007. A field experiment on spectrometry of crop response to soil salinity. *Agricultural Water Management* 89, 1-2: 39–48.

Letey J 1994. Is irrigated agriculture sustainable? In Baker RS, Gee GW & Rosenzweig (eds) *Soil and water science: Key to understanding our global environment*, 23 - 37. Madison: Soil Science Society of America.

Liebenberg L 1977. Die geologie van die gebied 2724D (Andalusia). Master's thesis. Bloemfontein: University of the Free State, Department of Geology.

Lillesand TM, Kiefer P w & Chipman JW 2004. *Remote sensing and image interpretation*. 5th ed. New York: John Wiley & Sons, Inc.

Lobell DB, Lesch SM, Corwin DL, Ulmer MG, Anderson KA, Potts DJ, Doolittle JA, Matos MR & Baltes MJ 2010. Regional-scale assessment of soil salinity in the Red River Valley using multi-year MODIS EVI and NDVI. *Journal of environmental quality* 39, 1: 35–41.

Lucas R, Rowlands A, Brown A, Keyworth S & Bunting P 2007. Rule-based classification of multi-temporal satellite imagery for habitat and agricultural land cover mapping. *ISPRS Journal of Photogrammetry and Remote Sensing* 62, 3: 165–185.

Macvicar C, De Villiers J, Loxton R, Verster E, Lambrechts J, Merryweather F, Le Roux J, TH Van Rooyen, Von H & Harmse M 1977. *Soil classification: A Binomial system for South Africa*. Report No S591 S6. Pretoria: Department of Agricultural Technical Services.

Maisela RJ 2007. Realizing agricultural potential in land reform: The case of Vaalharts irrigation scheme in the Northern Cape province. Master's thesis. Cape Town: University of the Western Cape, Faculty of Economic and Management Sciences.

Mashimbye EZ 2005. Remote sensing-based identification and mapping of salinised irrigated land between Upington and Keimoes along the lower Orange River, South Africa. Master's thesis. Stellenbosch: University of Stellenbosch, Department of Geography and Environmental Studies.

Mather P & Magaly K 2011. *Computer processing of remotely-sensed images*. 4th ed. Chichester: John Wiley & Sons.

McDonagh J & Bunning S 2009. *Field manual for local level land degradation assessment in drylands*. Norwich: Food and Agriculture Organization.

McFarlane DJ, George RJ & Caccetta PA 2004. *The extent and potential area of salt-affected land in western Australia estimated using remote sensing and digital terrain*

models. Proceedings of the 1st National Salinity Engineering Conference held November. Perth.

McGhie S & Ryan M 2005. *Salinity indicator plants*. New South Wales: Department of Infrastructure, Planning and Natural Resources.

Metternicht G & Zinck JA 2009. *Remote sensing of soil salinization: Impact on Land Management*. Boca Raton: CRC Press Taylor and Francis.

Metternicht GI & Zinck JA 2003. Remote sensing of soil salinity: Potentials and constraints. *Remote Sensing of Environment* 85, 1: 1–20.

Metternicht GI 1996. Detecting and monitoring land degradation features and processes in the Cochabamba valleys, Bolivia, a synergistic approach. Doctoral dissertation. Ghent: University of Ghent.

Mohamed ES, Morgun EG & Goma Bothina SM 2011. Assessment of soil salinity in the Eastern Nile Delta (Egypt) using geoinformation techniques. *Moscow University Soil Science Bulletin* 66, 1: 11–14.

Moolman J, Clercq W De, Wessels W, Meiring A & Molman C 1999. *The use of saline water for irrigation of grapevines and the development of crop salt tolerance indices.* Report No 303/1/1999. Pretoria: Water Research Commission.

Mougenot B, Pouget M & Epema G 1993. Remote sensing of salt affected soils. *Remote sensing reviews* 7: 241–259.

Mountrakis G, Im J & Ogole C 2011. Support vector machines in remote sensing: A review. *ISPRS Journal of Photogrammetry and Remote Sensing* 66, 3: 247–259.

Mucina L & Rutherford M 2006. *The vegetation of South Africa, Lesotho and Swaziland*. Pretoria: South African National Biodiversity Institute.

Muller SJ & Van Niekerk A 2016a. Identification of WorldView-2 spectral and spatial factors in detecting salt accumulation in cultivated fields. *Geoderma* 273: 1–11.

Muller SJ & Van Niekerk A 2016b. An evaluation of supervised classifiers for indirectly detecting salt-affected areas at irrigation scheme level. *International Journal of Applied Earth Observations and Geoinformation* 49: 138–150.

Myburgh G & Van Niekerk A 2013. Effect of feature dimensionality on object-based land cover classification : A comparison of three classifiers. *South African Journal of Geomatics* 2, 1: 13–27.

Myburgh G & Van Niekerk A 2014. Impact of training set size on object-based landcover classification: A comparison of three classifiers. *International Journal of Applied Geospatial Research* 5, 3: 49–67.

Naumann JC, Young DR & Anderson JE 2009. Spatial variations in salinity stress across a coastal landscape using vegetation indices derived from hyperspectral imagery. *Plant Ecology* 202, 2: 285–297.

Nell J & Van Niekerk A 2014. *Appropriate methods for monitoring salt accumulation and waterlogging on South African irrigation schemes*. Proceedings of the third International Salinity Forum. Riverside.

Nell J, Van Niekerk A, Muller S, Vermeulen D, Pauw T, Stephenson G & Kemp J 2015. *Methodology for monitoring waterlogging and salt accumulation on selected irrigation schemes in South Africa.* Report No TT 648/15. Pretoria. Water Research Commission.

Nikolakopoulos KG 2008. Comparison of nine fusion techniques for very high resolution data. *Photogrammetric Engineering & Remote Sensing* 74, 5: 647–659.

Novack T, Esch T, Kux H & Stilla U 2011. Machine learning comparison between WorldView-2 and QuickBird-2-simulated imagery regarding object-based urban land cover classification. *Remote Sensing* 3, 10: 2263–2282.

Oommen T, Misra D, Twarakavi NKC, Prakash A, Sahoo B & Bandopadhyay S 2008. An objective analysis of support vector machine based classification for remote sensing. *Mathematical Geosciences* 40, 4: 409–424.

Pal M & Mather PM 2005. Support vector machines for classification in remote sensing. *International Journal of Remote Sensing* 26, 5: 1007–1011.

Pal M 2005. Random forest classifier for remote sensing classification. *International Journal of Remote Sensing* 26, 1: 217–222.

PCI Geomatics 2014. *Geomatica Focus - User Guide*. Toronto: PCI Geomatics Enterprises Inc.

Peñuelas J, Isla R, Filella I & Araus JL 1997. Visible and near-infrared reflectance assessment of salinity effects on barley. *Crop Science* 37, 1: 198–202.

Phipson J 2012. *Agricultural and agribusiness status quo assessment.* Mtunzini: Uthukela District Municipality.

Pitman MG & Läuchli A 2002. Global impact of salinity and agricultural ecosystems. In Läuchli A & Lüttge U (eds) *Salinity: Environment-Plants-Molecules*, 3-20. Dordrecht: Kluwer Academic Publishers.

Platonov A, Noble A & Kuziev R 2013. Soil salinity mapping using multi-temporal satellite images in agricultural fields of Syrdarya province of Uzbekistan. In Shahid SA, Abdelfattah MA, & Taha FK (eds) *Developments in soil salinity assessment and*

reclamation: Innovative thinking and use of marginal soil and water resources in irrigated agriculture. Dordrecht: Springer.

Qureshi RH & Barrett-Lennard EG 1998. *Agriculture for irrigated land in a handbook.* Queanbeyan: Australian Centre for International Agricultural Research.

Rao BRM, Sankar TR, Dwivedi RS, Thammappa SS & Venkataratnam L 1995. Spectral behaviour of salt-affected soils. *International Journal of Remote Sensing* 16, 12: 2125–2136.

Rhoades JD 1997. *Sustainability of irrigation: An overview of salinity problems and control strategies*. Proceedings of the 50th Canadian Water Resources Association conference, Footprints of Humanity: Reflections on Fifty Years of Water Resource Developments. Lethbridge: 1-42.

Richards LA 1954. Diagnosis and improvement of saline and alkali soils. In *Agriculture Handbook No. 60*. Washington D.C.: Department of Agriculture.

Russ JC 1999. *The image processing handbook.* 3rd ed. Boca Raton: Taylor & Francis Group.

SASA 2007. *Soil, standards and guidelines for conservation and environmental management in the South African sugar industry*. Mt Edgecombe: Department of Environmental Affairs.

Schaffer C 1993. Overfitting avoidance as bias. *Machine Learning* 10, 2: 153–178.

Schmid T, Magaly K & Gumuzzio J 2009. Applications of hyperspectral imagery to soil salinity mapping. In Metternicht GI & Zinck J (eds) *Remote sensing of soil salinization: Impact on Land Management*, 113-140. Boca Raton: CRC Press, Taylor & Francis Group.

Schulze R 2006. *South African atlas of climatology and agrohydrology*. Report No 1489/1/06. Pretoria: Water Research Commission.

SEOS 2016 [online]. Supplement 1.2: Remote sensing instruments used in marine pollution monitoring. Available from: http://lms.seos-project.eu/learning_modules/marinepollution/marinepollution-c01-s02-p01.html [Accessed 25 June 2016].

Setia R, Lewis M, Marschner P, Raja Segaran R, Summers D & Chittleborough D 2013. Severity of salinity accurately detected and classified on a paddock scale with high resolution multispectral satellite imagery. *Land Degradation and Development* 24, 4: 375–384.

Shao Y, Hu Q, Guo H, Lu Y, Dong Q & Han C 2003. Effect of dielectric properties of

moist salinized soils on backscattering coefficients extracted from RADARSAT image. *IEEE Transactions on Geoscience and Remote Sensing* 41, 8: 1879–1888.

Sidike A, Zhao S & Wen Y 2014. Estimating soil salinity in Pingluo County of China using QuickBird data and soil reflectance spectra. *International Journal of Applied Earth Observation and Geoinformation* 26: 156–175.

Spies B & Woodgate P 2005. *Salinity mapping methods in the Australian context*. Canberra: Department of the Environment and Heritage and, Agriculture, Fisheries and Forestry.

Sreenivas K, Venkataratnam L & Rao PN 1995. Dielectric properties of salt-affected soils. *International Journal of Remote Sensing* 16, 4: 641–649.

Stals JP 2007. Mapping potential soil salinization using rule based object-oriented image analysis. Master's thesis. Stellenbosch: University of Stellenbosch, Department of Geography and Environmental Studies.

Steinberg D & Golovnya M 2007. *CART user's guide*. San Diego: Salford Systems.

Streutker A 1997. The dependence of permanent crop production on efficient irrigation and drainage at the Vaalharts government water scheme. *Water SA* 3, 2: 90-102.

Tajgardan T, Shataee S & Ayoubi S 2007. *Spatial prediction of soil salinity in the arid zones using ASTER data, Case study: North of Ag ghala, Golestan Province, Iran*. Proceedings of the 28th Asian Conference on Remote Sensing. Kuala Lumpur: 1712–1717.

Taylor GR, Mah AH, Kruse FA, Kierein-young KS, Hewson RD & Bennett BA 1996. Radar Imagery of Saline Soils Using Airborne. *Remote Sensing of Environment* 57: 127–142.

Tempfli K, Kerle N, Huurneman GC & Janssen LLF 2009. *Principles of remote sensing*. Enschede: ITC.

Tilley DR, Ahmed M, Son JH & Badrinarayanan H 2007. Hyperspectral reflectance response of freshwater macrophytes to salinity in a brackish subtropical marsh. *Journal of environmental quality* 36, 3: 780–789.

Tren R & Schur M 2000. *Olifants River irrigation schemes, Reports 1 & 2*. Colombo: IWMI.

Tso B & Mather PM 2009. *Classification methods for remotely sensed data*. 2nd ed. Boca Raton: CRC Press, Taylor & Francis Group.

Turhan H, Genc L, Smith SE, Bostanci YB & Turkmen OS 2008. Assessment of the effect of salinity on the early growth stage of the common sunflower (Sanay cultivar) using

spectral discrimination techniques. *African Journal of Biotechnology* 7, 6: 750–756.

Tzotsos A & Argialas D 2008. A support vector machine approach for object based image analysis. In Blaschke T, Lang S & Hay G (eds) *Object-Based Image Analysis*, 663–667. Berlin: Springer.

UCS 2016 [online]. UCS satellite database. Available from: http://www.ucsusa.org/nuclear-weapons/space-weapons/satellite-database#.V1Qprvl96Uk [Accessed 5 June 2016].

Umali DL 1993. *Irrigation − Induced salinity*. Washington D.C.: The World Bank.

USADA 2015 [online]. Soil Salinity Testing. Available from: http://www.nrcs.usda.gov/wps/portal/nrcs/detail/mt/home/?cid=nrcs144p2_057679 [Accessed 23 November 2015].

Van Rensburg L, Barnard J, Bennie A, Sparrow J & du Preez C 2012. *Managing salinity associated with irrigation at Orange-Riet and Vaalharts irrigation schemes.* Report No 1647/1/12. Pretoria: Water Research Commission.

Van Rensburg LD, De Clercq WP, Barnard JH & Du Preez CC 2011. Salinity guidelines for irrigation: Case studies from Water Research Commission projects along the Lower Vaal, Riet, Berg and Breede Rivers. *Water SA* 37, 5: 739–750.

Van Schilfgaarde J 1990. Irrigated agriculture: Is it sustainable? In Tanji K (ed) *Agriculture salinity assessment and management manual,* 584-594. New York: ASCE.

Viera AJ & Garrett JM 2005. Understanding interobserver agreement: The kappa statistic. *Family Medicine* 37, 5: 360–363.

Wang D, Poss JA, Donovan TJ, Shannon MC & Lesch SM 2002. Biophysical properties and biomass production of elephant grass under saline conditions. *Journal of Arid Environments* 52, 4: 447–456.

Weih RC & Riggan ND 2010. Object-based classification vs. pixel-based classification: Comparative importance of multi-resolution imagery. *The International Archives of the Photogrammetry, Remote Sensing and Spatial Information Sciences* 38: 1–6.

Wiegand C, Rhoades J, Escobar D & Everitt J 1994. Photographic and videographic observations for determining and mapping the response of cotton to soil salinity. *Remote Sensing of Environment* 49, 3: 212–223.

WRC 2010. *Knowledge review*. *Water research commission,* Report No K5/1880//4. Pretoria: Water Research Commission.

Wu J, Vincent B, Yang J, Bouarfa S & Vidal A 2008. Remote sensing monitoring of

changes in soil salinity: A case study in inner mongolia, China. *Sensors* 8, 11: 7035–7049.

Yu Q, Gong P, Clinton N, Biging G, Kelly M & Schirokauer D 2006. Object-based detailed vegetation classification with airborne high spatial resolution remote sensing imagery. *Photogrammetric Engineering and Remote Sensing* 72, 7: 799–811.

Zhang TT, Zeng SL, Gao Y, Ouyang ZT, Li B, Fang CM & Zhao B 2011. Using hyperspectral vegetation indices as a proxy to monitor soil salinity. *Ecological Indicators* 11, 6: 1552–1562.

Zhang Y 2002. Problem of fusion of commercial high-resolution satellite as well as Landsat 7 image and initial solutions. *International Archives of Photogrammetry Remote Sensing and Spatial Information Science* 34, 4: 587–592.

Zinck J 2000. *Monitoring soil salinity from remote sensing data*. Proceedings of the 1st Workshop for the Special Interest Group on Remote Sensing for Developing Countries by the European Association of Remote Sensing Laboratories. Gent: 359–368.